University of Stavanger

Faculty of Science and Technology

MASTER'S THESIS

Study program/Specialization: Petroleum Geosciences Engineering	Spring Semester, 2013 Open
Writer: Trine Mehus	_____ (Writer's signature)
Faculty supervisor: Udo Zimmermann Co- supervisor: Ingunn Cecilie Oddsen	
Title of thesis: From Cold to Hot: Post Hirnantian Sedimentary Basins in Bolivia- a Source Rock for Hydrocarbon Deposits in the Andes? – A Case Study of the Cancañiri Formation	
Credits (ECTS): 30	
Keywords: Bolivia Provenance Geochemistry Sedimentology Heavy minerals Cancañiri Formation Hirnantian glaciation	Pages: 70 pages + Enclosure: Appendix Stavanger…… date, year

From Cold to Hot: Post Hirnantian Sedimentary Basins in Bolivia- a Source Rock for Hydrocarbon Deposits in the Andes? – A Case Study of the Cancañiri Formation

by

Trine Mehus

Master Thesis

Presented to the Faculty of Science and Technology

The University of Stavanger

The University of Stavanger

June 2013

Acknowledgements

First I would like to thank my supervisor Dr. Udo Zimmermann, for giving me this research project, where I got the chance to travel to Bolivia which for me made this thesis unique and possible. Without Mr. Zimmermann's knowledge and guidelines this thesis would never have been written. I am also truly grateful for all your help and sharing of knowledge, and giving me a time full of long lasting experiences within geology and sedimentology, during my bachelor and master degree at UiS. I would also like to thank NPD (Norwegian Petroleum Directorate) for sponsoring me with the traveling cost to Bolivia.

Further, I would like to thank Ingunn Cecilie Oddsen, with her help and guidelines during the SEM and CL analysis, where she thought me how the machine worked and answered all my questions.

I also want to thank my fellow student Sveinung Hatløy, for cooperation throughout this whole semester, by shearing knowledge- and thoughts and giving me motivation, when my motivation was low.

Finally I want to thank my family and friends, for constantly support during this semester when writing my thesis, and throughout my whole study at UiS.

Abstract

From Cold to Hot: Post Hirnantian Sedimentary Basins in Bolivia- a Source Rock for Hydrocarbon Deposits in the Andes? – A Case Study of the Cancañiri Formation

Trine Mehus

The University of Stavanger, 2013

Supervisor: Udo Zimmermann

Co- supervisor: Ingunn Cecilie Oddsen

This thesis introduces to sedimentary rocks sampled in Bolivia, in the Eastern Cordillera. Samples were taken from two different outcrops of the Late Ordovician to Early Silurian Cancañiri Formation, and the comparison of these two localities will be drawn in the results. These rocks have been studied using petrography, geochemistry analysis, TOC, heavy minerals using SEM and CL detector analysis, to reveal the shape, composition and interesting features of the rocks. The Cancañiri Formation consists of interbedded sandstones and black shales with glacial diamictites of an Upper Ordovician age. This case study shows two sources of interest, one mafic and one felsic source, however an arc related source might also be possible. From the mineralogical analysis and petrography one can see that the rocks are mainly composed of quartz and pyrite, however with associated minerals like zircon, apatite, rutile and hematite. The total carbon content is very low and does not account for the black color but the high base metal content. This points to a deposition under water in an anoxic environment for the shales. The

facies change from one exposure to the other was accompanied by a change in the geochemistry with more felsic material stored in the more recycled rocks of the second exposure. The latter have one dimension higher abundances of organic matter. As both formations suffered the same p-T conditions during various tectonic events, it is argued that the black shales of CA, the oldest succession of the two sampled areas, has been deposited in a fjord-type environment without organic matter as a consequence of the mass extinction before. Transgression as a result of massive deglaciation provoked the facies changes to a shallow marine environment with some organic input.

Table of Contents

List of Tables

List of Figures

Often used abbreviations

BSE – Back-scatter Electron

CL – Cathodoluminescence

EDS – Energy Dispersive Spectrometer

Fm – Formation

HM – Heavy minerals

Myr – Million years

REE – Rare Earth Elements

SEM – Scanning Electron Microscope

TOC – Total Organic Carbon

UiS – University of Stavanger

1.0 Introduction

1.1 Objective

Bolivian rocks from Upper Ordovician to Silurian age (Table 1) are sampled to gain information about the depositional age by using heavy minerals and palaeoenvironment during deposition. I will as well try to determine the amount of organic carbon and see if there is source rock or hydrocarbons in central Andes. Different mineralogical and geochemical methods are going to be applied to reveal these conditions. These data are important for correlation and to understand the evolution and distribution of hydrocarbons. Some studies have been done in the stratigraphic proximity and those data will be compared here with the presented ones.

	Age	Period	Altiplano	Lithotypes
Cordilleran Cycle	**Silurian**	Pridoli to Ludlow	Catavi	Sandstone and shale
		Wenlock	Uncía	Shale
		Llandovery	Llallagua	Sandstone and shale
	Ordovician	**Ashgill**	**Cancañiri**	**Diamictite**

Table 1: Stratigraphy modified by Diaz – Martinez et al., (2006). The Cancañiri Formation and its related ages are marked in bold.

Department of Petroleum Engineering, University of Stavanger, Ullandhaug, 4036 Stavanger.

1.2 SAMPLING AND METHODOLOGY

This study will present results for four different analysis; i) Geochemistry, ii) petrography, iii) TOC (Total Organic Carbon) iv) heavy mineral determination and Cathodoluminescence (CL). Rocks where sampled at two different outcrops in Eastern Cordillera, S: 16° 19' 21.8'', W: 68° 01' 51.4'' long section Cancañiri Fm (CA), and S: 16° 24' 24.9'', W: 68° 02' 56.6'' Cancañiri Fm (CAN), (Figure 1). This case study will concentrate on these two Cancañiri Formations, which consist of *diamictites*. Diamictites are defined as: *[A terrigenous sedimentary rock that is not sorted or poorly sorted and contains particles of many sizes. Also known as mixtite]* McGraw-Hill 2003, (for Figures of the outcrops and rocks see appendix A).

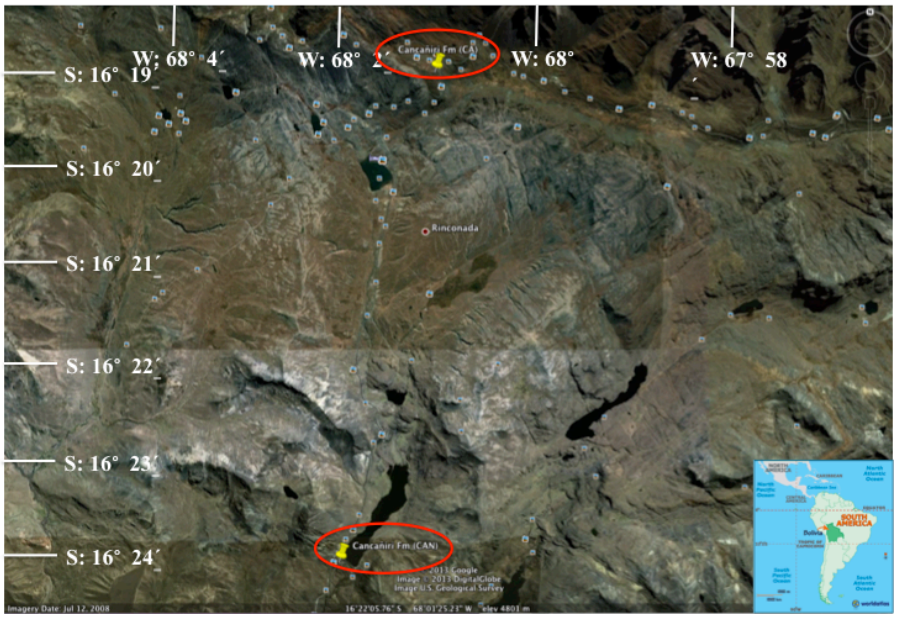

Figure 1: Overview of the formations sampled in Bolivia, where this research project concentrates around the two Cancañiri Formations (red circle), google earth 2013, i.e. www.worldatlas.com.

Department of Petroleum Engineering, University of Stavanger, Ullandhaug, 4036 Stavanger.

1.3 OUTLINE OF THE STUDY

First, I will describe the geological setting of the rocks, and the surrounding area at Eastern Cordillera/Bolivia, before I continue with the methodology, with the brief description of the preparation for all analysis types: i) Geochemistry, ii) petrography, iii) TOC (Total Organic Carbon) iv) heavy minerals and cathodoluminescence. The results of the analysis will then be described and interpreted, as well as a chapter of the application to the oil industry.

1.4 WORKING TITLE OF THE STUDY AND PROCEDURES

This research project is called ”From Cold to Hot: Post Hirnantian Sedimentary Basins in Bolivia- a Source Rock for Hydrocarbon Deposits in the Andes? – A Case Study of the Cancañiri Formation”. All the rocks were sampled in Bolivia, and prepared at the University of Stavanger (UiS). Some samples were milled in an agate mill and sent to Canada for geochemical analysis. SEM, CL and BSE (Back-Scatter Electron) images combined with EDS (Energy Dispersive Spectrometer)- and heavy mineral studies however, where also carried out at UiS.

1.5 HIRNANTIAN GLACIATION

The Hirnantian glaciation has caused the second largest mass extinction during the Phanerozoic after the Permo-Triassic, as 85 % of the marine species disappeared. This major extinction event is considered to be related directly to the effects of glacial conditions established in the Late Ordovician, and is the first of five major mass extinctions during the Phanerozoic (Delabroye and Vecoli., 2009). However the Hirnatian had only a duration of about 2 Myr, and therefore had happened in a short time interval, also in a middle of a greenhouse (Kaljo et al., 2008).

In the Hirnatian there has been recognized two faunal extinctions. One is linked to the onset of the glaciation, the other one is related to the melting of the Gondwana ice sheets and its associated transgression. It is the second one, which is more related to the sampled rocks from Bolivia. This is due to the anoxic water conditions, associated with the deposition of black shales close to the Ordovician-Silurian boundary found in the offshore environments of Gondwana, Laurentia and south China (Delabroye and Vecoli., 2009).

Peri-Gondwanan areas are where the glacial-related deposits occur, one can therefore correlate directly between the glacial events and faunal dynamics in these regions. Many of the index fossils used for the Hirnatian global chronostratigraphy do not occur in Gondwanan localities, it is therefore problematic to do the biostratigraphy on the Gondwanan glacial-related sedimentary strata. Due to this dating problem and also the correlation between the glacially influenced

Gondwanan areas and the faunal dynamics, it is difficult to do a fully reconstruction of the Hirnatian global event stratigraphy (Delabroye and Vecoli., 2009).

Ordovician and Silurian rocks are mostly dominated by different fossils, however due to the lack of fossils in the rocks from Bolivia, it can be problematic to pin-point the exact age of the sampled rocks as other dating methods include errors far above the assigned 2 Myr duration of the Hirnantian glaciation. Based on facts that there were positive carbon 13 excursions in the Hirnantian glaciation, Carbon isotopes are a practical method to test the timing and dating of rocks and events. However, the sampled rocks in Bolivia are not carbonates.

Within the Cancañiri Formation in Bolivia, diamictites are found interbedded with sandstones and shales, these diamictites can be correlated to other formations in other countries in South America i.e. San Gabán Formation in Peru and Zapla Formation in northern Argentina, and the Vargas Peña Formation in eastern Paraguay and the Vila María Formation in southern Brazil also show some similarities in age (Díaz- Martiínez and Grahn., 2006).

However, the age of these formations are highly discussed, due to lack of fossils, however a late Ordovician age (Ashgillian) of the Zapla Formation in Argentina is suggested due to the findings of the trilobite genus *Dalmanitina.* Based on this trilobite, the genus is characteristic and can be correlated to the Upper Ordovician series in sequences of North America, Asia, North Africa and Europe, also known as the "*Dalmanitina* beds". Based on findings and correlation with other alleged Hirnantian fauna. The Cancañiri Formation also assigned a late Ashillian age, however

more studies are needed in this area to get a more understanding of the age and correlations of these rocks (Díaz- Martiínez and Grahn., 2006). For this study detrital zircons had been separated but could not be measured during the MSc thesis because of time constraints.

Tectonic setting

The Cancañiri Formation is interpreted as a lowstand deposits (see below) while a large part of the region was glaciated and was related to regional extension. However several large-scaled tectonic events induced resedimentation events during deposition (Díaz- Martiínez and Grahn., 2006).

1.6 GEOLOGICAL SETTING AND STRATIGRAPHY

Bolivia is today located on the boundary of the South American- and the Nazca plates (Figure 2). The Cordillera Occidental or Altiplano contains most of the world-famous mineral resources, and the rock here consists of Tertiary to Quaternary volcanic complexes. Most of the volcanic rocks have been dated to the Late Miocene. The Nazca plate is still subducting and cause active volcanism (House, 2010).

Towards the west, the Altiplano is located (Figure 3); the rocks here are Tertiary red-beds volcanic complexes and domes deposited in high (3500-5000 m) intermontane basins, which have been formed with the Andean mountain range (House, 2010).

This region is formed, caused by several geological processes. In combination with eastward thrusting of the Proterozoic and Paleozoic basement of the Cordillera Occidental, and the westward thrusting of the Paleozoic orogenic basins of the Cordillera Oriental during on-going subduction processes, the crust was shortened. These thrusts formed foreland basins, which have c. 15000 m of sediments that are interlayered with volcanic rocks during the Mesozoic and Cenozoic era. Crustal shortening then tectonically inversed to extensional movements when subduction processes slowed down during the Phanerozoic (House, 2010).

Between the Oligocene and Miocene, during the deformation of the Andes, several volcanic and plutonic complexes were emplaced along the Altiplano, especially along the eastern margin with the Cordillera Oriental. Marked contrasts between Tertiary intrusive complexes and Devonian–Silurian phyllites can be seen in the Cordillera Oriental (House, 2010).

Recent alluvial sediments dominate as response to up-lift of the Andes, where in the east Proterozoic basement with schist-belts and Mid-Proterozoic mobile belts are exposed. In horst structures near the surface massive mineralization in weathered bedrocks are observable and in deeper crustal levels massive sulphide deposits have been formed (House, 2010).

Southern Bolivia consists of the sub-Andean zone, which is an active foreland-fold and thrust belt along the eastern margin of the Andean orogeny. It is c. 150 km wide and 400 km long. The southern sub-Andean belt is characterized by several north to north-northeast trending, narrow, continuous surface anticlines (Tankard et al., 1995).

A continuous stratigraphy and efficient detachment horizons are suggested due to the structural style of long, thin ranges. In the late Oligocene, the Andean shortening began, and after 10 Ma the sub-Andean zone occurred (Tankard et al., 1995).

Complex maturation history and facies variations are the likely factors controlling the distribution of oil and gas in Bolivia`s hydrocarbon province (Tankard et al., 1995).

Eastern Cordillera (Altiplano)

The Eastern Cordillera stretches from northeast as an extension of the same chain as in Peru, and continuous southwards to Argentina. The Coniri and San Vicente faults separate it from the Altiplano in the west. In the east there is a Main Front Thrust, which is a limit to the Sub-Andean Ranges (Suarez Soruco et al., 2000).

With Proterozoic to recent rocks with marine to continental sequences, the Eastern Cordillera holds the country`s most complete stratigraphic sequences (Suarez Soruco et al., 2000).

Cordilleran Cycle

The sediments from the Cordilleran Cycle are distributed from the Peruvian border to the Argentine border within the Huarina Fold Belt and in the Sub-Andean Belt. These sediments were deposited as infill of wide intracratonic basins, where the material derived from both south and west (Suarez Soruco et al., 2000).

The Cordilleran outcrops consist of two sectors; the western sector and the eastern sector. Both sectors have similar sequences and different names. The western sector is the Huarina Fold Belt; this sector is located to the west and southwest, where one contains the lineament, which is formed by the Cordillera Real fault zone and its extension into the city of Sucre, and further south with the Tocloca fault. Different formations represents the stratigraphic sequence of this sector i.e. the Cancañiri, Huanuni, Llallagua, Uncía and Catavi Formations, for the Silurian, and

the Vila Vila, Belèn, Sicasica, Collpacucho Formations and the Ambo Group, for the Devonian and Lower Carboniferous (Suarez Soruco et al., 2000).

Andean and Sub-Andean Belt represents the eastern sector, this sector was tectonically transported from the NE and E by the Cordillera Real fault zone and the lineament described above. The Aiquile-Vallegrande basins are located in the central part, while the Zudanes-Azurduy and Tarija-Padcaya basins goes further towards the meridian stretching even to northern Argentina. Formations defined for the Silurian age for this sector are Cancañiri, Kirusillas and Tarabuco, while the defined formations from the Devonian and Lower Cretaceous are Santa Rosa, Icla, Huamampampa, Los Monos, Iquiri and Saipurù. However the Los Monos, Iquiri and Saipurù Formations are rare to find in the Eastern Cordilleran sector (Suarez Soruco et al., 2000).

In the Cordilleran cycle reworked marine sediments are what have composed the Cancañiri Formation. Heterogeneous glaciomarine deposits, slope deposits, detrital flow and diamictites are what the Cancañiri Formation relates to at Altiplano. These outcrops are starting 8 km east of the Uyuni and ending at the confluence of the Alota and Grade de Lipez rivers, south of the San Cristobal village (Suarez Soruco et al., 2000).

The Huarina Fold Belt

The Oclóyic movements in northern Argentina caused two effects: 1. The Tacsarian Cycle sequence, in which Cambro-Ordovician rocks have been formed. 2. A normal deep fault (*the Cordillera Real lineament-Tocloca Fault*) which separates the formations as an asymmetrical

distensive basin, with a deep western sector (the Chayanta and Tica Tica basin of up to a 1500 m thickness), from the eastern sector characterized by shallow marine environments (20 to 100 m) (Suarez Soruco et al., 2000).

Cancañiri Formation

The Cancañiri Formation appears often as diamictites and is composed of material deposited in poorly bedded strata sequence, large fallen blocks, slipped layers and abundant clasts of different materials and origins. This material came from the erosion of the Ordovician and Pan-Brasilian rocks (Neoproterozoic to Cambrian) and was then denudated and accumulated in a deep basin. Within these sediments diamictites developed unbedded massive bodies with arenaceous parts that slipped and got mixed within the sediments. The Cancañiri Formation lies unconformable on Tremadocian to Arenigian rocks in the south and on upper Ordovician rocks in the Cochabamba region. While the diamictites rest upon the Caradocian rocks, in the Independencia-Inquisivi-Milluni region. The Cochabamba sector is the only region of the country with diagnostic fossils (Suarez Soruco et al., 2000). Sediments of the Catavi, Uncía and Cancañiri Formations, as well as Ordovician rocks in the region: i.e. the Coroico and An´mutara Formations were all affected by very-low grade metamorphism. This metamorphic event is called the "*cordillera Real Slates*" (Suarez Soruco et al., 2000).

Andean-Subandean Belt

The stratigraphy of the western sector is similar to both the central and western sector, the eastern border of the Eastern Cordillera and the Interandean. In the Department of Chuquisaca in

El Poter-Tarabuco-Icla-Supaymayu area, and in the Cajas-Jarcas Yesera and the Department of Tarija, in Angosto de Alarache region is where the most complete Silurian succession is located. However, in these departments there are no Silurian outcrops east of E 64°15´ (Suarez Soruco et al., 2000).

In the eastern sector, the thickness for the Cancañiri Formation is much less than for the western sector. The thicknesses in the eastern sector ranges from 20 to 200 m, minimum values when compared with the western sector (Tica Tica and Chayanta basins of Huarina Fold Belt), while in the western sector it shows thicknesses over 1000 m. In the eastern sector the Cancañiri Formation consists of shallower shelf marine sediments characterized by diamictites with a silty matrix, with abundant and more or less uniform quartzitic sandstones, rounded clasts in the central part, a greater variety of lithotypes, and large clasts diameters towards the south. Some alpine-type valley glaciation to the south is also indicated in this sector due to striated and faceted clasts. However, in the central part one can see that the basin is shallower and displays development of carbonatic rocks in the upper part, which cause an ongoing debate about the stratigraphic relation. Landoverian trilobites, corals, brachiopodes, and molluscs (*Paraencrinurus boliviensis* zone) and the basal Wenlockian *Ozarcodina sagitta rhenana* association, contain abundant fauna from silts (Lampaya and Pojo), limestones and limey sandstones (Tunari Cordillera). As well as a chitinozoan of the high part of the Middle Llandoverian was found in the La Cumbre section. However, the age of the Cancañiri Formation in still under debate, due to unclear chronological position of some of the taxons (Suarez Soruco et al., 2000).

Department of Petroleum Engineering, University of Stavanger, Ullandhaug, 4036 Stavanger.

Towards eastern Bolivia the thickness of the Cancañiri Formation is petering out. However, this trend is also found in the western boarder of the meridional Sub-Andean, particularly in the Condado and Negro rivers, where the thickness is only a few tenths of meters. The lithology of the sediments of the Cancañiri Formation is the same as in the west of the country, but here the marks produced by glacier action, i.e. as polished and striated facets, are more visible in the clasts incorporated in the diamictite matrix, mostly in granodiorite and quartzite boulders. Here in this region, the Cancañiri Formation lies on top of Lower Ordovician sediments (Suarez Soruco et al., 2000).

Department of Petroleum Engineering, University of Stavanger, Ullandhaug, 4036 Stavanger.

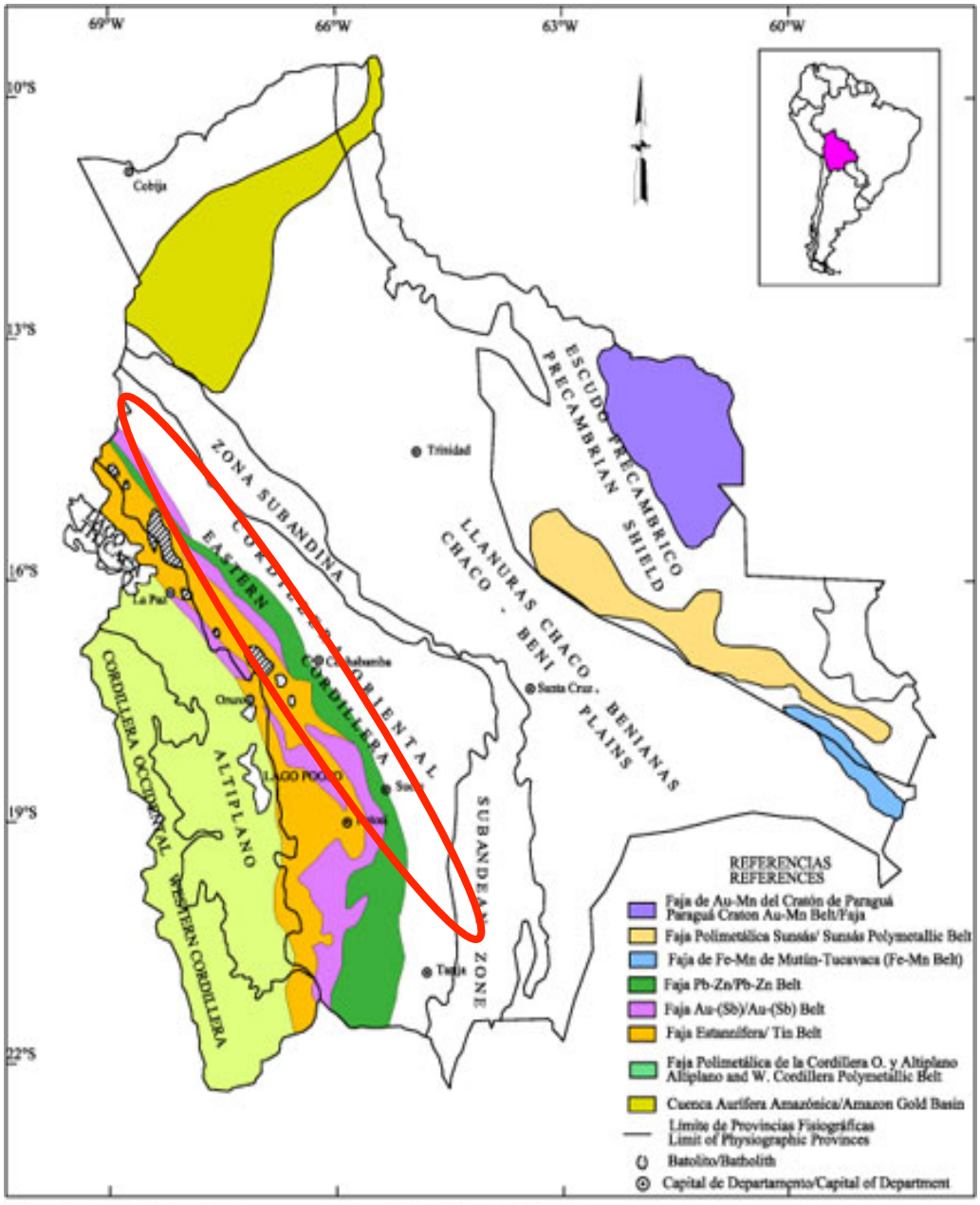

Figure 2: Geological map of Bolivia, Eastern Cordillera is marked in the red circle, after Arce-Burgoa and Goldfarb., (2009).

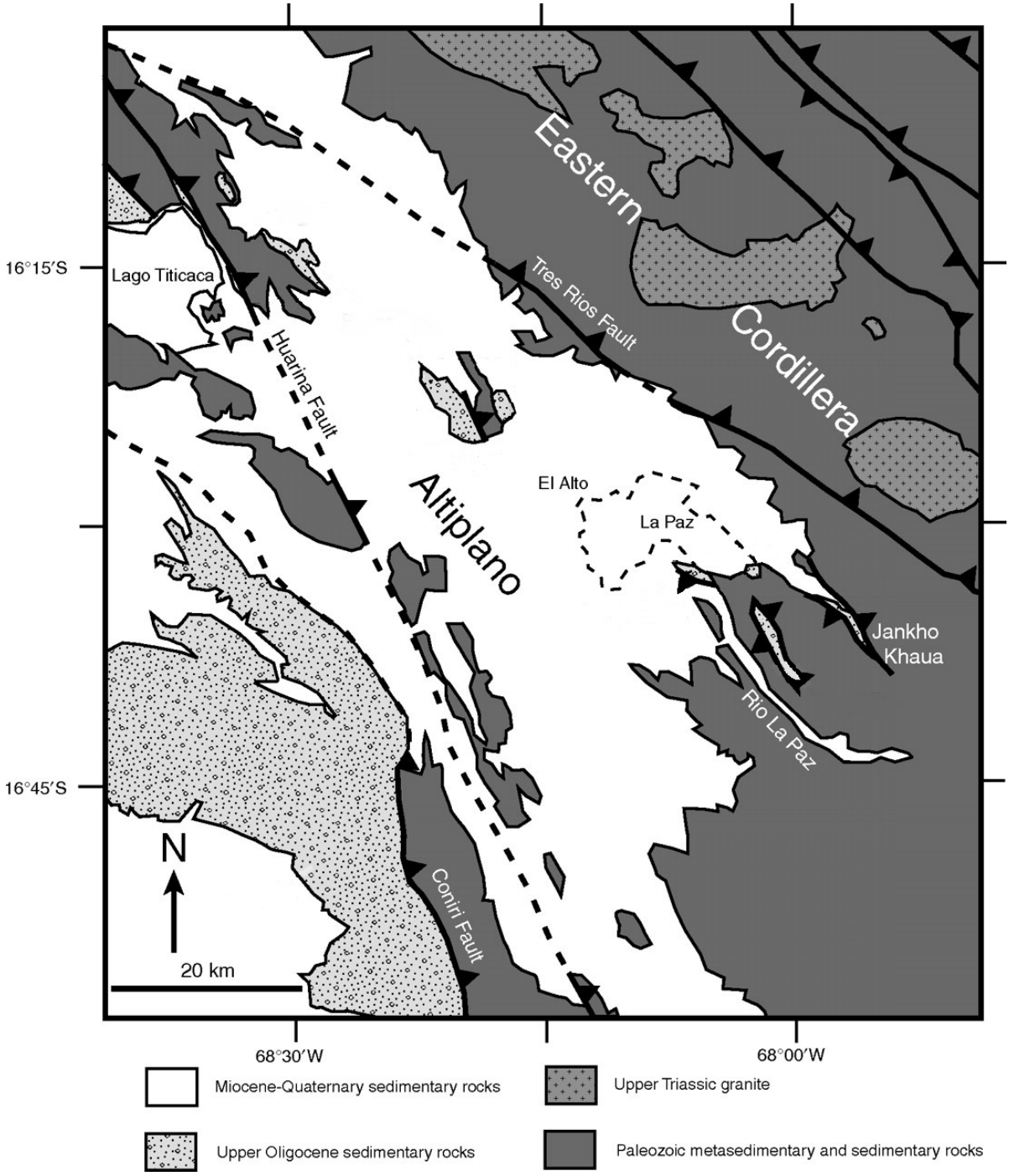

Figure 3: More detailed geological map of Altiplano and Eastern Cordillera, where one also can see the different faults from the text above, modified after Murray et al., (2010).

2.0 Methodology and preparation

2.1 PETROGRAPHY

Some of the thin sections have been pre-prepared at UiS, and then sent to a laboratory in Canada, due to soft characteristics for the rock, while some have been prepared and finished at UiS. For preparation I cut the sample so I had a flat surface that showed the most important features in the rock. Then I polished this surface by using water that contained a powder on a glass plate, and moved the rock on this plate. I used powder (silica carbon pwder) with different type of grain size, started with the coarsest powder 220, moved over to 320, then 600 and last 1000 (which was very fine grained). A different glass plate for each type of polishing powder was absolute necessary, because if the coarse powder still was on the plate after I had washed it this would scratch the surface and one then would have needed to start over. It was also important to wash the plates between each polished sample for the same reason.

After this I had to polish the rectangular glass plate and measure the thickness in the middle of it, before I glued the glass plate to the rock sample. The reason for polish the glass plate was because then the glue and the polished rock sample would better bind the sample to the glass. I also had to write the thickness with a regular pen- and the rock sample with a diamond pen, on the glass plate, so I would know how thick the glass plate and the sample was- and so the name of the rock sample did not get polished away.

The glue consisted of two components: the glue and a liquid that makes the glue hard. The glue is called SpeciFix Resin, and the liquid that hardens the glue is called SpeciFix–20 Curing Agent.

The way to mix the SpeciFix–20 Technical Data: First I mixed the two components, with the mixed ratio of: 7 parts of Resin/1 part of curing agent by weight. Than I mixed this amount correctly and stirred for approximately 3 minutes, after this the glue had to rest for 2 minutes and pour the epoxy carefully cover the specimen. When the glue was ready, I put the glue onto the polished glass plate, and put the plate on top of the polished rock sample. Then I had to move and press the plate over the rock, so all the bobbles were gone. The samples were then placed under pressure for the next 24 hours.

After 24 hours the samples were ready for further preparation. Struers Actom-50 cutting machine cuts the rock samples that a small layer of the sample was left. Then I had to polish these samples on the glass plate with the powder of 220, 320, 600 and 1000. Here one needs to be very careful when polish, because if one polished too much (more than 25 micron thick), the sample might disappear, and then one need to do the whole procedure again.

Petrography analyses where conducted in a light microscope; Zeiss AXIO, Lab.A1, where the camera name was AxioCam ERc 5s, for Figures see appendix B.

2.2 HEAVY MINERALS

For preparation of heavy minerals I got grains from the samples CA 24, CA 31 (first outcrop-long section), and CAN (second outcrop). The grains consisted of tree different powder, CA 24 Apatite Fraction, CA 24 Horizon Frantz Magnetic fraction and CA 24 Zircon Fraction, the same powder were also given for the CA 31 and CAN samples respectively. I needed a glass plate and a two- side tape, the tape was then glued to the glass plate. A round form called a mound, were then set on top of the tape. Two mound forms were placed next to each other, where two equal samples where made, (this was done in case one of the samples was contaminated, 18 mounds were therefore made). The grains from the samples were then distributed in the mounds. It was very important to not use the whole sample, as one might make some more mound samples if needed.

After the grains were placed in the mound I had to take 2/3 of glue in the mound, this was the same glue used for petrography. The mounds with the glue would then dry over night. However it was important to mark the samples correctly, so one would not mix them with each other. It is therefore vice to write the sample name with a diamond pen on the mound, hence when polishing the sample name will maintain. These mounds will then be used in the SEM (Scanning Electron Microscope).

Before analyzing the samples (mounds) in the SEM with the Cathodoluminescence (CL) detector and BSE images combined with EDS, I had to polish the mounds with a machine called Struers, Terga Force -5 and Terga Doser –5. Two different cloths "Pan" and "Nap" was needed to polish the samples, where Pan polished the samples for 3 micron, and Nap for 1 micron. Each sample was polished with both cloths for approximately 5 minutes.

The next step was to coat the samples with a machine called Leica EM SCD 500 where each sample was coated with carbon. When the coating was done, the samples were ready for further process: the SEM and CL detector. With a SEM the sample can be observed using a BSE detector and the EDS detector measures semi-quantitative chemistry of the minerals to facilitate its identification. The CL detector analysis was compared with backscatter electron images of the same samples, at 20 kV. EDAX Genesis software was used on a Zeiss Supa 35 VP machine (for Figures of equipment and methodology, see appendix B).

2.3 GEOCHEMISTRY INCLUDING RARE EARTH ELEMENTS

For geochemical analysis I had 59 samples from the long section (first outcrop, CA), and 13 samples from the second outcrop (CAN), which were going to be analyzed and therefore needed to be prepared- and milled in the milling machine. I needed 10 grams of each sample for geochemistry results and 10 grams of each sample for TOC results. The milling machine milled the rock into finest mesh. Milled samples were sent to Canada for geochemical analysis.

The milling machine was manufactured by Retsch (Retsch RS 200). The program was set on manual operation, with the speed on 700 rpm. In between every rock sample that I milled, I had to clean all the instrument I used with acetone. It was very important that everything was clean so the tests would be as accurate as possible.

Before starting to mill I needed to clean all the equipment. Then I hammered the sample into smaller pieces, so there were smaller rocks pieces in the bowl, which was to be placed in the milling machine. I milled the samples in the milling machine until I could not feel any grains and the sample was very fine- grained mesh, like dust (for Figures of the equipment, see appendix B).

3.0 Results

3.1 PETROGRAPHY IN LIGHT MICROSCOPY AND SEM

A total of three thin sections were studied with light microscopy:

Sample CA 25

From the light microscope one can observe that it is clearly a mudrock. Where quartz, mica, and feldspar occur, as well as a zircon. Observable is also crenulation hence the rocks are strongly deformed.

Sample CA 39

Quartz, pyrite, organic shell fragments and traces of pore can be observed in this fine-grained rock. However this sample is composed mostly of quartz with few grains of muscovite, biotite and feldspar. Quartz grains are rounded to angular and up to 40 micrometer in diameter. Matrix is abundant and makes up c. 80 % of the sample. However, heavy minerals are found in-between these minerals and consisted of 64 % pyrite (Figure 4), monazite, rutile, with few apatite grains.

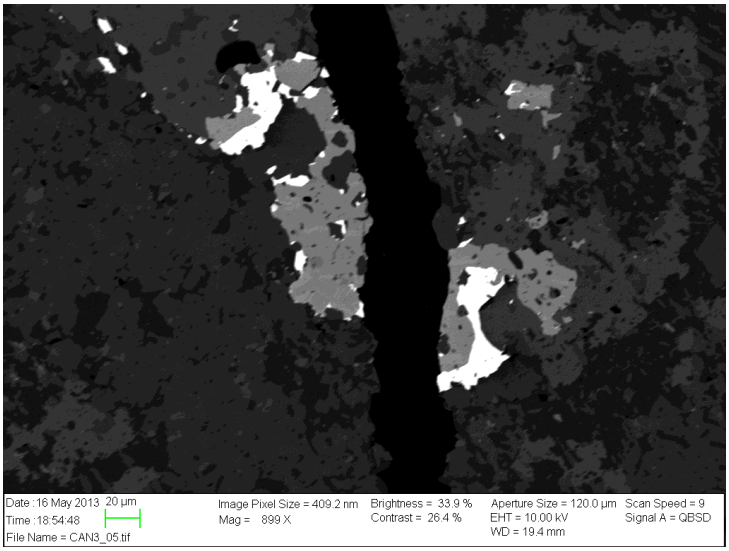

Figure 4: A crack divides this mineral in two pieces; the grey is pyrite while the white grain is Pb.

Sample CAN 3

Sample CAN 3 from the second Cancañiri Formation show a more variety of mineral- grains in the rock, and less abundant matrix c. 60 to 70 %. The matrix is composed of quartz, feldspar, muscovite and biotite (mica). However the quartz grains in this thin section is larger than for CA 39, here the grains are mostly well rounded to angular in shape and up to 500 micrometer in diameter, however poorly sorted grains. The overall grains are larger in this thin section, than for CA 39. Where one can observe big quartz grains, most of the quartz is not ondulose derived therefore from non-metamorphic sources. However in smaller lithoclast two different metasedimentary rock fragments have been observed, which allows to model a multiple recycling for the detritus. The abundant chlorite comes from a mafic source rock material or is a

weathering product after deposition of numerous minerals derived from mafic rocks, like gabbros etc. Heavy minerals are found in this rock as well, in-between the matrix, where 38 % were pyrite, 30 % zircon (where zonation are observed, Figure 5 and Figure 6), however also apatite and rutile where observed, (for Figures of the microscope and petrography, see appendix B).

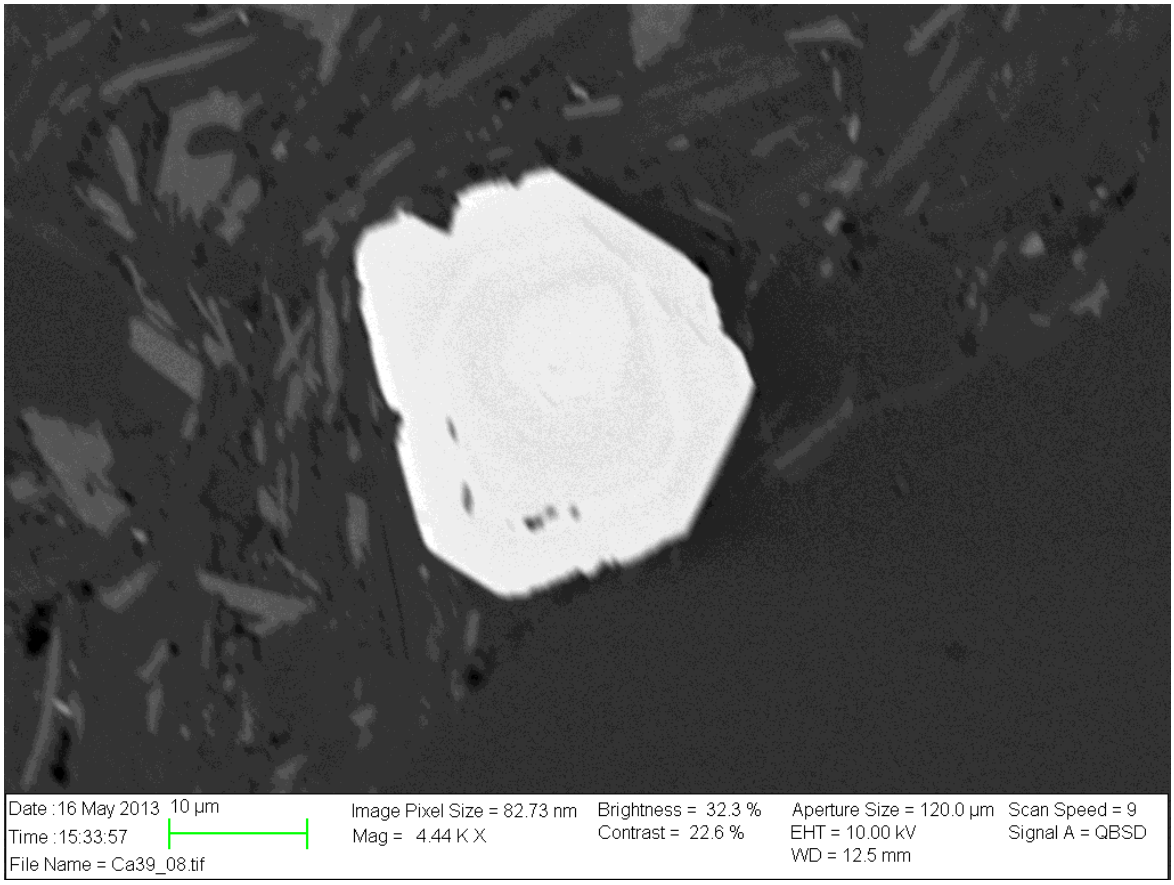

Figure 5: Well rounded zircon.

Figure 6: Zonations in this rounded zircon (same as above), taken with the CL detector.

3.1.1 Implication of the petrography results

When one compare both petrography samples it seems like the CA 39 has overall smaller grains than CAN 3. Both rocks show rounded to angular gains, however the quartz grains for the CAN 3 can be up to 500 micrometer in diameter and are well rounded. CAN 3 have overall rounder grains than CA 39, which however, has more angular once. The quartz grains for CA 39 are only up to 40 micrometer, and have much finer grains and are most likely shale. There is therefore

more matrix in CA 39 than CAN 3. Heavy minerals can be found in both rocks. However, slightly more heavy mineral grains are seen and found in the CAN 3 sample.

As one can see, the Cancañiri Formation is well sorted, and consists of mainly quartz, but also with some mica and feldspar, and lithoclasts derived from schist and metasiltstone. Some rutile and zircon were found as well. Due to the fine sorting and round grains, either the environmental area allowed reworking or the source rocks contain already recycled material.

3.2 HEAVY MINERAL FRACTION

The heavy minerals analyses from the samples CA 24, CA 31 and CAN will be described below, starting with the Apatite fraction (unmagnetic grain with a specific density between 2.75 and 3.3 g/cm^3), further the Magnetic fraction (magnetic minerals with a specific density above 2.75 g/cm^3) and finally the Zircon fraction with the highest specific density (>3.3 g/cm^3). All samples are analyzed in a SEM under BSE conditions and with a CL detector. The semi-quantitative chemistry has been measured with an EDS.

3.2.1 Sample CA 24

3.2.1.1 Apatite fraction

As this sample was from apatite fractions one should expect to find some apatite grains in this sample, I found one among 65 measured grains.

This sample is dominated by pyrite (93.8 %). However, the Pyrite grains occur rarely alone (4.6 %), the most often rock fragment in conjunction with the pyrite is muscovite (in 64.6 % of the cases). Rutile intergrowth with muscovite also occurs in 4.6 % of the 65 measured cases. Feldspar, biotite and quartz are other minerals, which are as well intergrown with pyrite to gain the necessary density. One zircon was as well found within muscovite. This shows the fine-grained character of the sample.

Pyrite

The pyrite ranging from 2 to 20 micrometer in diameter, as rounded to sub rounded grains, indicating less transported grains, but transported. This implies that pyrite was transported under anoxic conditions as anoxic environment destroys quickly the mineral. In all Figures pyrite is the white fragments while the grey is usually muscovite or other intergrown minerals (as described above).

Apatite

One single apatite grain was observed in this sample (where a total of 65 grains where measured, Figure 7). The shape was angular, indicating that is has not traveled far from its source.

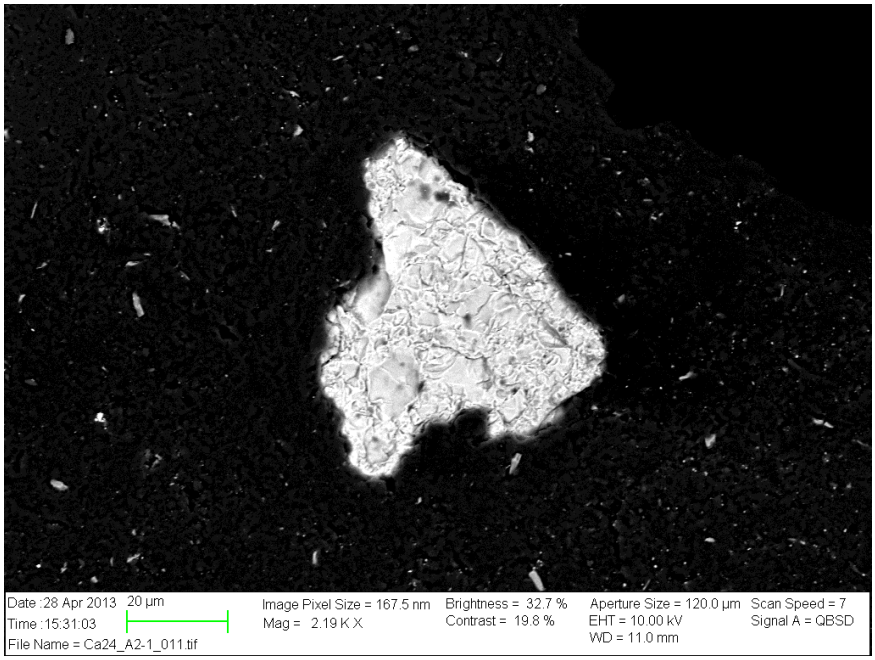

Figure 7: One single apatite fraction in this sample.

Other minerals

Other minerals found where zircon and rutile. The zircon in this sample did not show any zonation, and was intergrown with other minerals to reduce the specific density, Figure 8 and Figure 9. Rutile occurs as impurities in mica and is mostly intergrown and not a single grain.

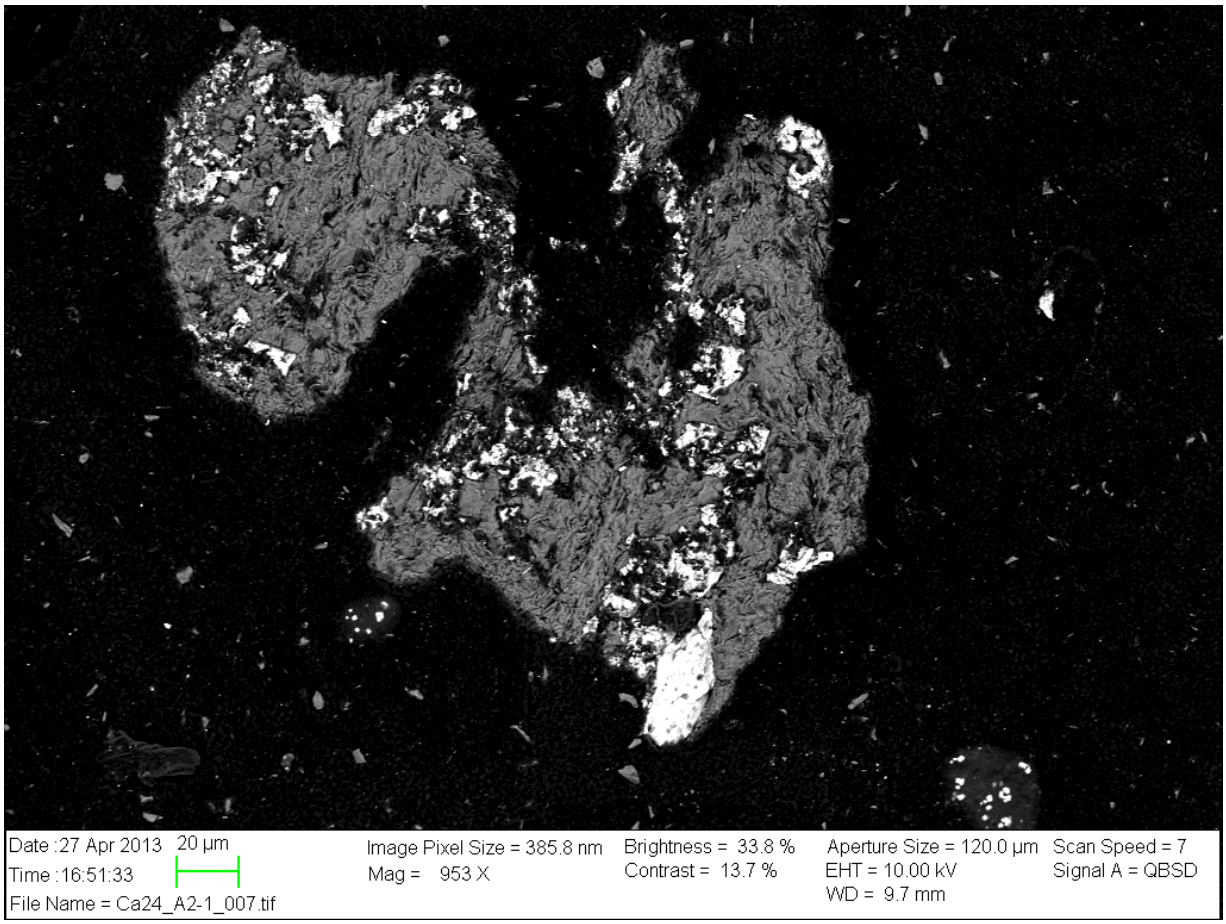

Figure 8: Dark gray: muscovite, while the big white angular grain in the middle is zircon and all other white fragments are pyrite.

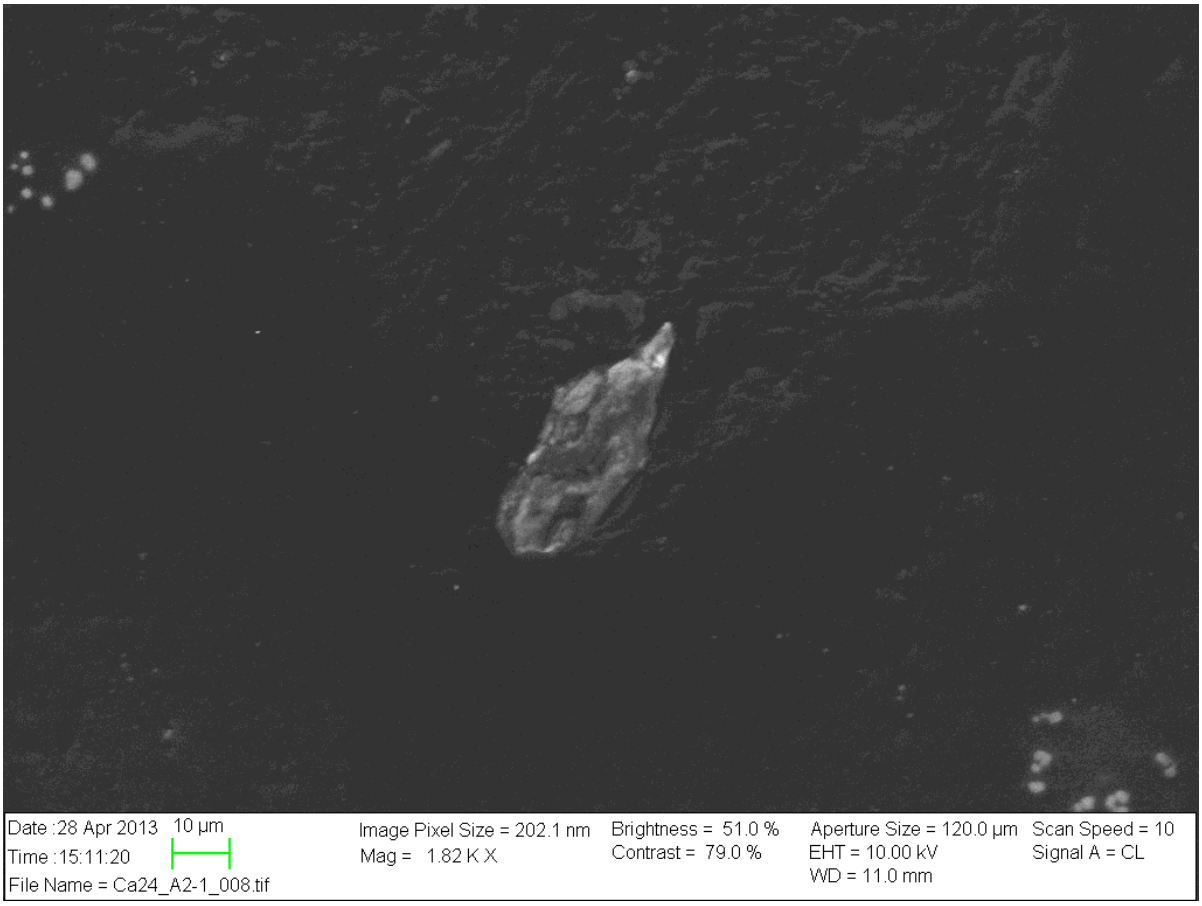

Figure 9: Zircon fragment of the same sample as above, taken with the CL detector.

3.2.1.2 Magnetic fraction

146 grains were measured in this magnetic sample. This sample is dominated by pyrite (40 %), however rutile and monazite are shown in smaller amounts. Apatite also occurs, as well as ilmenite. All the heavy minerals operate seldom alone, often with intergrown minerals like muscovite, biotite and quartz. The minerals differ in size and shape, from well rounded to more angular, indicating two different sources, one transported further than the other.

Pyrite

The pyrite ranging from 5 to 60 micrometer in diameter, also here rounded to sub rounded grains, Figure 10. However a more squared pyrite grain is also observed (Figure 11), this can indicate that the grain was close to the source when it deposited or even grow post-depositional.

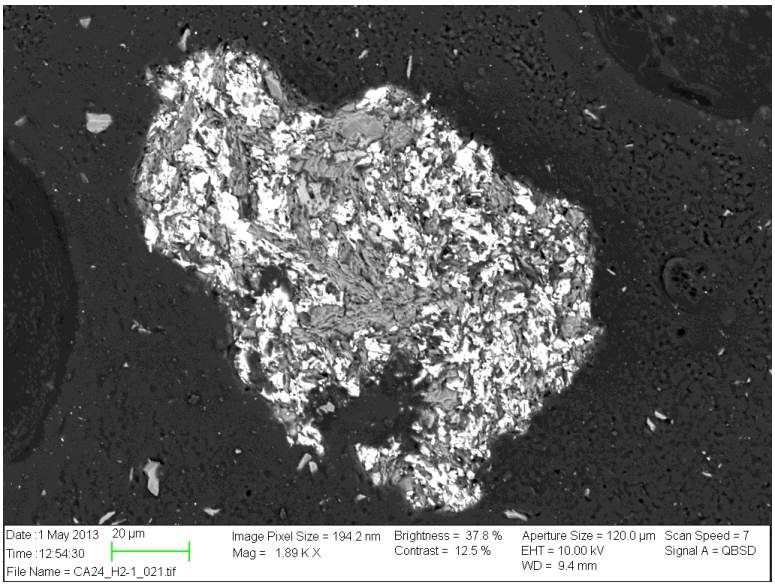

Figure 10: Framboise pyrite (white) in muscovite (grey).

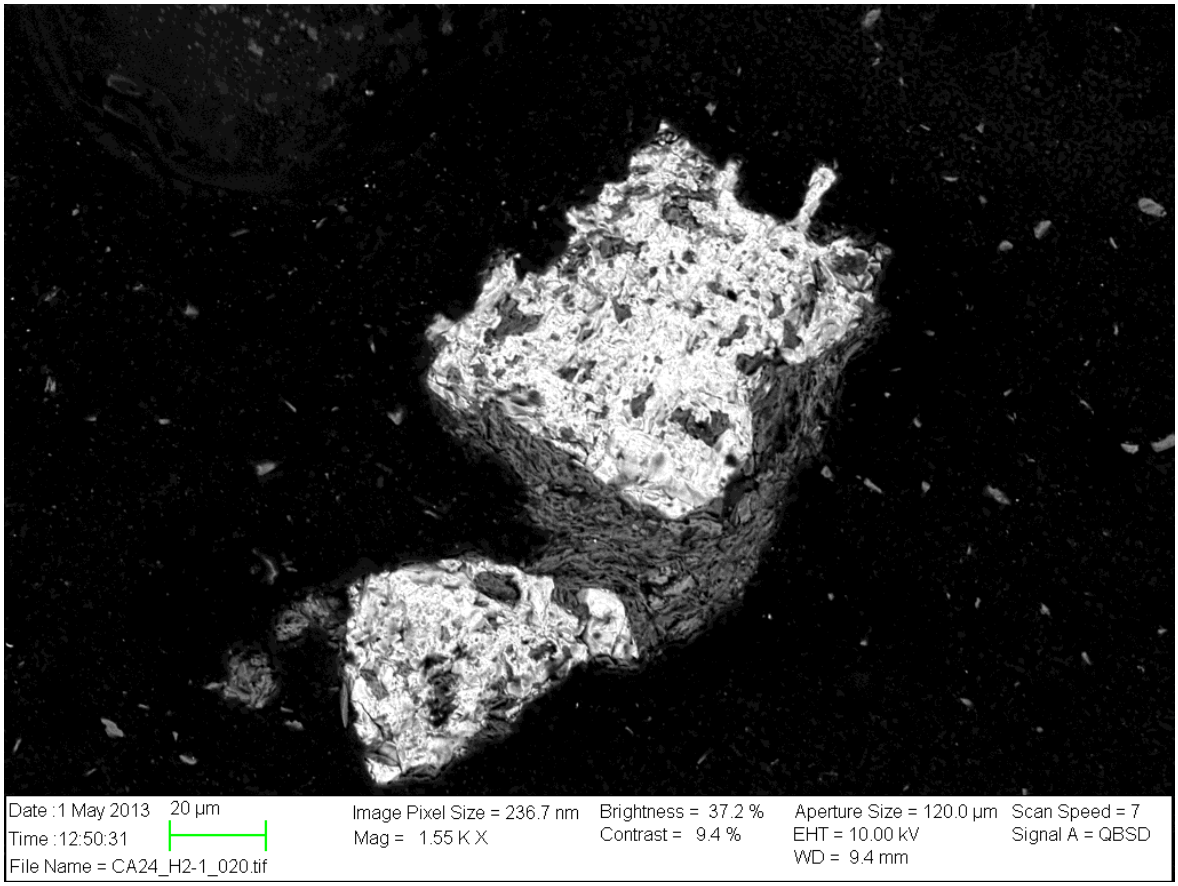

Figure 11: Squared pyrite (white) in muscovite (grey).

Other minerals

Other minerals found where elongated ilmenite (30 micrometer wide) and titianite (15 micrometer wide) Figure 12, well rounded rutile (Figure 13) and sub rounded to rounded apatite (20 micro meter in diameter).

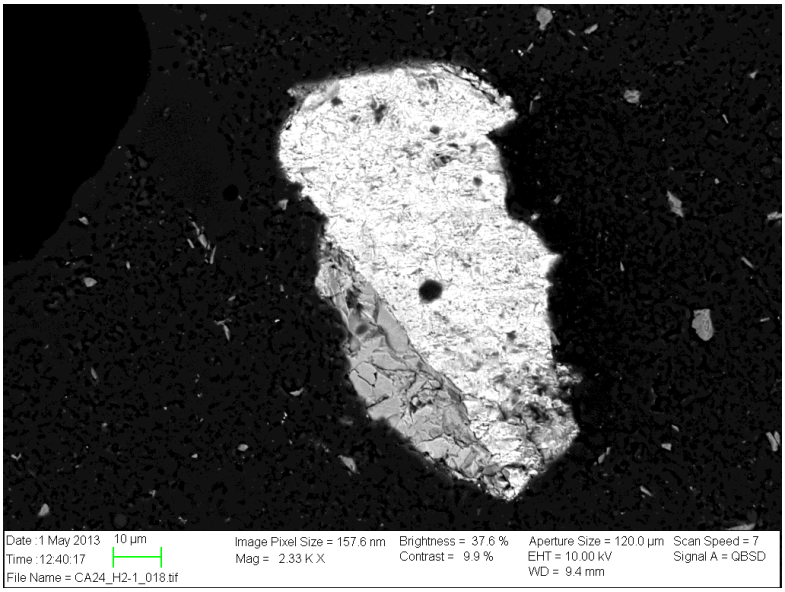

Figure 12: Ilmenite (white) and titanite (grey).

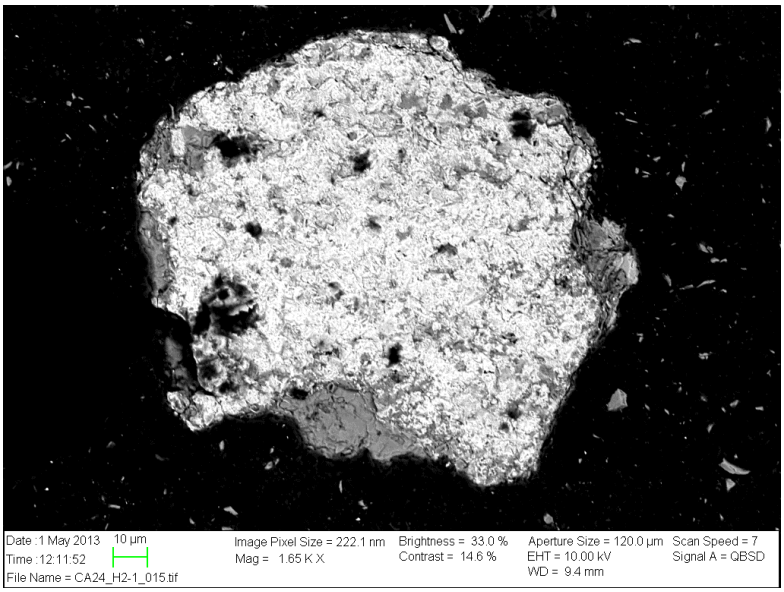

Figure 13: Rutile (white) in muscovite (grey).

3.2.1.3 Zircon Fraction

Zircon and pyrite dominate this sample with 60 % and 40 %, respectively, where a total of 119 grains were measured. The Zircon, and pyrite occurs alone in some causes, however also in quartz and mica (biotite and muscovite). Some rutile where also observed however with associated minerals as mica.

Zircon

The Zircon grains ranging from 20 micrometer to 100 micrometer in diameter and are relatively angular, however well rounded zircons are also observed. This indicates two types of sources, one transported further than the other. Some zonation can be seen in this sample.

Pyrite

Pyrite for this sample is more angular in shape and varies from 20 micrometer to 100 micrometer in diameter, indicating that the source is closer, (Figure 14).

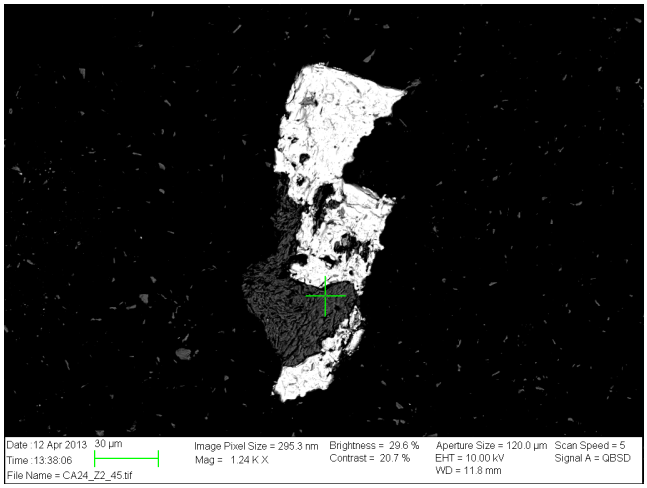

Figure 14: Pyrite (white) with mica (dark gray), seen with the BSE detector.

Rutile

The rutiles in this sample are well rounded with a range of 20 to 60 micrometer in diameter, and 30 to 80 micrometer long, Figure 15.

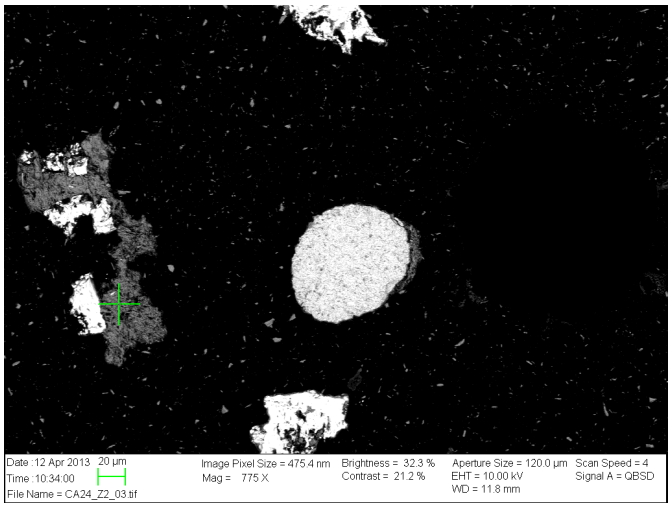

Figure 15: The rounded grain is a single rutile (in the middle of the figure), while the dark mineral to the left of the rutile (green cross, grey) is feldspar and pyrite in white. The two other white minerals above and below the rutile are also pyrite.

3.2.2 Sample CA 31

3.2.2.1 Apatite fraction

The apatite sample from CA 31 consisted of 70 % pyrite with intergrown minerals like quartz, mica (biotite and muscovite), and feldspar. Apatite was found as a single grain in 4% of the studied grains, 134 in total, however also as inclusions in quartz and mica. Rutile, hornblende and chromite were found as well. All grains differs in shape and size, some are well rounded others angular, indicating different sources, one closer than others in regard of the depositional area.

Pyrite

In this sample the pyrite grains were more angular and elongated in shape than in other samples. However round and squared grains also do occur ranging from 5 to 50 micrometer in diameter. The smaller pyrite grains are more rounded than the bigger grains, indicating a longer transportation or a denser transport medium causing more frequent grain-grain collision to grind the components more rapid.

Apatite

The apatite grains were rounded to sub rounded in shape, and ranging from 20 to 40 micrometer in size. Accompanied mostly by pyrite (Figure 16) and quartz (Figure 17), however it appears also as single-grain.

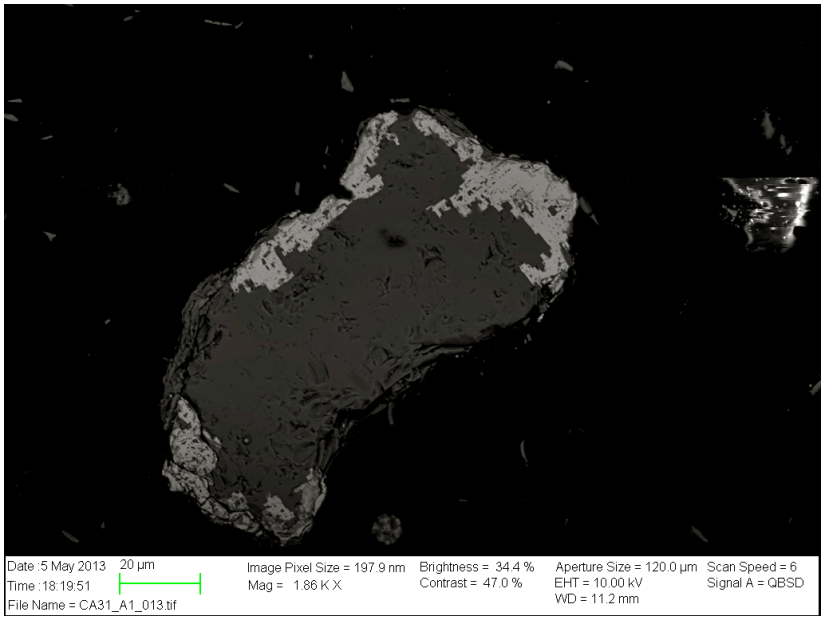

Figure 16: Pyrite (light gray) accompanied with apatite (dark gray).

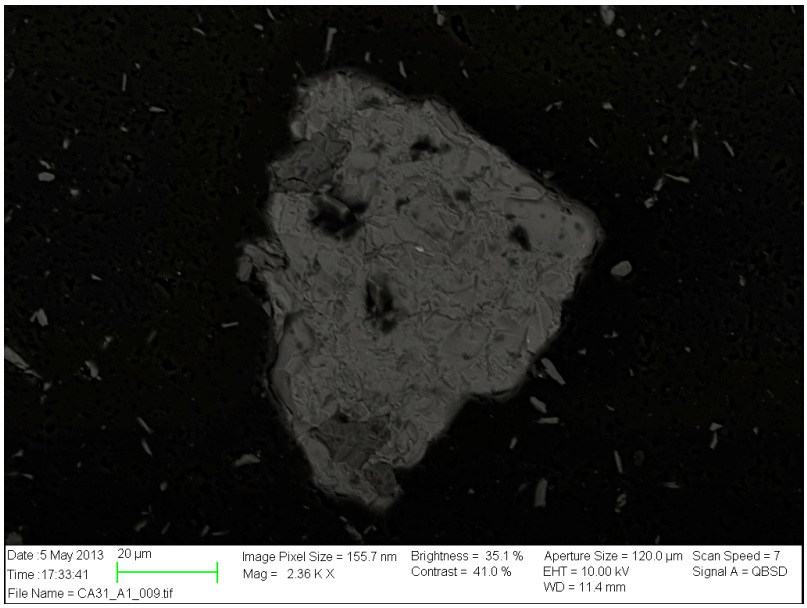

Figure 17: Quartz in dark gray, while the surrounding gray and white is apatite.

Other minerals

Other minerals found where hornblende, chromite and well-rounded rutiles often with intergrown minerals like quartz or muscovite, 20 to 30 micrometer in diameter, Figure 18.

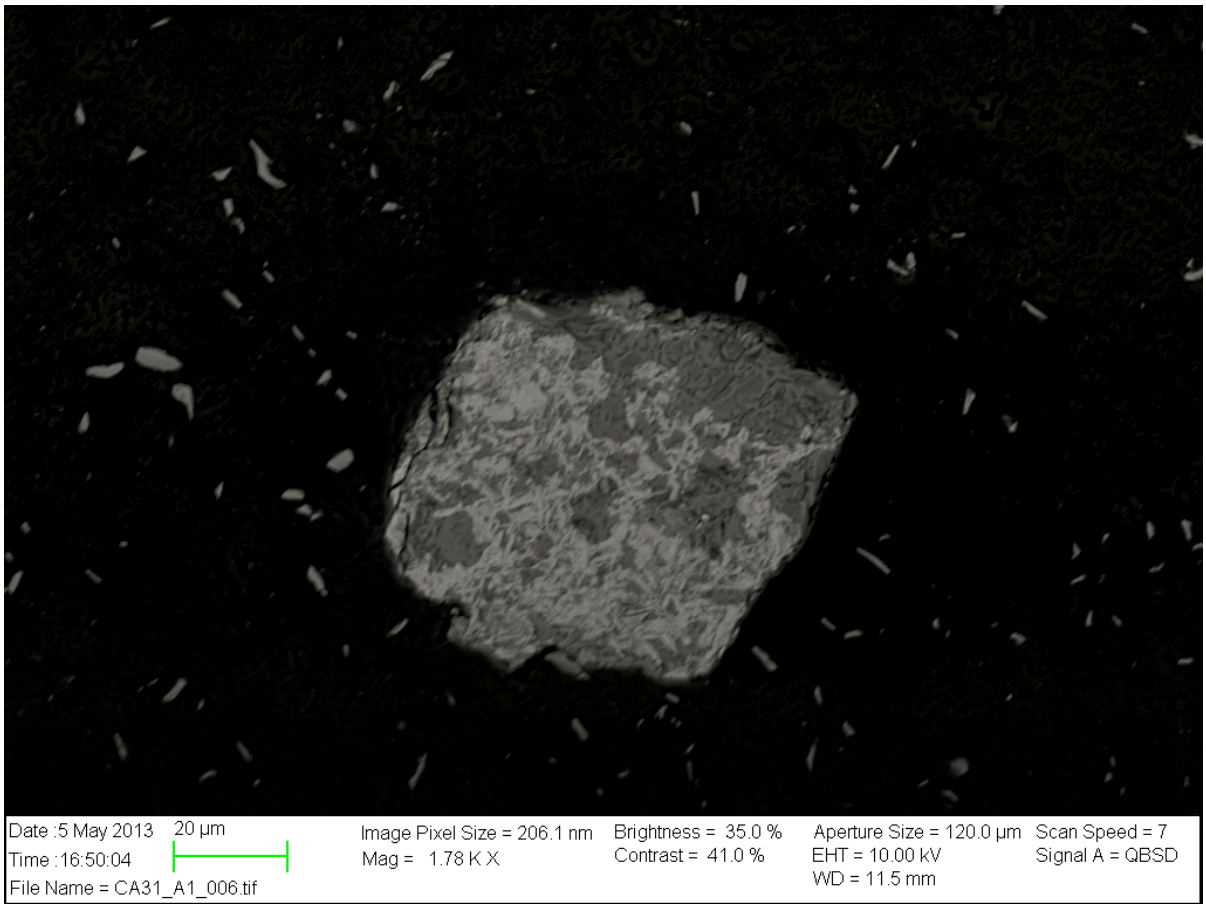

Figure 18: Rutile (light grey) and quartz (dark grey).

3.2.2.2 Magnetic fraction

Magnetic fraction of CA 31 is dominated by pyrite in lithoclasts with muscovite (mica), feldspar and quartz in 90 % of the total 253 measured grains. Some apatite, zircon, rutile and ilmenite are also found in smaller amounts 10 %. The minerals differ in size from well rounded (rutile and zircon) to more angular and elongated (apatite), however some pyrites are squared.

Pyrite

Pyrite in this sample ranging from 10 to 20 micrometer, rounded to angular in shape, a squared pyrite is also observed. The pyrite operates seldom alone (10 %), and in most of the cases here pyrite is intergrown with muscovite or quartz. Again the shape indicates different sources of material, where one has been transported further than the other.

Other minerals

Other minerals found where well-rounded zircons approximately 30 micrometer in diameter, where some zonation can be observed from the CL detector, (Figure 19). However, magnetic zircons are mostly metamict and should not show intensive zonation. Apatite is rare and small (i.e. 40 micrometer in diameter), and intergrown with muscovite which is the most abundant variation found in this sample. However, some of the grains were found with intergrown minerals as feldspar, biotite or quartz.

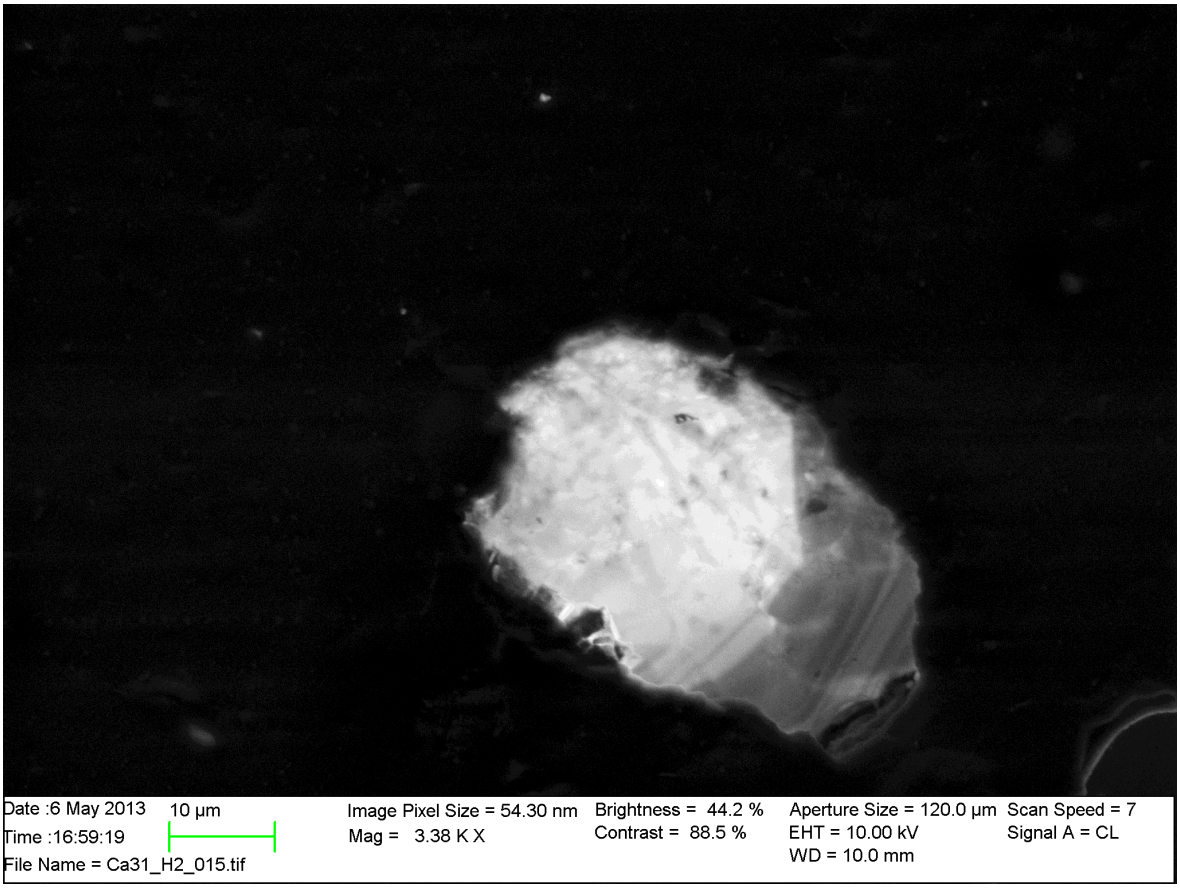

Figure 19: Zircon. One can observe zonation down to the right, taken by the CL detector.

3.2.2.3 Zircon fraction

Zircon fraction of CA 31 is as well dominated by pyrite in 90 % of the cases (were 258 grains were measured), as the rest of the CA 31 fractions (apatite and magnetic fraction). The pyrite is intergrown with muscovite, biotite (mica) or quartz (50 % of the cases), in 40 % of the cases the pyrite occurs alone. All grains have different shapes and forms, from angular, squared, to elongated or well rounded. Zircon, apatite and rutile are observed in smaller amounts (10 %).

Pyrite

The pyrite differs in size and shape, from small well rounded grains to larger elongated and angular once, ranging from 5 to 80 micrometers in diameter. As said above, the intergrown minerals with pyrite is mostly quartz or mica. Based on the shape and form of the grains the sources are different. Squared minerals might be post-depositional while well-rounded grains have been transported. This transport had to be necessarily under anoxic condition.

Other minerals

Other minerals found in this sample were small well-rounded zircons (10 to 20 micrometer in diameter), well-rounded rutiles (i.e. 50 micro meter in diameter), apatite and ilmenite. Also in these grains, minerals like mica and quartz are found, however they also occur as single-grains in some cases (3 %).

3.2.3 Sample CAN

3.2.3.1 Apatite fraction

This succession represents the Cancañiri Formation in a different exposure (CAN) (see Figures in appendix A) and its heavy minerals in the apatite fraction consist mainly of quartz (60 %) with other fragments. Heavy minerals as rutile, zircon, pyrite and apatite were found in 15 to 20 % of the determined grains (a total of 277 grains were measured). Intergrown minerals with the heavy minerals are muscovite or biotite (mica), quartz and feldspar. The shape and form differs from well rounded to elongated, however also angular.

Zircon

Most of the zircons are well-rounded 30 to 60 micrometer in diameter, however elongated zircons are also found 10 to 20 micrometer wide and 20 to 50 micrometer long. In Figure 20, a rare squared one is shown. The different shape can indicate different sources and/or different sedimentation mechanisms.

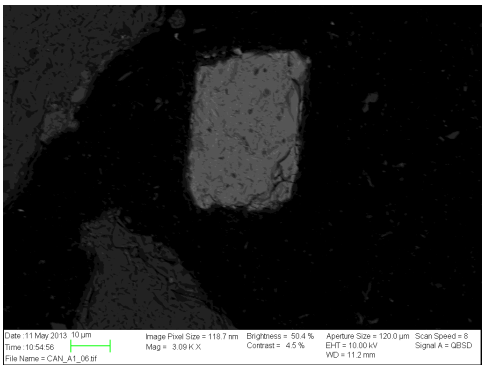

Figure 20: Squared zircon.

Apatite

Most abundant are apatite grains with shape variations from sub-rounded to rounded 30 to 50 micrometer in diameter, and only few more elongated grains are observed, 20 micrometer wide and 30 to 40 micrometer long. Again different source rock material can be implied.

Rutile

Rutiles are observed as squared minerals, angular to rounded or sub rounded i.e. 20 micrometer in diameter, often with intergrown quartz.

Other minerals

Other minerals found in this sample were pyrite 10 to 20 micrometer in diameter, hematite, with intergrown minerals like quartz, feldspar and mica. All grains differ in size and shape indicating different sources of material.

3.2.3.2 Magnetic fraction

This sample consisted of rutile in 65 % of the cases, 20 % zircon and 10 % pyrite, with intergrown minerals as mica, quartz and feldspar. 222 grains in total were measured in this sample. Other minerals found were apatite, hematite and gypsum in 5 % of the 222 incidences. Many of the grains where well rounded however some angular and elongated were also observed, indicating different sources.

Rutile

Rutiles where often intergrown with quartz however, also in mica or alone, as rounded grains (diameter 20 to 45 micrometer), Figure 21. Elongated rutile grains are c. 20 micrometer wide and 50 micrometer long. Based on the different shapes and form this sample indicates at least two different sources.

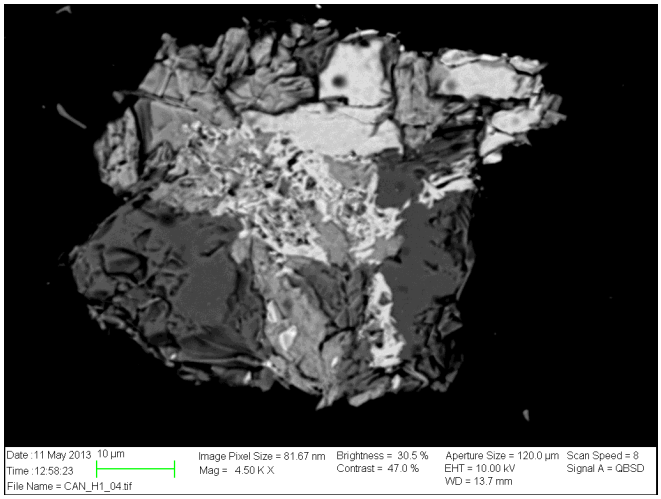

Figure 21: Dark grey: quartz, light grey: rutile, mixed: mica.

Zircon

Zircons are in its shape squared or elongated but also commonly rounded as a single grain or in a small lithoclast. Well-rounded zircons ranging from 30 to 40 micrometer in diameter, while more elongated grains ranging from 10 to 20 micrometer wide and 30 to 40 micrometer long. Again the form might indicate different sources. Zonation can be observed form the CL detector (Figure 22).

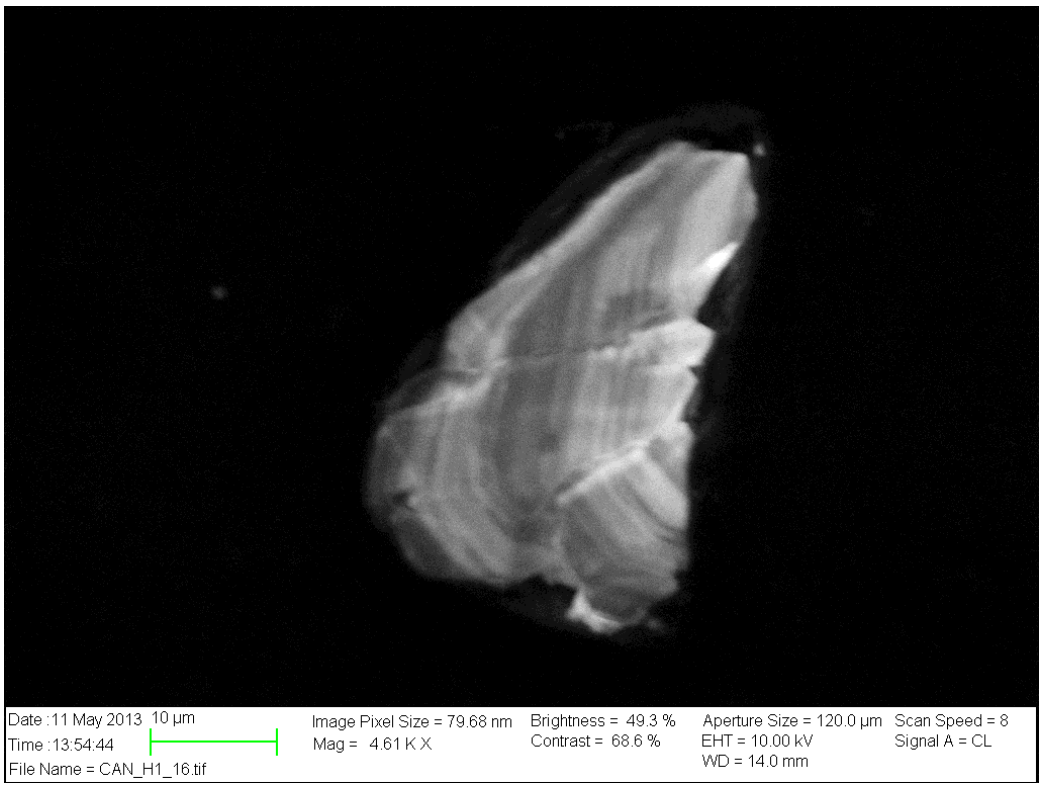

Figure 22: From this zircon one can clearly recognize zonation by the use of the CL detector and see that the original grain was very large.

Pyrite

Pyrite is often found with intergrown minerals as quartz or mica, sub rounded to rounded. Compared to the other samples the pyrite here can be large, up to 200 micrometer in diameter, however angular and elongated pyrite are also observed i.e. 40 to 60 micrometer wide and 80 to 100 micrometer long, which are more a common size for the pyrites related to the other samples. The large grains may indicate that the source is close or that large quantities of S and Fe had been available if this grain type is secondary.

Other minerals

Besides apatite, gypsym and Nb-rich rutile, few grains of hematite (Figure 23) could be identified.

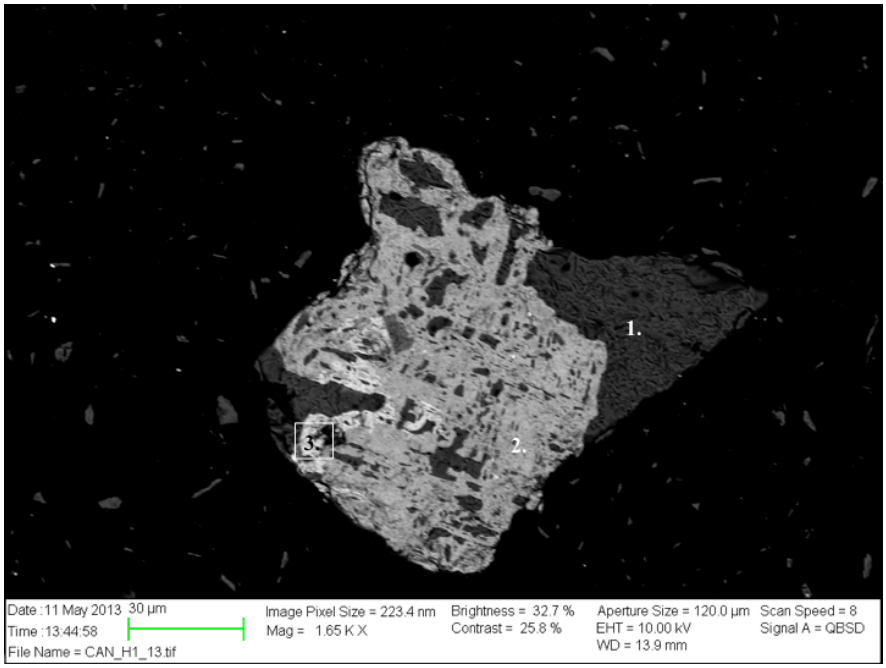

Figure 23: 1. Quartz, 2. Hematite, 3. Pyrite.

3.2.3.3 Zircon fraction

This zircon sample was dominated by zircons, as expected, in 80 % of the measured grains (506 in total). However, rutile (15 %) and pyrite (3 %) were also observed, intergrown and occurring in lithoclasts with quartz, mica and feldspar (2 %). All grains vary in form and shape from well rounded to elongate and angular, indicating different source material.

Zircon

Well-rounded zircons ranging from 30 to 70 micrometer in diameter, squared and angular zircons as well as elongated are also observed 20 to 40 micrometer wide and up to 80 micrometer long, as well indicating different sources.

Rutile

Rutiles vary in shape and form from rounded to elongated and angular, ranging from 20 to 40 micrometer wide and up to 70 micrometer long, for rounded grains the diameter ranges from 10 to 20 micrometer.

Other minerals

Pyrite in this sample occurs as larger grains compared to all other mineral grains, although few smaller grains have been identified. Elongated grains ranges from 50 to 60 micrometer wide, up to 120 micrometer long. The ranges in diameter are 40 to 50 micrometer for more rounded grains. Hematite where also observed together with the pyrite as can be seen in Figure 24 below.

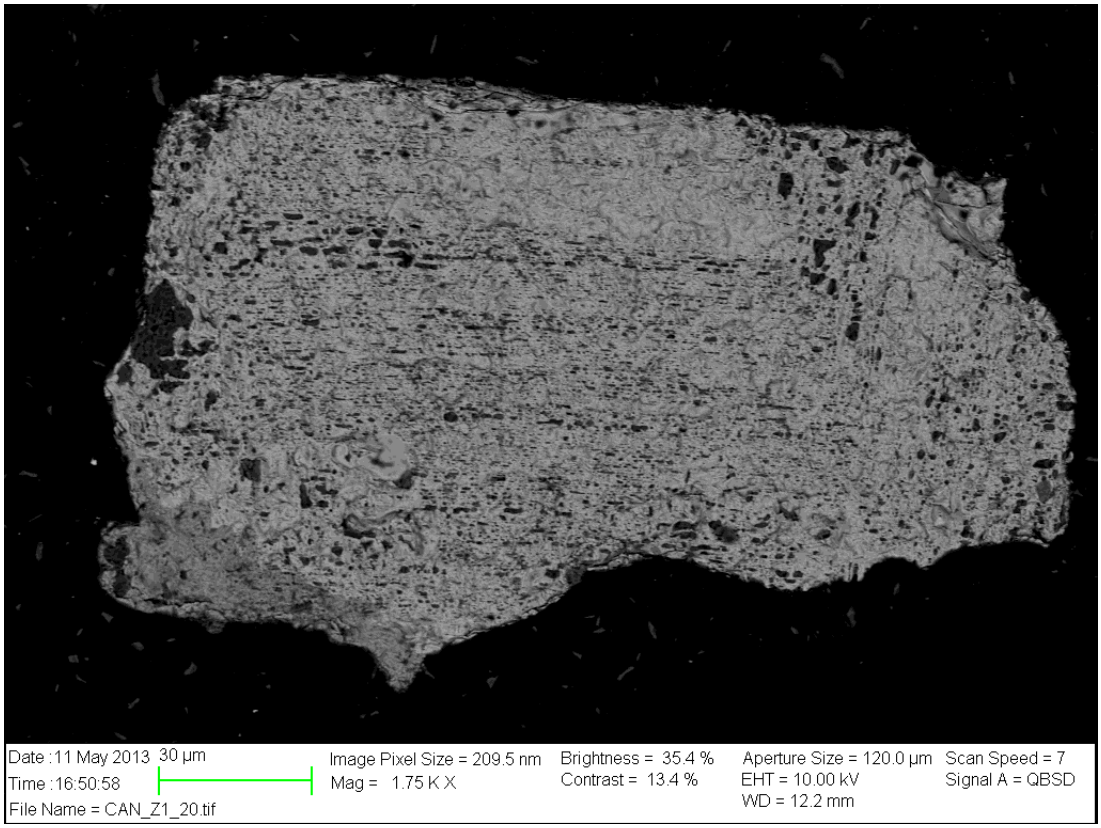

Figure 24: Large pyrite (light grey), with hematite (grey bottom left corner) and feldspar and mica (dark grey).

3.2.4 Implication of the heavy mineral data

CA 24 consists of mainly pyrite 70 %, with some input of zircon 20 %, rutile and apatite. Some intergrown minerals like biotite, muscovite, quartz, hematite occur in smaller detail 10 %. The huge amount of pyrite indicates anoxic condition, where organic carbon content is preserved up to 0.63 %. Since there are different shapes and sizes of heavy minerals one can suspect that the detritus came from different sources.

CA 31 dominates and consists of 80 to 85 % pyrite, the rest is mostly zircon, apatite and rutile. However, i.e. hematite, ilmenite and pyrope are found alone or within the other minerals. The intergrown minerals are dominated by muscovite, biotite (mica) or quartz. CA 31 compared to CA 24 are more or less the same, however slightly more pyrite is discovered in CA 31. Anoxic conditions can therefore be revealed in this sample as well, as not all pyrites are rounded but angular. Different shape and form are observed, from well rounded (travelled further) to more angular and elongated (close to source), indicating different sources, some closer than others.

CAN

One can clearly see a difference of the two Cancañiri outcrops, CA 24 and CA 31 samples compared to the CAN samples. CA consisted mainly of pyrite, while the grains in the CAN Formation had a lot of variety, with zircons, rutiles, apatite and pyrite occurring the most. However the shape and form of the grains are more or less the same for CA and CAN, some are well rounded others more elongated or angular, all these shapes and form indicates different sources, some closer than the other. Since the pyrite grains in the CAN formation are larger than for CA, this might indicate that the source for the pyrite in this case is closer than for CA. Table 2 below shows the summary of the heavy minerals analysis. For more Figures from the heavy minerals analysis and the chemical composition of the minerals see appendix C.

Formation	Fraction	Mineral (%, size, form)	Mineral (%, size, form)	Mineral (%, size, form)	Others
Cancañiri (CA 24)	Apatite	Pyrite (94 %, 2-20 µm, sub rounded)	Rutile (4.6 %, 2-20 µm, rounded)	Apatite (1.5 %, 25 µm, angular)	Zircon
	Magnetic	Pyrite (40 %, 5-60 µm, sub rounded)	Rutile (13 %, >80 µm, rounded)	Monazite (13 %, 20-30 µm, angular)	Ilmenite, titanite, apatite, zircon
	Zircon	Zircon (60 %, 20 -100 µm, rounded to angular)	Pyrite (40 %, 20 - 100 µm, angular)	Rutile (2.4 %, 50 -60 µm, rounded)	None
Cancañiri (CA 31)	Apatite	Pyrite (70 %, 5-50 µm, rounded to angular)	Apatite (4 %, 20-40 µm, rounded)	Rutile (2.5 %, 20-30 µm, rounded)	Hornblende, chromite
	Magnetic	Pyrite (90%, 10-20 µm, rounded to angular)	Rutile (5 %, µm, rounded)	Zircon (3 %, 30 µm, rounded)	Apatite, pyrope, ilmenite
	Zircon	Pyrite (90 %, 5-80 µm, rounded to angular)	Zircon (5 %, 10-20 µm, rounded)	Rutile (1.2 %, 50 µm, rounded)	Apatite
Cancañiri (CAN)	Apatite	Zircon (15 %, 10-50 µm, rounded to elongated)	Rutile (10 %, 20 µm, rounded)	Apatite (9 %, 30-50 µm, rounded to elongated)	Pyrite
	Magnetic	Rutile (65 %, 20-50 µm, rounded to elongated)	Zircon (20 %, 10-40 µm, rounded to elongated/angular)	Pyrite (10 %, >200 µm, rounded to angular)	Apatite, hematite
	Zircon	Zircon (80 %, 30-70 µm, rounded)	Rutile (15 %, 20-40 µm, rounded to angular)	Pyrite (3 %, 20-120 µm, rounded to angular)	Hematite

Table 2: A summary table for the heavy minerals from the SEM analysis, of the two formations and their different fractions.

Department of Petroleum Engineering, University of Stavanger, Ullandhaug, 4036 Stavanger.

3.3 GEOCHEMISTRY

Major element geochemistry

The first exposure (indicated by CA) contains rocks with a slightly lower silica concentration than those from the second outcrop (now named CAN). From table 5, Appendix D one can observe a typical continental crust composition (UCC; after McLennan et al., 2006), where CaO values are relatively low, mostly below 0.5 %, however, some samples show values above 0.5 %. This indicates only a minimal input of calcite and that CaO is mainly stored in plagioclase (for calculated values, see appendix D, Table 6).

3.3.1 Trace elements and Rare Earth Elements (REE)

Composition

A Zr/Ti versus Nb/Y plot (Figure 25) was made to estimate the composition of the sedimentary rocks, as these elements are strongly immobile (Zimmermann and Spalletti 2009). Both formations do fall in the center of the diagram. CA Formation (blue) is concentrated in the lower rhyodazite dazite region, towards an andesite trend or composition. CAN Formation (green) has slightly higher Zi/Ti ratios and indicates a rhyolite and rhyodazite dazite trend or composition. These samples are slightly more felsic. UCC is plotted as a black circle in the middle of the diagram, where the two formations are plotted in the diagram slightly above (CAN), or slightly below (CA), the UCC, indicating a felsic component and a mafic component respectively.

Alternatively, it could be argued that the two formations represent unrecycled detritus, which is not the case, as framework minerals like quartz and heavy minerals are often well rounded. The CAN Formation has the overall highest values in both Zr/Ti, ranging from c. 0.015 to 0.15, and Nb/Y, ranging from 0.15 to 0.8, the CA values for Zr/Ti ranging from approximately 0.013 to 0.12, while the Nb/Y values are from 0.12 -1, as one can see from Figure 25 below.

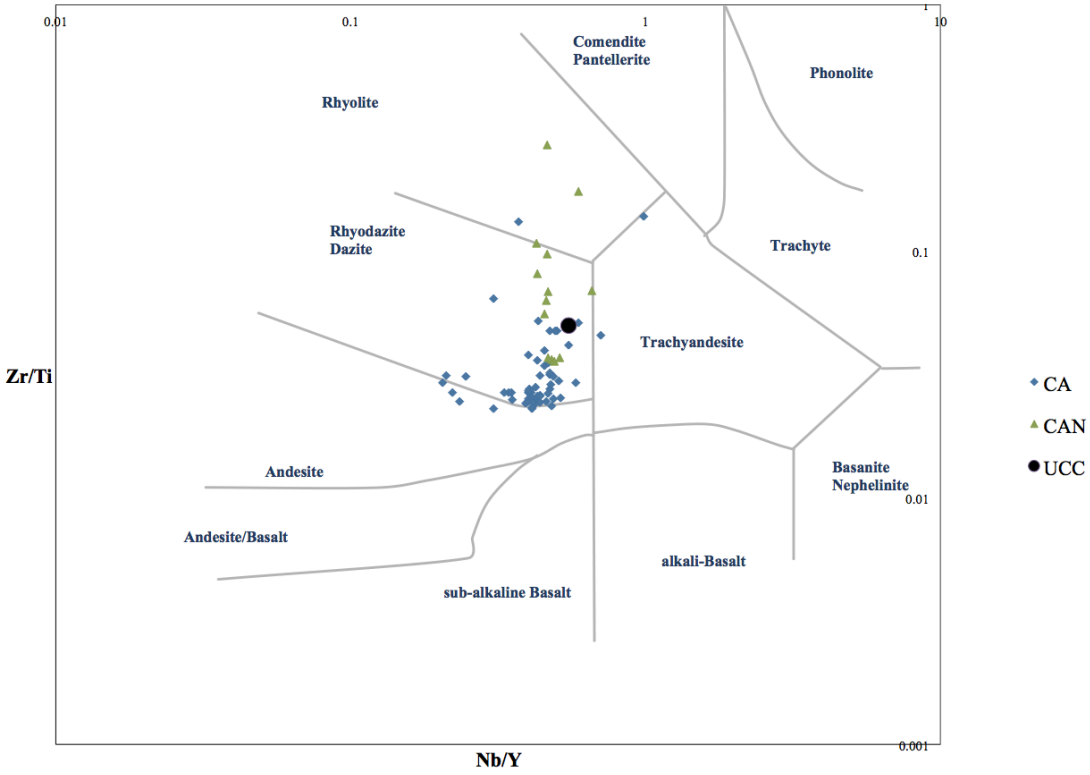

Figure 25: Zr/Ti versus Nb/Y diagram (after Winchester and Floyd., 1977), CA values in blue, CAN vales in green. UCC is after McLennan et al., (2006).

Both formations are slightly enriched compared to UCC in elements like U, P, Cr, Ta, Pb, Zr and Ce, however also Th and Hf. Sr is highly depleted, together with Rb, V, Nb, Ti and Sc which is

only slightly depleted (Figure 26) (Figure 146 in Appendix D shows major trace elements, for all rock samples from both formations). Both formations reflect a typical UCC in most of the elements, and SiO_2, Al_2O_3, Fe_2O_3, CaO, Na_2O, K_2O and TiO are all enriched (Table 5, appendix D).

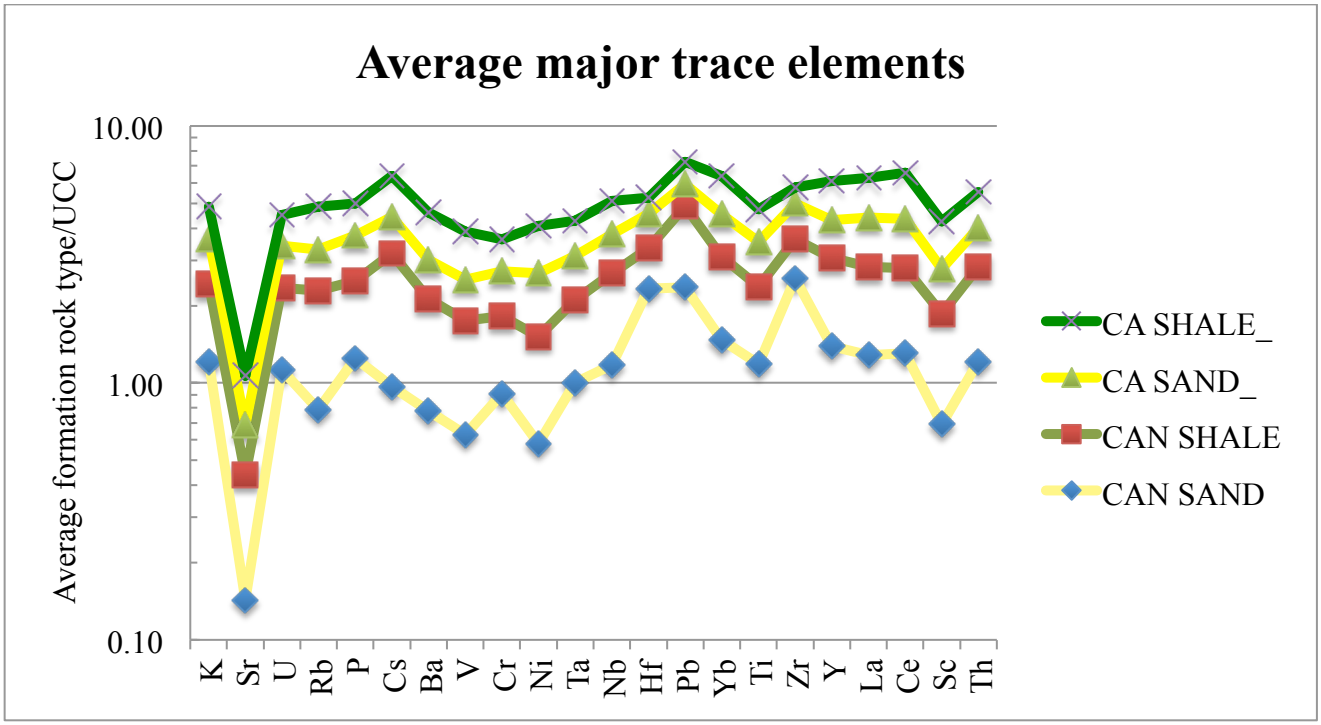

Figure 26: Average major trace elements for both formations.

Some trace elements are useful for provenance analysis due to their insoluble and immobile conditions, Ti, Th, Sc and Zr and REE are some of them, and these elements can preserve the characteristics of the source rock in the sedimentary record and can be robust provenance indicators (Zimmermann and Spalletti., 2009).

Trace elements

By plotting Rare Earth Elements (REE) one can find out the composition of sedimentary rocks. Figure 27 below show the average REE values for each formation normalized to UCC values (for detailed REE- normalized to UCC plot, in both formations, for all samples see appendix D, figure 147). By using this diagram one can see the different trends related to UCC for the two formations. The CA values seem to have significantly higher values than the CAN Fm. Most of the CA samples have high values in Ce, this trend can be seen in nearly all CA samples (appendix D, Figure 115). Five samples starts with values below 1 (CAN 6 and 7, and CA 7, 22, and 33 (appendix D, Figure 147)) all other samples start with values above 1. As one can see from Figure 27 below, the trend and form for the two different formations are more or less the same, however in average the CA samples are enriched in REE.

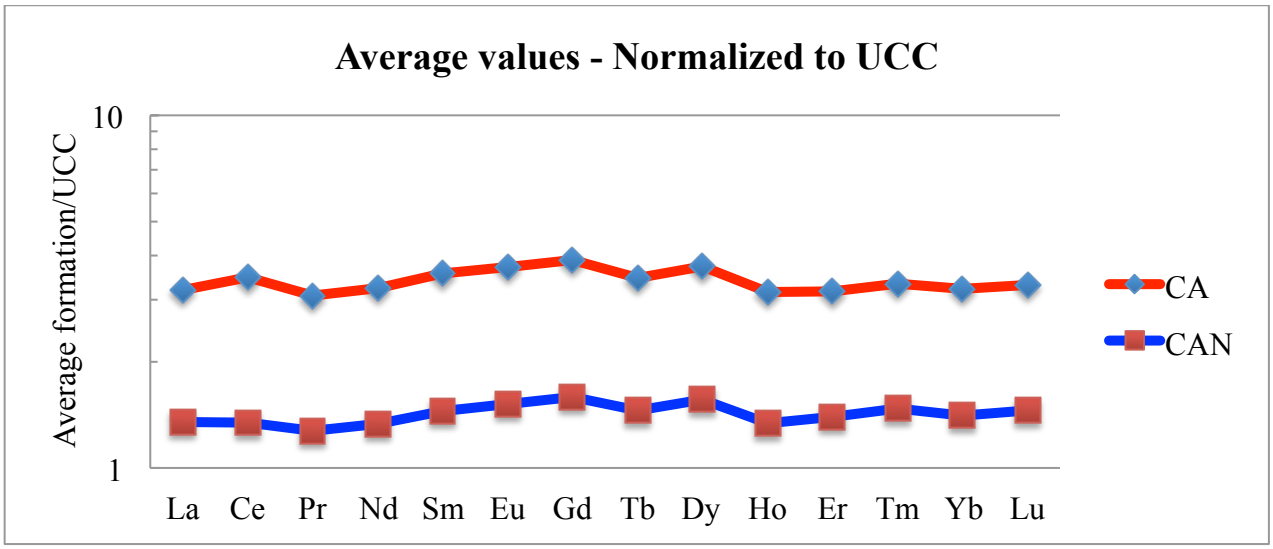

Figure 27: Average REE values for the two Cancañiri Formations (CA in red, and CAN in blue) normalized to UCC (after McLennan et al., 2006).

Figure 28 shows the average REE normalized to chondrite (after Taylor and McLennan., 1985) for the two Cancañiri Formations (CA in red and CAN in blue) (all samples for REE- normalized to chondrite, for both formations are plotted in appendix D, figure 148). For both formations the trend is more or less the same, with lower Eu values (depleted) and higher Gd values (enriched) resulting in a similar shaped pattern. CAN 6 and 7 and CA 7, 22, and 33 are lower than the others (appendix D, figure 148), however the difference is not that much for this diagram. This is a typical REE pattern for modern deep-sea turbidites from a continental arc (McLennan et al., 1990).

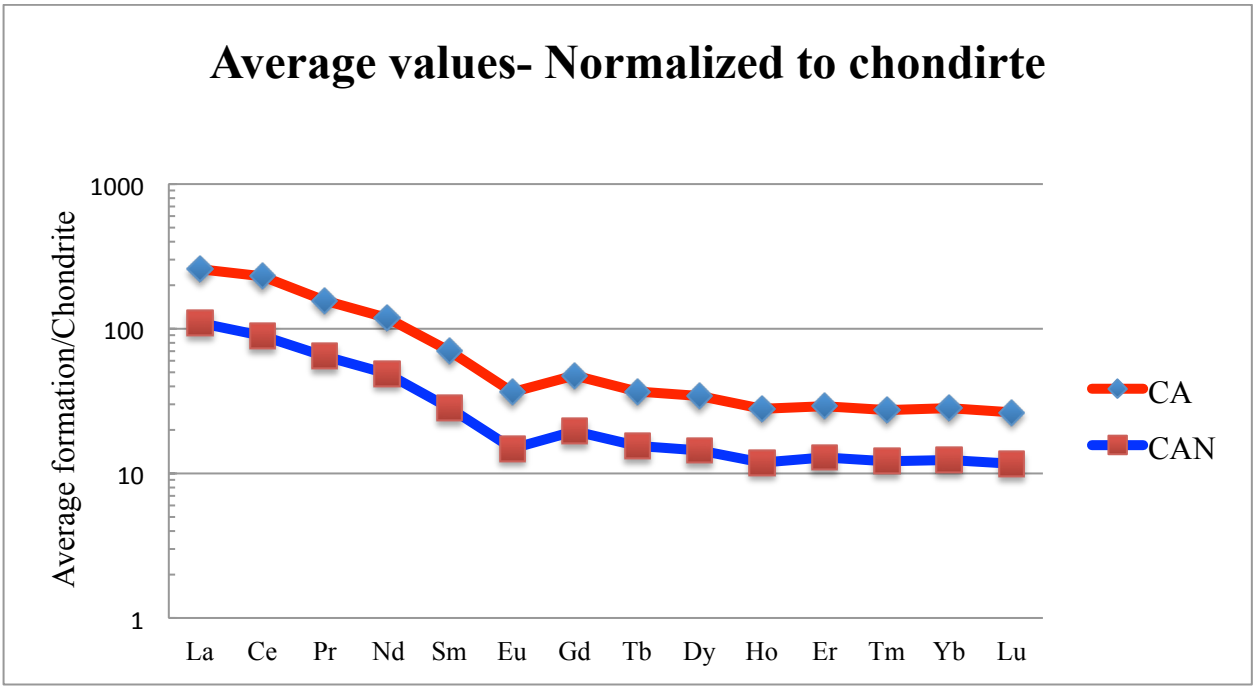

Figure 28: Average values REE- normalized to chondrite (after Taylor and McLennan., 1985). The y-axis indicates rock normalized to chondrite.

Chemical Index of Alteration (CIA)

By calculate the CIA one can measure the degree of chemical weathering. During diagenesis, ratios of major elements and abundances need to be checked for mobility. As long as the bulk composition is not strongly affected by diagenesis, geochemical analysis can be used on sedimentary rocks and can be a valuable tool for provenance studies of matrix-rich sandstones (Zimmeramnn and Bahlburg., 2003).

The mobile oxides in sediments can reflect the alteration of feldspar and volcanic glass to clay minerals, where CIA measures the molecular proportion of Al_2O_3. Petrographical and geochemical composition are affected by sorting, i.e. for sedimentary rocks as heavy minerals, the heavy minerals are rich in high field strength and REE and included in sandstones (Bahlburg et al., 2009).

The CIA values are high and more or less concentrated around the same area and therefore the same trend. The trend indicates an illite trend, which indicates K- addition (Zimmermann et al., 2009, Figure 29). The overall values are ranging approximately between 73 to 81 %, which is highly weathered. Three of the CAN values (yellow, CAN 6, 7 and 10) are shown with lower values (around 70 %, however still significantly weathered). One very low value for the CA sample is also observed (approximately around 40 %, and is the sample CA 33). A reason for this low CA 33 sample might be due to the large amount of CaO, with a value of 11.41 (appendix D, Table 5), which typically lowers the CIA.

The sample is highly reworked and the values for the major elements and the alkalis are very low and therefore prone to error, (for calculated values see Appendix D, table 6).

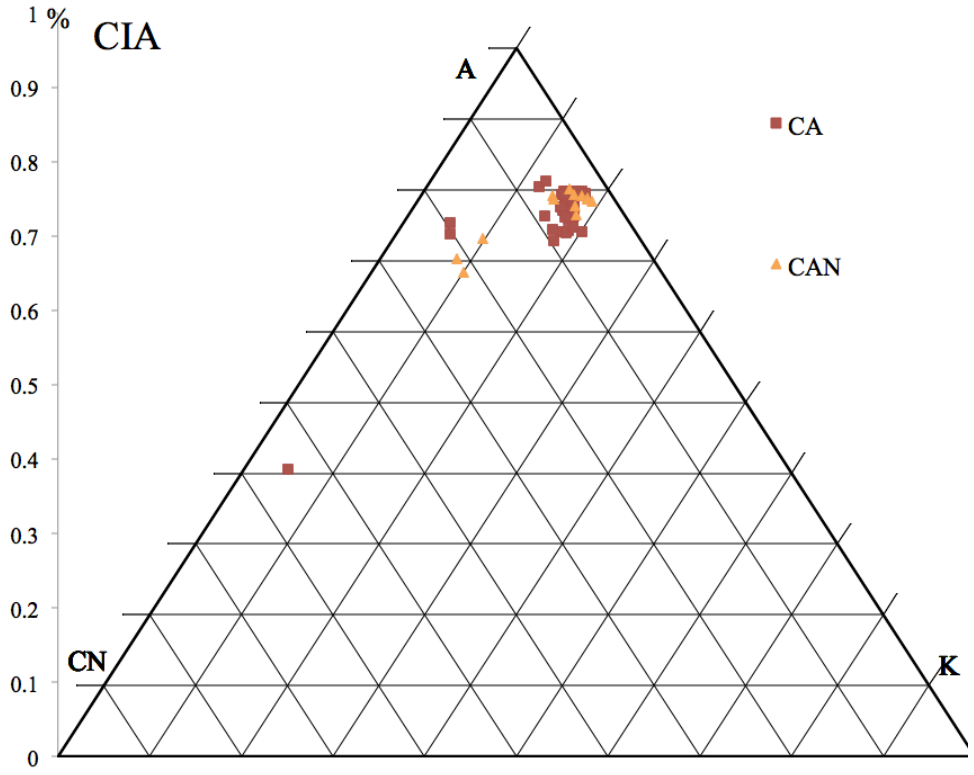

Figure 29: CIA plot, CA values in red, CAN values in yellow.

Samples from glaciogenic successions from the Devonian and Carboniferous from elsewhere, plots in the same area as the rocks from Bolivia. This might support the theory about the existence of the Hirnantian glaciation in Bolivia.

3.3.2 Provenance

Th/Sc versus Zr/Sc

Figure 30 (after McLennan et al., 1990) shows compositional trends of the succession using Th/Sc versus Zr/Sc ratios. Zr/Sc indicates the degree of reworked detritus, while Th/Sc shows the grade of fractionation.

CAN samples are shown in green and all samples are above the UCC, showing a strong reworked component. Most CA samples (blue) are below the UCC indicating compositional variations, however some samples (sandstones) plot close to 100 in the Zr/Sc ratio (sample CA 22 and 27). The CAN Formation shows more reworked sediments with Zr/Sc ratios between 10 to nearly 1000. The CA Formation is less fractionated with Zr/Sc values mostly below 10. The two formations show two different trends, which indicate two different detrital mixes. Zr is depleted in nearly all samples below typical UCC. Both formations are enriched in silica, however depleted in Zr and strongly enriched in Sc.

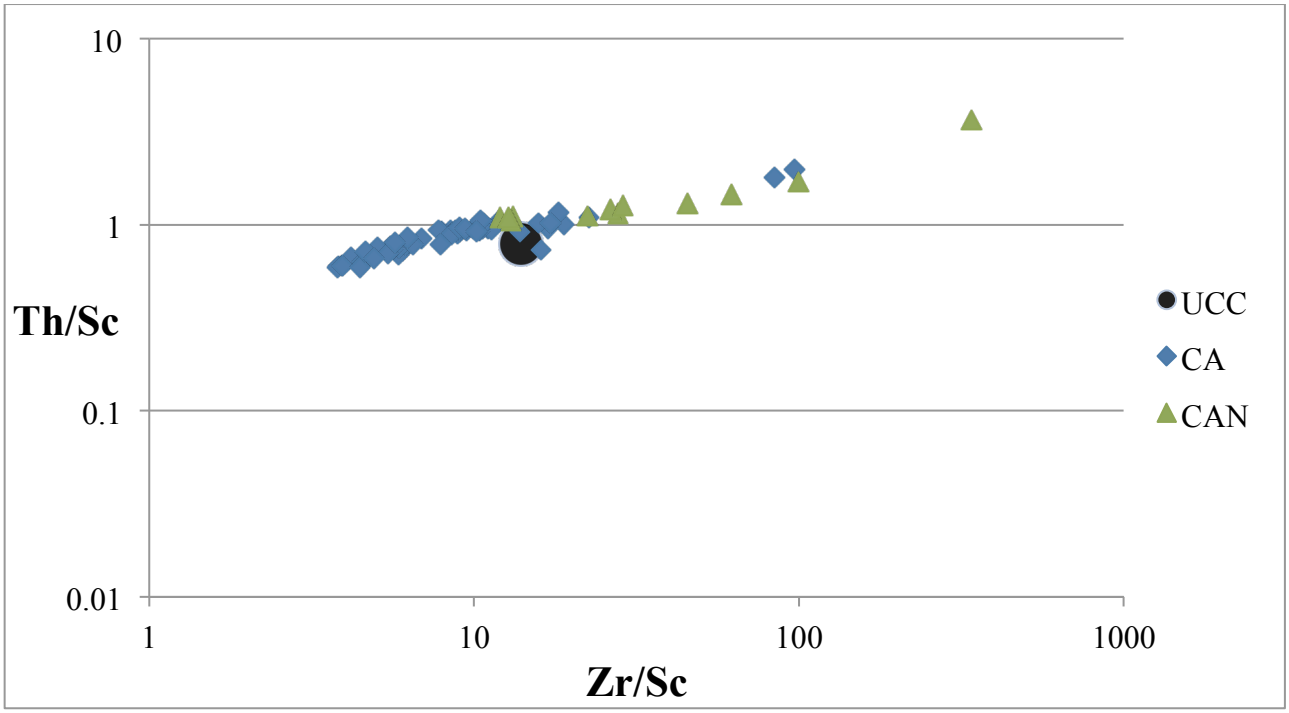

Figure 30: Th/Sc versus Zr/Sc plot, CA values in blue, CAN values in green.

Ti/Zr versus La/Sc

By using the diagram below (Figure 31) one can find out the paleotectonic setting of clastic sedimentary rocks with the help of the trace elements Ti, La, Sc, Th and Zr (Zimmermann et al., 2009).

The Ti/Zr versus La/Sc diagram shows the palaeotectonic setting of the detrital mix for the two formations. Only in very special cases this diagram can be used to identify the paleotectonic setting of the depositional rocks (Zimmermann et al., 2009), it mostly reflects the averaged tectonic setting of the detritus. One can clearly see that the detritus are composed of different

sources. CAN values (green) are plotted in active continental margin, continental island arc (shales) and passive rifted margin (sandstones). CA values are not defined that good, indicating more reworked sediments. However the trend is going from oceanic island arc towards an active continental margin (shales) and two samples fits into the passive rifted margin (sandstone), this shows more or less the same results as the Th/Sc plot above, for both formations. Low Ti/Zr values indicate reworked or dominance of felsic source material (Zimmermann et al., 2010), which can be observed more often in the CAN Formation (between approximately 4 to 28). However the La/Sc values vary within this formation from approximately 3 to 10. This can therefore indicate different portions of felsic material and less fractionated sources. The CA Formation has higher Ti/Zr values (approximately 20 to 42, however two samples are close to 5) compared to the CAN Formation, and the La/Sc ratios for CA are between 2 and 7. This indicates the abundance of a mafic source rock material.

This trend can also be observed in the tri-plot Th-Sc-Zr/10 (Figure 32). Here, CAN is clearly dominated by felsic material while CA has a higher amount of mafic input into the detritus.

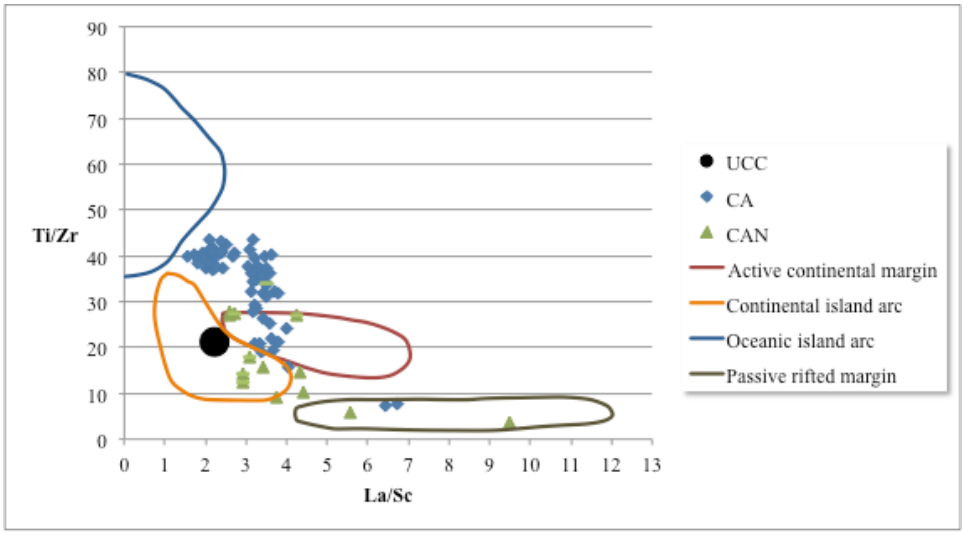

Figure 31: Ti/Zr versus La/Sc plot, CA values in blue, CAN values in green.

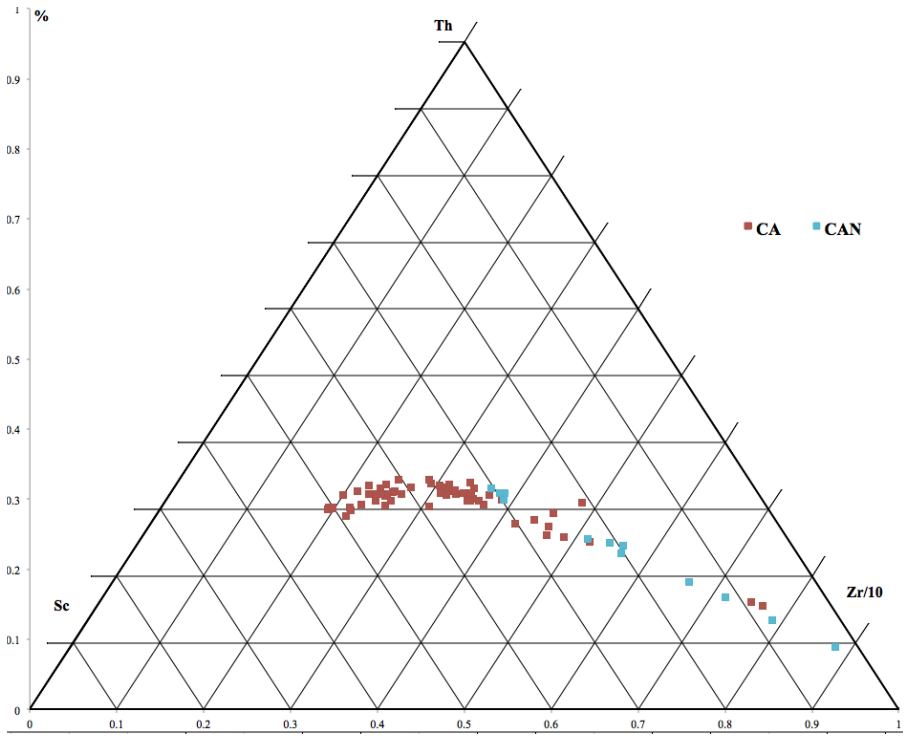

Figure 32: Th/Sc plot, CA values in red, CAN values in blue.

To find out if there is a possible arc signature, one can use some trace elements and their ratios, a table is as well conducted for this reason, Table 3, (Zimmermann et al., 2009). La_N/Yb_N rations in nearly all samples are above typical arc UCC value (<6), and Eu/Eu* values are below 1, which is the typical arc UCC value, (McLennan et al., 1993). As the Table shows, red indicates an arc setting, while orange show relatively close to an arc values. Based on the abundance of the arc related geochemical proxies it can be assumed that one of the sources had been related to arc setting. However, this does not mean that the Cancañiri Formation has been deposited in such a setting.

Sample	Rock type	SiO2	La/Sc	Th/Sc	Zr/Sc	Ti/Zr	Eu/Eu*	LaN/YbN	TiO2	Nb	Ta
CA1	Sand	64.83	3.22	0.74	16.08	21.04	0.63	10.23	0.79	14.20	1.10
CA2	Shale	61.41	3.22	0.95	10.62	29.23	0.65	10.87	0.88	15.90	1.10
CA3	Shale	61.09	3.43	1.04	11.89	26.40	0.64	11.19	0.89	15.70	1.10
CA4	Sand	69.79	3.68	1.01	18.89	19.53	0.72	12.77	0.80	14.00	1.10
CA5	sand	65.07	3.58	1.05	12.85	25.20	0.63	10.58	0.81	14.90	1.10
CA6	Shale	61.10	3.27	0.95	11.01	28.52	0.64	10.02	0.89	16.10	1.20
CA7	Shale	61.52	3.16	0.95	11.35	27.65	0.62	9.09	0.89	16.40	1.10
CA8	Shale	59.12	3.71	0.93	9.44	32.09	0.58	9.25	0.91	16.40	1.10
CA9	Shale	56.29	3.23	0.93	8.42	39.65	0.61	9.20	1.17	21.50	1.50
CA10	Shale	55.68	3.47	0.94	8.74	39.78	0.65	10.87	1.16	20.20	1.30
CA11	Shale	57.75	3.50	0.92	8.98	37.45	0.64	10.78	1.01	17.10	1.30
CA12	Shale	55.23	3.08	0.92	7.93	41.20	0.63	9.84	1.09	18.90	1.50
CA13	Shale	54.29	3.15	0.84	6.90	43.47	0.65	11.38	1.05	18.10	1.40
CA14	Shale	57.24	3.12	0.89	8.85	36.35	0.65	10.03	1.02	18.80	1.30
CA15	Shale	56.72	3.27	0.96	9.96	34.77	0.63	9.45	1.04	18.90	1.40
CA16	Shale	57.26	3.47	0.93	10.37	31.94	0.63	10.45	1.05	19.30	1.40
CA17	Shale	56.38	3.58	0.95	8.98	36.07	0.60	10.19	1.08	18.80	1.40
CA18	Shale	54.02	3.62	0.94	7.78	40.10	0.65	11.10	1.04	18.60	1.40
CA19	Shale	55.79	3.37	0.89	8.52	36.61	0.65	10.78	1.04	18.10	1.50
CA20	Shale	55.58	3.38	0.97	9.02	35.58	0.61	10.81	1.07	19.00	1.50
CA21	Sand	66.03	3.62	0.92	13.86	22.00	0.61	13.51	1.17	22.00	1.50
CA22	Sand	88.05	6.43	1.97	96.80	7.23	0.69	10.78	0.35	8.50	0.50
CA23	Shale	54.81	3.41	1.03	10.67	31.76	0.67	10.20	1.13	19.90	1.40
CA24	Shale	56.35	3.49	0.98	10.49	31.28	0.63	11.26	1.04	19.00	1.40
CA25	Shale	56.11	3.50	1.05	10.44	33.54	0.65	9.50	1.11	21.30	1.40
CA26	Shale	56.73	2.52	0.78	7.89	42.36	0.64	9.64	1.06	14.90	1.00
CA27	Sand	84.84	6.73	1.80	84.20	7.59	0.57	5.88	0.32	6.40	0.50
CA28	Shale	53.81	3.17	0.95	9.39	34.26	0.63	10.70	1.18	22.00	1.50
CA29	Shale	58.15	3.13	0.92	10.18	32.11	0.62	9.48	1.09	19.90	1.40
CA30	Shale	62.92	3.33	0.95	16.92	21.02	0.63	9.23	0.89	16.20	1.30
CA31	Sand	66.52	3.79	1.02	15.81	21.13	0.66	11.37	0.78	13.80	1.10
CA32	Shale	64.87	3.99	1.17	18.13	24.02	0.60	9.81	1.09	18.80	1.50
CA33	Shale	54.60	3.38	1.03	17.24	19.13	0.63	8.45	0.44	7.80	0.70
CA34	Sand	69.61	4.03	1.09	22.54	15.58	0.60	7.33	0.82	14.00	1.20
CA35	Shale	64.42	1.73	0.60	3.93	40.09	0.63	7.30	0.63	11.80	0.70
CA36	Shale	57.67	1.81	0.60	3.83	38.53	0.62	8.33	0.59	11.30	0.80
CA37	Shale	61.13	1.58	0.59	3.80	39.80	0.64	7.76	0.63	12.40	0.80
CA38	Shale	60.65	1.93	0.67	4.17	40.59	0.67	8.74	0.65	12.60	0.90
CA39	Shale	55.95	2.01	0.62	4.55	37.30	0.65	8.10	0.68	13.30	1.20
CA40	Shale	41.62	2.37	0.60	3.94	40.55	0.59	7.32	0.56	10.80	0.70
CA41	Shale	53.28	2.10	0.63	4.53	41.33	0.60	9.46	0.75	13.80	1.00
CA42	Shale	55.50	2.45	0.74	5.58	37.37	0.60	8.41	0.73	13.50	1.10
CA43	Shale	60.34	3.28	0.59	4.46	37.54	0.61	8.38	0.67	12.70	0.90
CA44-1	Shale	53.36	2.72	0.73	5.41	40.64	0.64	8.61	0.77	14.70	1.20
CA44-2	Shale	54.23	2.66	0.77	5.53	39.73	0.64	9.40	0.77	14.40	0.90
CA45	Shale	56.20	1.96	0.74	5.77	39.48	0.64	7.44	0.76	14.30	1.10
CA46	Shale	55.52	2.25	0.78	6.10	39.80	0.65	7.88	0.81	14.20	1.00
CA47	Shale	55.56	2.11	0.73	6.04	38.77	0.61	8.20	0.82	14.90	1.20
CA48	Shale	53.96	2.19	0.72	5.09	41.79	0.67	8.58	0.78	16.00	1.30
CA49	Shale	55.72	2.24	0.70	5.84	37.32	0.58	9.06	0.80	13.40	1.10
CA50	Shale	54.84	2.16	0.79	6.13	36.89	0.61	8.40	0.83	15.50	1.10

CA51	Shale	54.05	2.11	0.75	5.86	38.57	0.58	8.52	0.83	15.30	1.10
CA52	Shale	54.71	2.37	0.74	5.60	41.13	0.57	7.85	0.73	14.50	1.00
CA53	Shale	56.71	2.28	0.79	6.50	37.84	0.57	9.01	0.82	15.20	1.40
CA54	Shale	51.92	2.38	0.76	5.02	43.19	0.65	9.77	0.76	14.20	0.90
CA55	Shale	53.79	3.04	0.85	6.23	37.53	0.69	8.41	0.78	14.90	1.00
CA56	Shale	54.83	2.16	0.70	5.43	40.89	0.66	8.57	0.74	13.80	0.90
CA57	Shale	47.55	3.80	0.80	5.72	31.92	0.60	8.60	0.64	13.20	0.90
CA58	Shale	54.03	2.11	0.71	4.64	43.45	0.62	7.72	0.74	12.00	0.90
CA59	Shale	52.14	3.48	0.66	4.91	34.07	0.68	8.19	0.67	13.30	0.80
CAN1	Sand	73.55	2.92	1.15	27.76	12.37	0.65	6.76	0.63	13.00	0.80
CAN2	Sand	72.27	2.91		24.94	14.42			0.66	17.50	75.40
CAN3	Shale	65.59	4.26	1.11	13.14	27.04	0.65	12.43	0.83	17.30	1.10
CAN4	Shale	64.08	2.73	1.09	12.03	27.58	0.68	8.58	0.83	15.60	1.20
CAN5	Sand	66.05	3.09	1.11	22.36	18.00	0.64	7.95	0.94	16.90	1.30
CAN6	Sand	85.26	3.76	1.46	61.92	9.29	0.54	5.72	0.48	9.20	0.70
CAN7	Sand	88.25	5.58	1.70	99.60	5.72	0.59	10.25	0.38	7.50	0.60
CAN8	Shale	59.20	2.59	1.05	13.01	27.11	0.61	8.15	1.00	18.40	1.00
CAN9	Shale	55.90	2.61	1.09	12.77	27.91	0.60	7.49	1.07	20.70	1.10
CAN10	Sand	89.55	9.50	3.65	340.63	3.70	0.60	6.62	0.84	14.80	1.20
CAN11	Sand	65.79	3.43	1.21	26.21	15.85	0.68	7.60	0.97	18.10	1.20
CAN12	Sand	68.22	4.32	1.26	28.72	14.61	0.67	9.20	0.91	19.60	1.30
CAN13	Sand	75.79	4.39	1.31	45.43	10.29	0.61	9.76	0.78	13.90	0.90
Arc			**<3**	**<0.81**	**<10**	**>20**	**1.00**	**<6**	**<0.68**	**<12**	**<1**
	Arc										
	Close to arc										

Table 3: Arc related setting for the two formations, defining trace element abundance and ratios. *N* indicates normalization to chondrite. Red values indicates arc setting, while orange indicates values close to an arc. Table after Zimmermann et al., 2010.

3.4 IMPLICATION OF THE PROVENANCE DATA

Petrographic studies have shown that the main source of the two Cancañiri Formations was composed of quartz-rich sedimentary rocks. The CAN Formation is stronger reworked than the CA Formation.

The provenance of the Cancañiri Formation points to two significant source types; one felsic and one mafic, however maybe one arc related as well, which is observed in ancient retro-arc (foreland) basins.

Not all elements points to a mafic source, due to the fact that trace elements like Sc, Ti and Nb are not strongly enriched, rather the opposite. It is therefore interpreted two source composition, one felsic and one mafic, where diagrams and petrography points to an active continental margin or a continental island arc, a table is as well conducted for a possible arc related setting (Table 3 above). Only some of the characteristic geochemical parameter point to an arc provenance as such that it is argued that a variety of sources have been eroded into the Cancañiri basin: a) felsic, b) mafic and c) arc related.

A number of compatible elements are enriched in CA even in the sandstones (Figure 26) and would, under normal circumstances support the influence of a mafic component. However, the fact that the rocks are related to the Hirnantian glacial event and the black color of the shales

might indicate a different depositional environment form the rocks of CAN. In anoxic environments base metal like Cu, Co, Cr, V etc. are enriched and pyrite grows enhanced to the abundant organic material with the existence of S. This would explain the enriched values for these base metals and the enormous high abundance of pyrite in the heavy mineral fraction.

Based on the dominance of the pyrite in the heavy minerals analyses for the Cancañiri Formations, a deep-sea environment can be suggested, due to the anoxic conditions. However due to the poorly sorted grains in the petrography, it could be argued that the depositional environment might be not as deep. The appropriate depositional environment might therefore be suggested as a slope to deep-sea basin deposits, with turbidity currents and might be compared to a fjord or estuary. However, this environment was only poorly ventilated either because of very steep basin margins or because of partly ice cover. To support this hypothesis the black shales are studied for the amount of organic carbon. Total carbon varies only between 0.03 % and 0.63 %, Table 4.

	Organic C (%)	Total C (%)
CA37	<0.02	0.53
CA39	0.05	0.51
CA45	<0.02	0.51
CA55	0.04	0.04
CA57	0.03	0.63
CAN1	0.13	0.17
CAN8	0.19	0.27
CAN9	0.22	0.32
CAN10	<0.02	0.03

Table 4: Total and organic carbon for the two Cancañiri Formations.

Table 4 shows that either only little organic matter had been deposited as a consequence of the mass extinction or that all the organic matter is already migrated. However, the black color of the black shales is derived from the high amount of base metals and not from organic matter.

4.0 Application for the Petroleum Industry

During a fieldtrip in Bolivia black shales have been identified and were target for this research study to reveal the composition of the detritus and to identify the amount of organic matter. Unbelievably, the dark color of the shales is not related to organic matter. Amounts of organic carbon is far below 0.1 % for CA and slightly higher for CAN. The dark color is controlled by the high amount of base metal input. These high abundances are related to an anoxic environment (supported by the heavy mineral studies and the high amount of detected pyrite, even detrital grains) but in this environment either no organic matter was deposited as the rock is slightly younger than the Hirnantian mass extinction or the organic matter already migrated.

5.0 Conclusion

This research project shows how I have used different whole rock analyses on several rock samples, from Bolivia. It shows the preparation and methodology, further geochemical analyses to gain information about the source and provenance study in Bolivia. Two outcrops from the Upper Ordovician, Cancañiri Formation in "La Cumbre/Eastern Cordillera" was sampled, "CA" and "CAN" respectively.

The petrography showed us well-rounded grains, of different minerals i.e. mica, feldspar, muscovite, quartz etc. indicating an environment dominated by sorting and reworking. However, we do not know if the source rocks already had been composed of recycled material or if all the rounding and sorting had happened throughout the sediment transport. The existence of angular grains and even of rounded pyrite and apatite points for certain source components to a shorter transportation and less reworking in the depositional area. It is therefore argued for a slope environment with channel systems fed by higher mountain areas close to the depositional basin.

Pyrite dominates the two formations, when studying the heavy mineral fraction, besides the common candidates of zircons, rutile and apatite. However, in this study pyrite is not only preserved as squared minerals then most likely grown during post-depositional processes but also as rounded detrital grains. This implies short transport under anoxic conditions. The latter are supported by the high amount of redox-sensitive base metals. This fact is bothering the interpretation of the provenance based on compatible elements.

Geochemical constraints for these two exposures point to a stronger input of mafic material (independent of base metals) for the samples of the first exposure CA, while rocks from CAN are slightly more recycled and dominated by felsic sources. Organic matter was never stored or is migrated as in the current situation total organic carbon lies in dimensions below 0.1 %.

It can therefore be argued that the depositional environment for CA has been in an anoxic facies without the deposition of organic matter like in a fjord. The lack of organic matter can be supported by the mass extinction during the Hirnantian. In contrast, the rocks of CAN are probably deposited in a facies with stronger recycling and more abundant organic matter. An environment like a shallow marine beach deposit could be imagined established after the expected transgression after the melting of the ice. Although organic carbon is not high in CAN – it is one dimension higher than in CA and suffered the same p-T conditions during orogenic events. This let argue for the absence of organic matter during the deposition of CA.

References

Arce-Burgoa, O, R., and Goldfarb, R, J., (2009): *Metalliferous ore Deposits of Bolivia*, SEG (Society of Economic Geologists) Newsletter, No. 79, USA.

Bahlburg, H., and Dobrzinski, N., (2009): *A review of the Chemical Index of Alteration (CIA) and it's application to the study of Neoproterozoic glacial deposits and climate transitions.* The Geological Record of Neoproterozoic Glaciations. Geological Society, London, memoir.

Bahlburg, H., Vervoort, J, D., Du Frane, S, A., and Bock B., (2009): *Timing of crust formation and recycling in accretionary orogens: Insights learnd from the western margin of South America.* Earth-science Reviews 97, 215-241.

Delabroye, A., and Vecoli, M., (2009): *The end- Ordovician glaciation and the Hirnantian stage: A global review and questions about Late Ordovician event stratigraphy.* Earth- Science Reveiws 98 (2010) 269-282, Elsevier.

Díaz-Martínez, E., and Grahn, Y., (2006): *Early Silurian glaciations along the western margin of Gondwana (Peru, Bolivia and northern Argentina): Palaeogeographic and geodynamic setting.* Palaeoecology 245, 62- 81. Elsevier.

Gradstein, F., Ogg, J., and Smith, A., (2004): *A geological Time Scale 2004*. Cambridge: Cambridge University press 2004.

Google earth., (2013).

House, A., (2010): *Mining Journal A supplement to Mining Journal Bolivia*, established 1835, Aspermount UK, I Singer Street London EC2A 4BQ.

Kaljo, D., Hints, L., Männik, P., and Nolvak, J., (2008): *The succession of Hornantian events based on data from Baltica: brachiopods, chitinozoans, conodonts, and carbon isotopes.* Estonian Journal of Earth Sciences, 2008, 57, 4, 197-218.

McGraw-Hill., (2003): *Dictionary of Geology and Mineralogy,* second edition. The McGraw-Hill Companies.

McLennan, S, M., Taylor, S, R., McCulloch M, T., and Maynard, J, B., (1990): *Geochemical and Nd-Sr isotopic composition of deep- sea turbidites: Crustal evolution and plate tectonic associations.* Vol. 54, pp. 2015-2050. Pergamon Press plc.

McLennan, S, M., Hemming, S., McDaniel D, K,. and Hanson, G, N., (1993): *Geochemical approach to sedimentation, provenance, and tectonics.* Geological Society of Amrica, Special Paper 284, 1993.

McLennan, S., Taylor, S., and Hemming, S., (2006): *Composition, differantiation, and evolution of continental crust: constrains from sedimentary rocks and heat flow*. In M. Brown, & T. Rushmer, Evolution and differentiation of the continental crust (pp. 92-135).

Murray, B. P., Horton, B. K., and Heizier, M. T., (2010): *Oligocene- Miocene basin evolution in the northern Altiplano, Bolivia: Implication of evolution of the central Andean backthrust belt and high plateau.* Geological Society of America Bulletin 2010; 122; No. 9-10; 1443-1462.

Suares Soruco, R., Estenssoro, S, C., and Zapata, C, M., (2000): *Compendio de Geologia de Bolivia*, Volumen 18 numero 1-2 junio 2000.P. 29, 39-76. Revista Tecnica De Yacimentos Petrolliferos Fiscales Bolivianos.

Tankard, A, J., Soruco R, S., and Welsink H, J., (1995): *Petroleum Basins of South America*, AAPG Memoir 62. p.523.

Taylor, S, R., and McLennan, S, M., (1985): *The Continental Crust; Its composition and evolution; an examination of the geochemical record preserved in sedimentary rocks*. Blackwell, Oxford.

Winchester, J, A., and Floyd, P, A., (1977): *Geochemical discrimination of different magma series and their differentiation products using immobile elements.* Chem. Geol. 20:325-343.

Zimmermann, U., and Bahlburg, H., (2003): *Provenance analysis and tectonic setting of the Ordovician clastic deposits in the southern Puna Basin, NW Argentina.* Sedimentology (2003) 50, 1079-1104. International Assosiation of Sedimentologists.

Zimmermann, U., Niemeyer, H., and Meffre, S., (2009): *Revealing the continental margin of Gondwana: the Ordovician arc of the Cordón de Lila (Northern Chile).* Springer- Verlag 2009.

Zimmermann, U., and Spalletti, L, A., (2009): *Provenance of the Lower Paleozoic Balacrce Formation (Tandilia System, Buenos Aires Province, Argentina): Implication for paleogeographic reconstructions of SW Gondwana.* Elsevier, Sedimentary Geology 219 (2009) 7-23.

Zimmermann, U., Poiré D, G., and Peral, L, G., (2010): *Neoproterozoic to Lower Palaeozoic successions of the Tandilia System in Argentina: implication for the palaeotectonic framework of southwest Gondwana.* Springer- Verlag 2010.

www.worldatlas.com, 2013.

Appendix

Often used abbreviations

BSE – Back-scatter Electron

CL – Cathodoluminescence

EDS – Energy Dispersive Spectrometer

Fm – Formation

HM – Heavy minerals

REE – Rare Earth Elements

SEM - Scanning Electron Microscope

APPENDIX A – ROCKS FROM THE TWO CANCAÑIRI OUTCROPS

Cancañiri Formation (CA Fm)

Figure 33: Long section Cancañiri Fm (CA), the numbers and arrows are indicating where some of the samples were sampled (for more information about the samples see Figures below).

Figure 34: CA 1, sandstone, GC.

Figure 35: CA 2, shale, GC.

Figure 36: CA 3, shale, GC.

Figure 37: CA 4, sandstone, GC.

Figure 38: CA 5, sandstone, GC.

Figure 39: CA 6, shale, GC.

Figure 40: CA 7, shale, GC.

Figure 41: CA 8, shale, GC.

Figure 42: CA 9, shale, GC.

Figure 43: CA 10, shale, GC.

Figure 44: CA 11, shale, GC.

Figure 45: CA 12, shale, GC.

Figure 46: CA 13, shale, GC.

Figure 47: CA 14, shale, GC.

Figure 48: CA 15, shale, GC.

Figure 49: CA 16, shale, GC.

Figure 50: CA 17, shale, GC.

Figure 51: CA 18, shale, GC.

Figure 52: CA 19, shale, GC.

Figure 53: CA 20, shale, GC.

Figure 54: CA 21, sandstone, GC.

Figure 55: CA 22, sandstone, GC.

Figure 56: CA 23, shale, GC.

Figure 57: CA 24, shale, GC, HM fractions; apatite-, magnetic- and zircon fraction (SEM).

Figure 58: CA 25, shale, GC, petrography.

Figure 59: CA 26, shale, GC.

Figure 60: CA 27, sandstone, GC.

Figure 61: CA 28, shale, GC.

Figure 62: CA 29, shale, GC.

Figure 63: CA 30, shale, GC.

Figure 64: CA 31, sandstone, GC, and SEM fractions; apatite-, magnetic- and zircon fraction (HM).

Figure 65: CA 32, shale, GC.

Figure 66: CA 33, shale, GC.

Figure 67: CA 34, sandstone, GC.

Figure 68: CA 35, shale, GC.

Figure 69: CA 36, shale, GC.

Figure 70: CA 37, shale, GC.

Figure 71: CA 38, shale, GC.

Figure 72: CA 39, shale, GC, petrography- and HM fractions; apatite-, magnetic- and zircon fraction (SEM).

Figure 73: CA 40, shale, GC.

Figure 74: CA 41, shale, GC.

Figure 75: CA 42, shale, GC.

Figure 76: CA 43, shale, GC.

Figure 77: CA 44, shale, GC.


Figure 78: CA 45, shale, GC.


Figure 79: CA 46, shale, GC.

Figure 80: CA 47, shale, GC.

Figure 81: CA 48, shale, GC.

Figure 82: CA 49, shale, GC.

Figure 83: CA 50, shale, GC.


Figure 84: CA 51, shale, GC.

Figure 85: CA 52, shale, GC.

Figure 86: CA 53, shale, GC.

Figure 87: CA 54, shale, GC.

Figure 88: CA 55, shale, GC.

Figure 89: CA 56, shale, GC.

Figure 90: CA 57, shale, GC.

Figure 91: CA 58, shale, GC.

Figure 92: CA 59, shale, GC.

All rocks from CA 1 to CA 39 were sampled with c. 10 m distance from each other, while samples from CA 39 to CA 59 were sampled c. every meter.

Cancañiri Formation (CAN Fm)

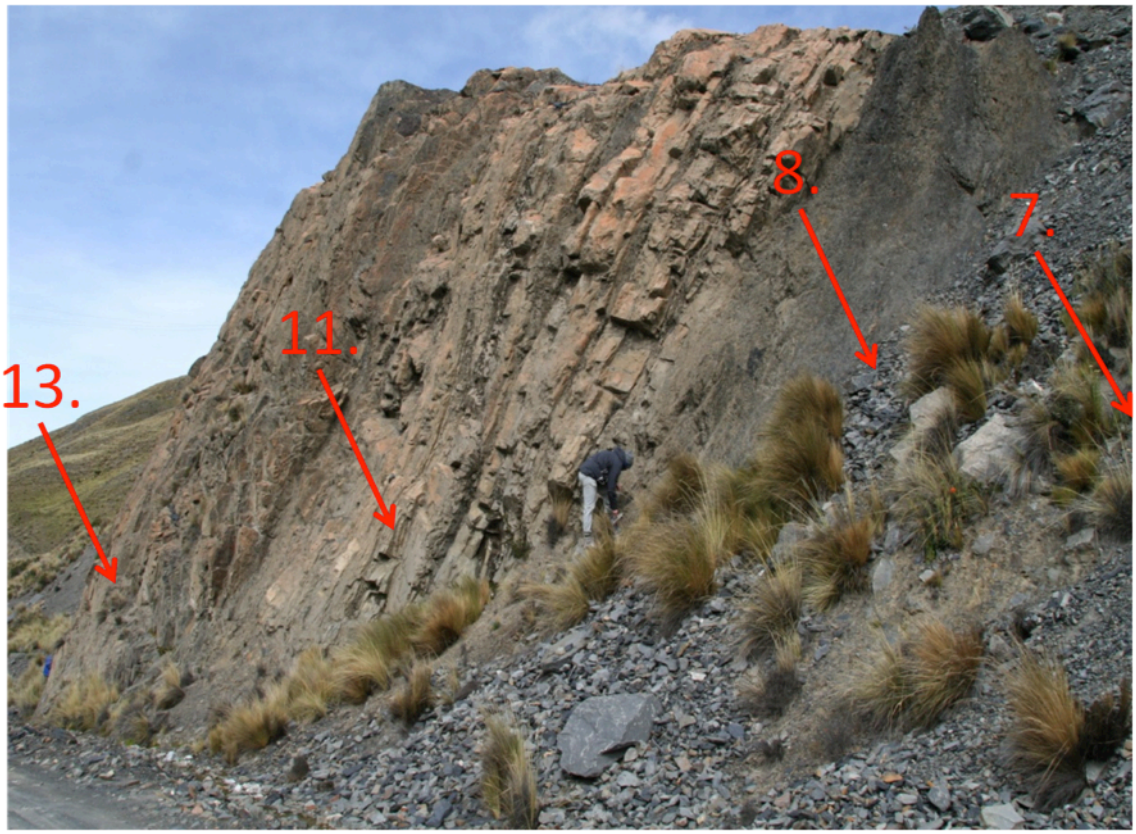

Figure 93: Second Cancañiri Fm (CAN), arrows and numbers indicating some of the sampled samples (for more information about the samples, see Figures below).

Figure 94: CAN 1, sandstone, GC.

Figure 95: CAN 2, sandstone, GC.

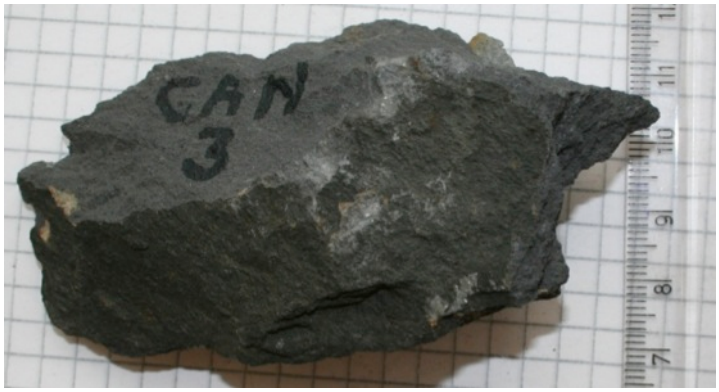

Figure 96: CAN 3, shale, GC, petrography- and HM fractions; apatite-, magnetic- and zircon fraction (SEM).


Figure 97: CAN 4, shale, GC.

Figure 98: CAN 5, sandstone, GC.

Figure 99: CAN 6, sandstone, GC.

Figure 100: CAN 7, sandstone, GC.


Figure 101: CAN 8, shale, GC.

Figure 102: CAN 9, shale, GC.

Figure 103: CAN 10, sandstone, GC.

Figure 104: CAN 11, sandstone, GC.

Figure 105: CAN 12, shale, GC.

Figure 106: CAN 13, sandstone, GC.

Every rock from this Formation was sampled with c. one meter distance from each other.

In both formations detrital zircons had been separated but could not be measured during the MSc thesis because of time constraints.

APPENDIX B -EQUIPMENT AND METHODS

Preparation for petrography

Light microscope:

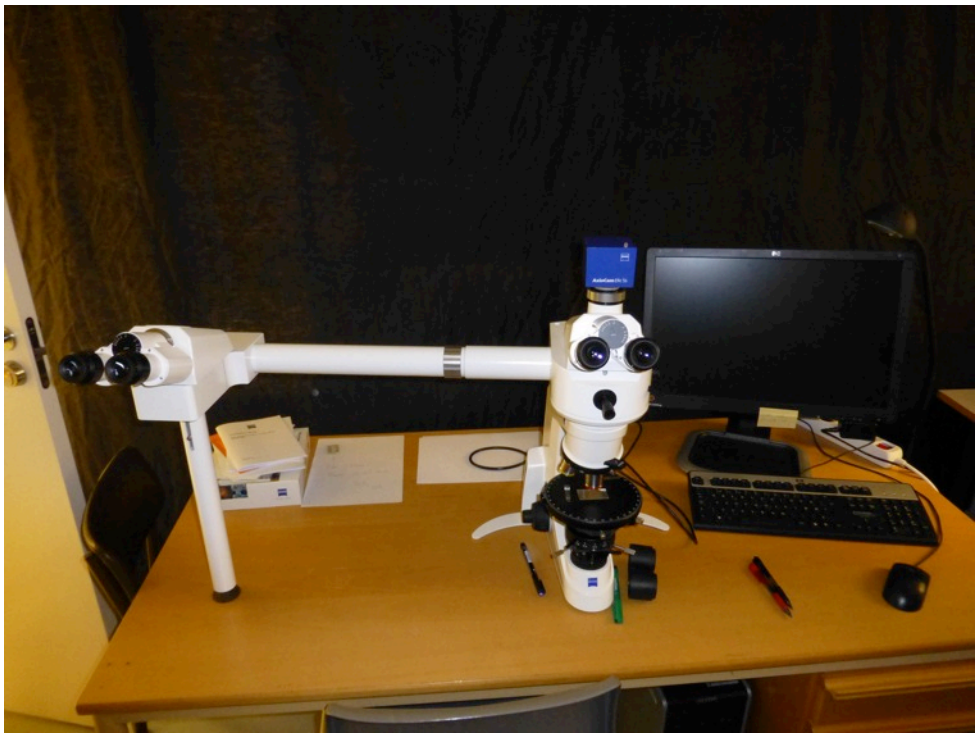

Figure 107: A light microscope used to observe the minerals in the petrography, photos below are taken with the camera on this microscope.

Sample CA 39

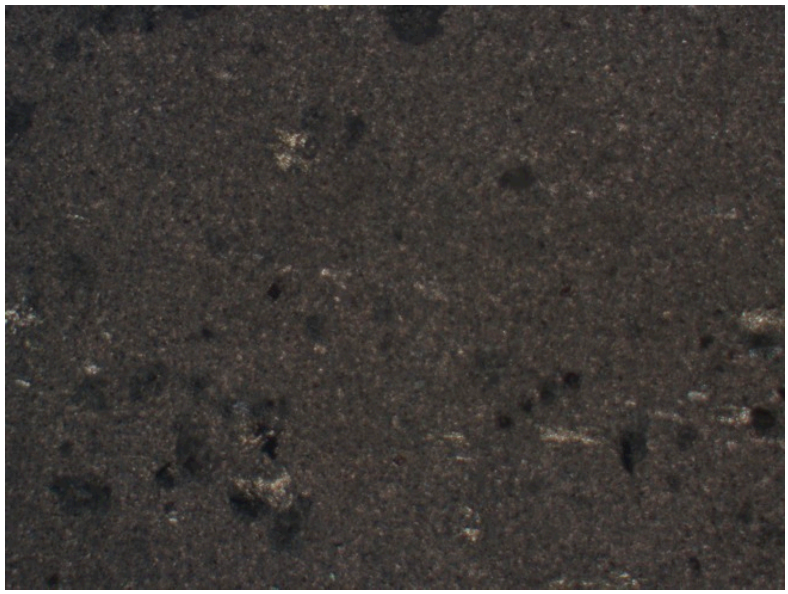

Figure 108: Petrography of Ca 39, taken with a light microscope. Surrounding matrix is quartz, mica (biotite and muscovite) and feldspar. Heavy minerals are mostly pyrite.

Sample CAN 3

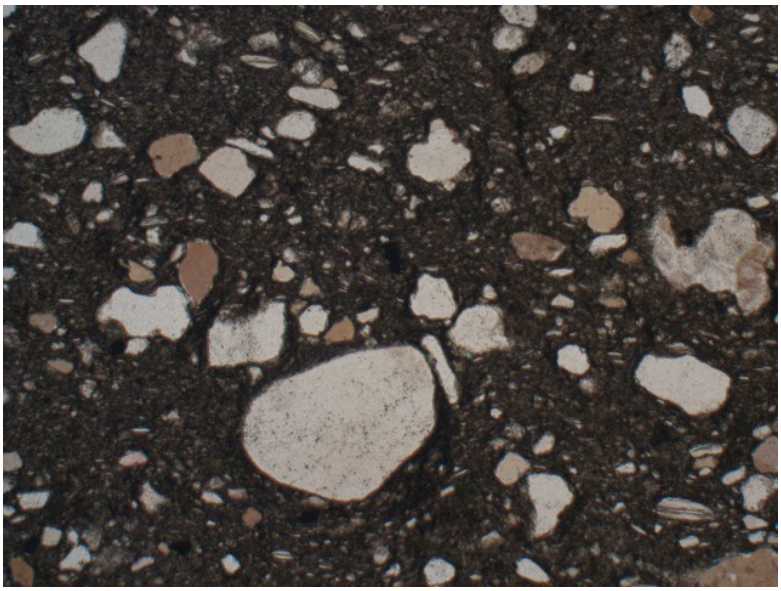

Figure 109: Petrography of CAN 3, taken with a light microscope. Large white mineral is quartz. Surrounding matrix is quartz, mica (biotite and muscovite) and feldspar. Heavy minerals are pyrite, zircon, apatite and rutile occurring the most.

Preparation for mounds, coating, SEM, CL detector and heavy minerals.

Figure 110: Making of mounds, for heavy minerals and SEM analysis, i.e. CAN Formation.

Figure 111: Powder from the rocks, used for heavy minerals and SEM analysis.

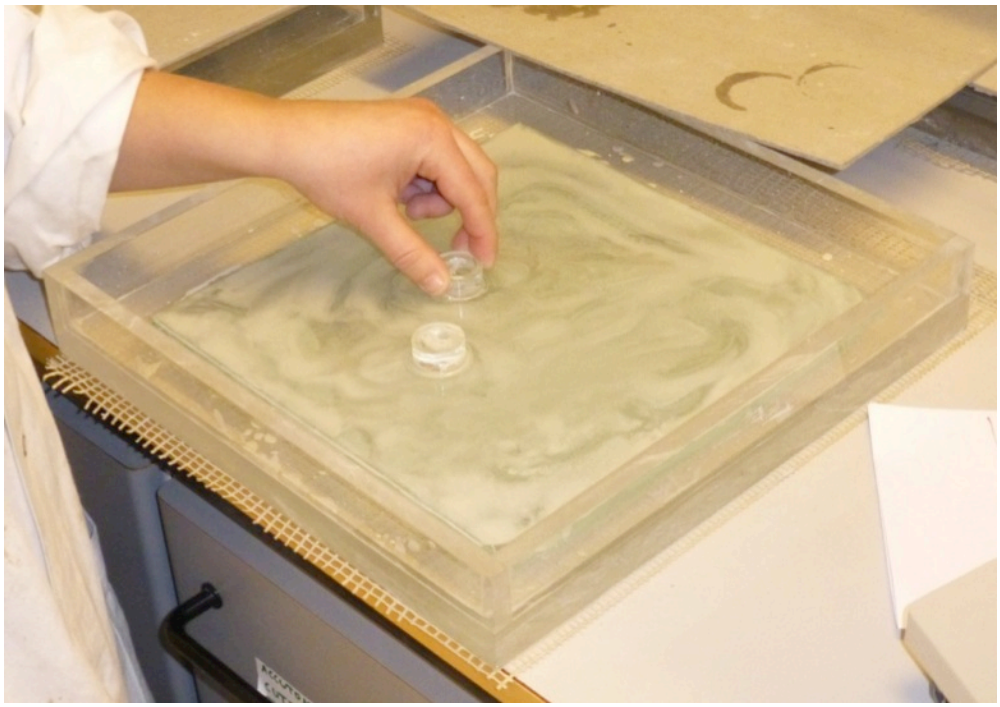

Figure 112: Mounds polished by hand with the 1000 powder, before more polishing in the polish machine.

Figure 113: Mounds ready for further preparation (polishing machine).

Figure 114: Polishing machine.

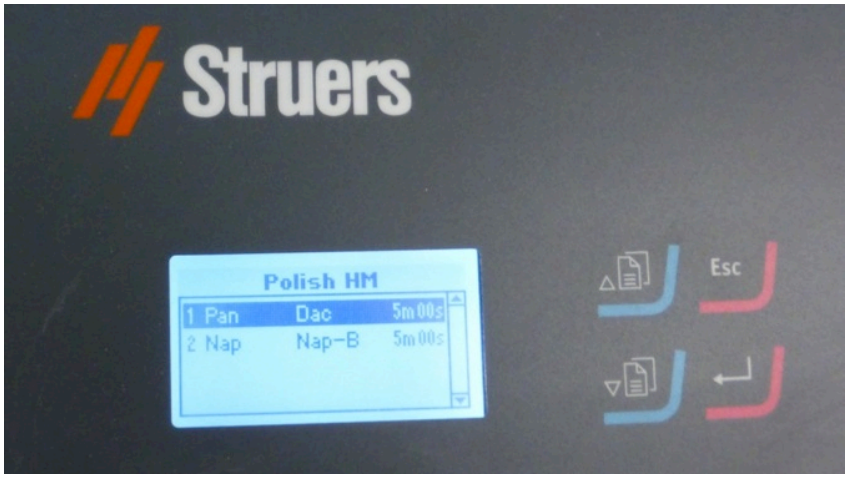

Figure 115: “Pan” and “Nap” were the two polishing program we used, one polished for 3 micron (Pan), the other one for 1 micron (Nap).

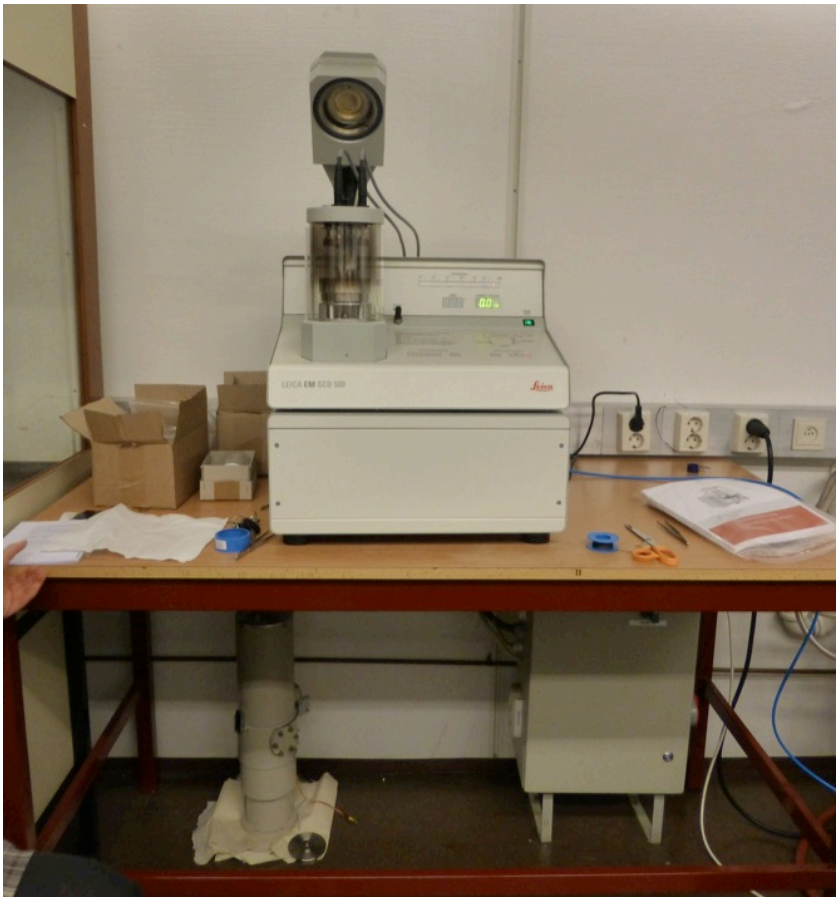

Figure 116: Coating machine, all mounds were coated with carbon.

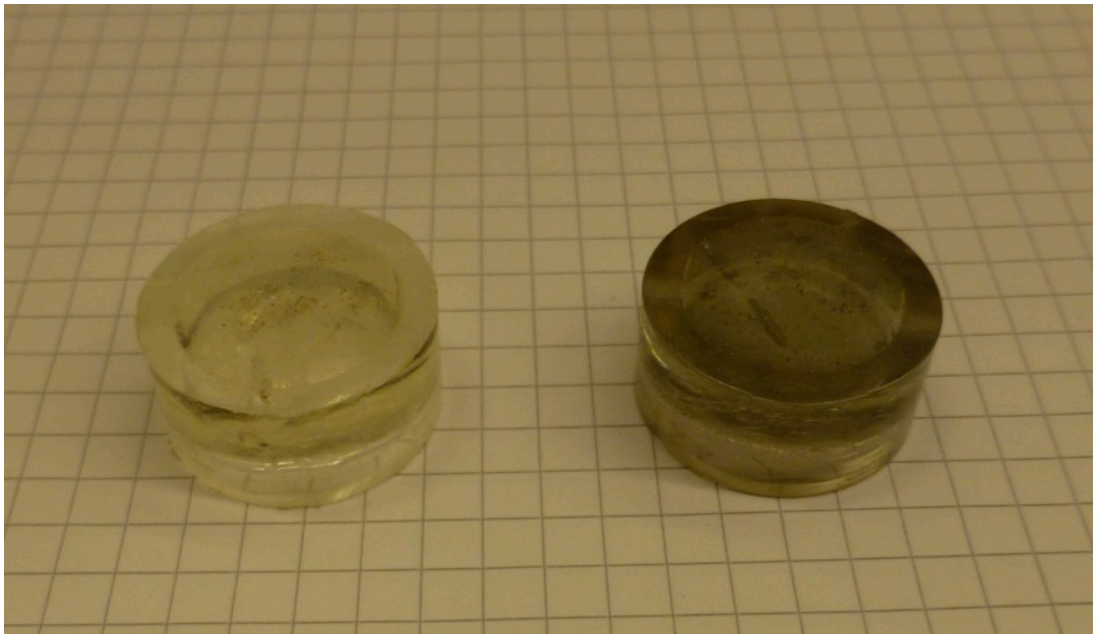

Figure 117: Two mounds, the mound to the right has been coated with carbon, the one to the left is ready to be coated. After coating, the sample is ready to further analysis; Heavy minerals, SEM and CL detector.

SEM

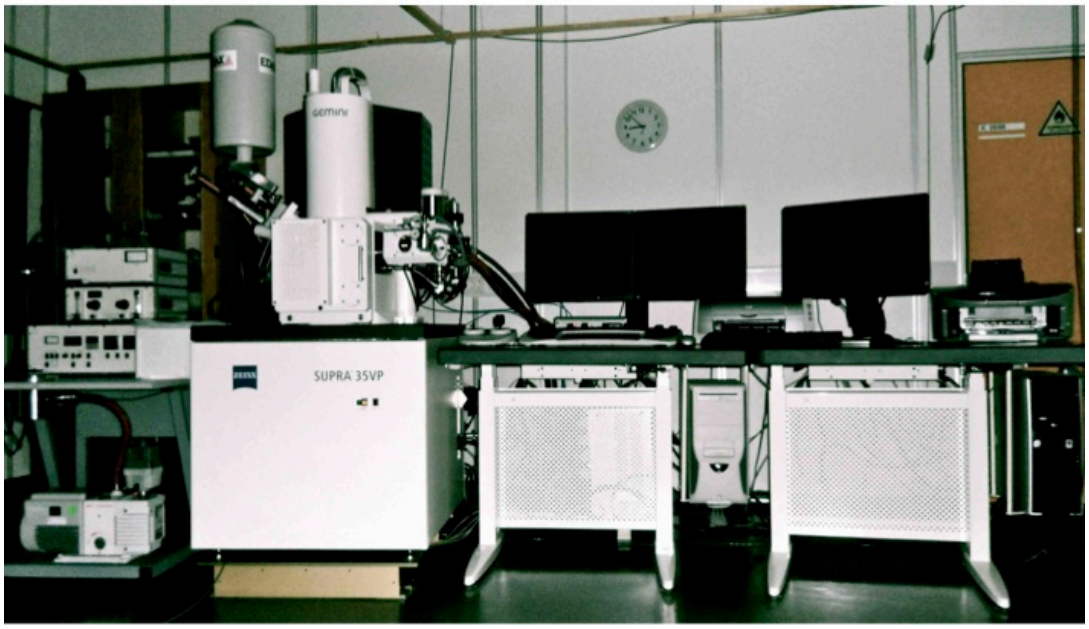

Figure 118: The SEM machine used for heavy minerals analysis, including BSE, EDS and CL detector, (photo taken by Sveinung Hatløy).

Preparation for milling

Milling

Figure 119: Milling machine, Retcsh RS 200.

Figure 120: Agate beaker (made by quartz arenite) used in the milling machine.

APPENDIX C – HEAVY MINERALS (HM)

Pyrite

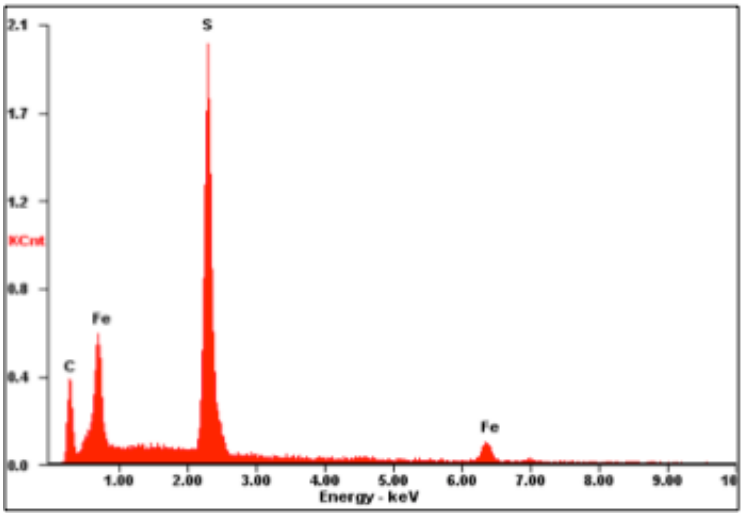

Element	Wt %	At %
FeL	31.50	24.55
S K	38.16	51.80
FeK	30.35	23.65

Figure 121: Main chemical composition of pyrite, together with a table containing the amount of each element present.

Zircon

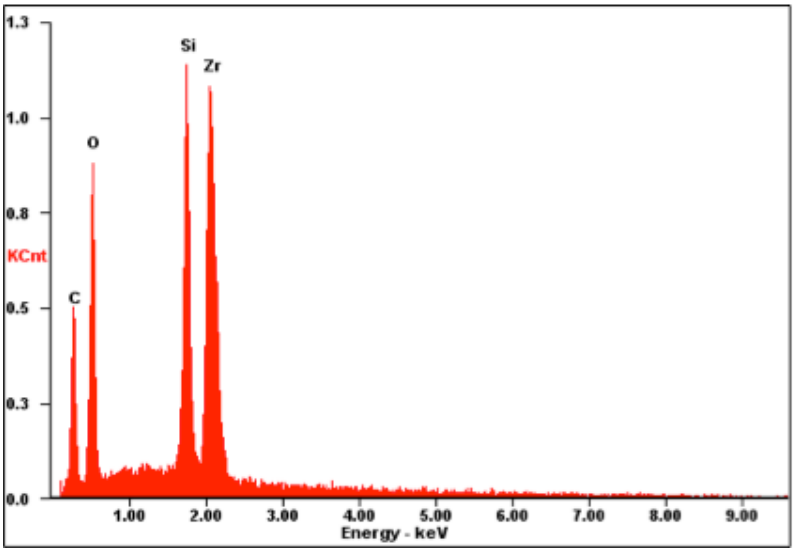

Element	Wt %	At %
SiK	22.30	48.25
ZrL	77.70	51.75

Figure 122: Main chemical composition of zircon, including a table with amount of elements present.

Rutile

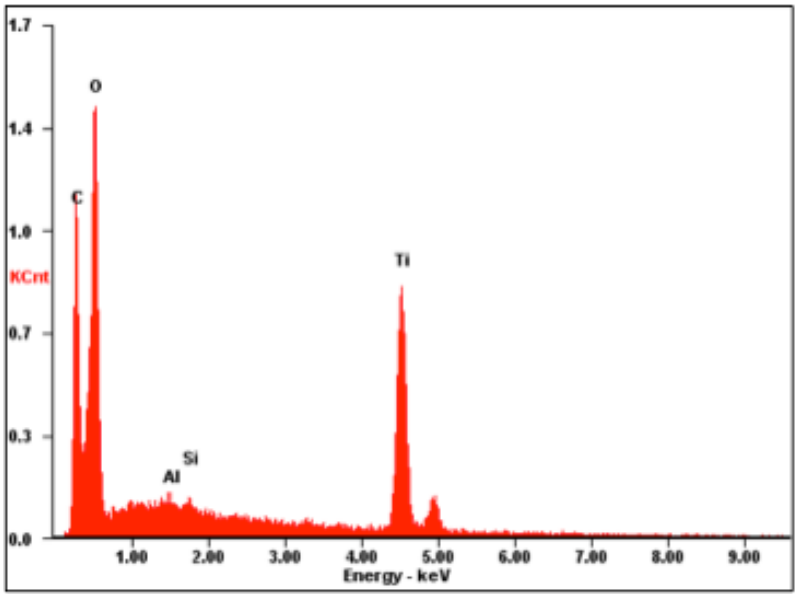

Element	Wt %	At %
AlK	00.99	01.74
SiK	01.00	01.69
TiK	98.00	96.57

Figure 123: Chemical composition of rutile, including a table with the amount of elements present.

Apatite

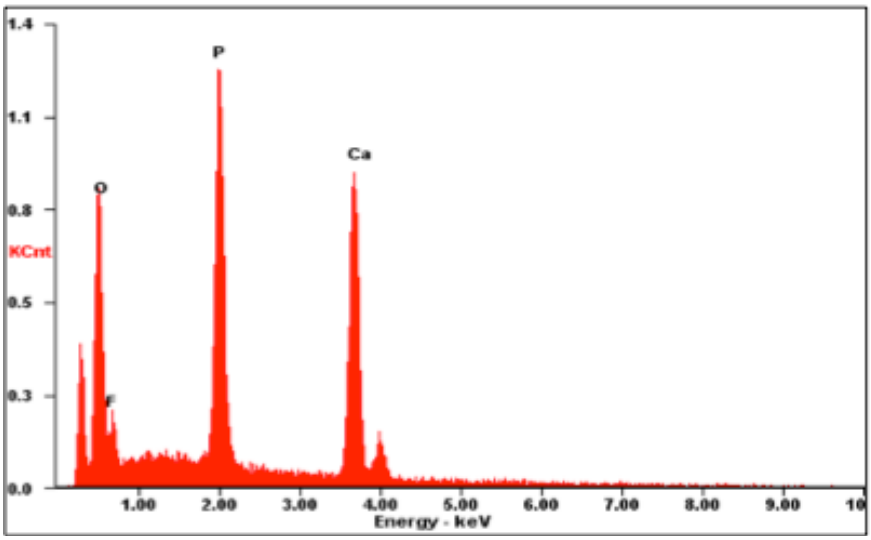

Element	Wt %	At %
F K	06.22	11.21
NaK	00.34	00.50
MgK	00.34	00.47
AlK	00.44	00.55
P K	32.25	35.64
CaK	60.43	51.62

Figure 124: Chemical composition of apatite, including a table with the amount of elements present.

Hematite

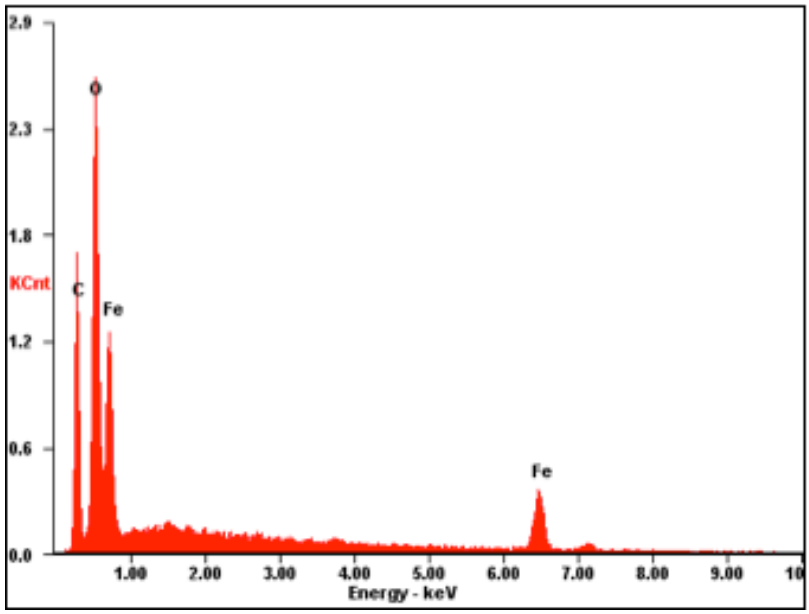

Element	Wt %	At %
AlK	00.71	01.44
SiK	00.37	00.72
CaK	01.24	01.71
FeK	97.68	96.13

Figure 125: Chemical composition of hematite, including a table with the amount of elements present.

Ilmenite

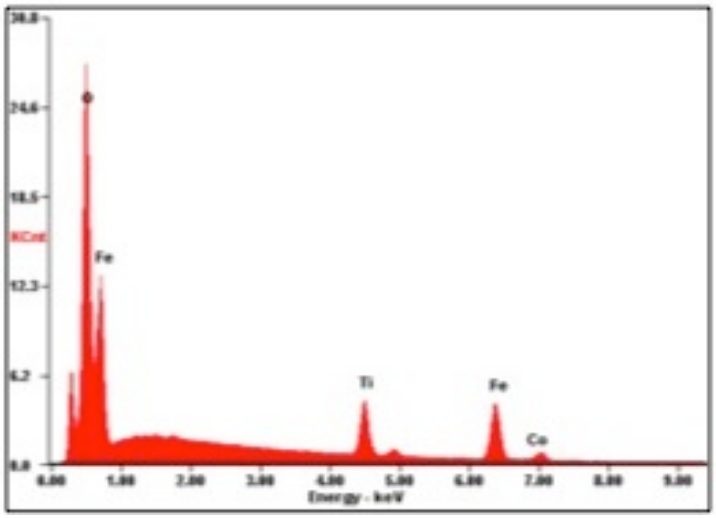

Element	Wt %	At %
FeL	79.13	78.27
TiK	06.63	07.65
FeK	14.01	13.86
CoK	00.23	00.21

Figure 126: Chemical composition of ilmenite, including a table with the amount of elements present.

Titanite

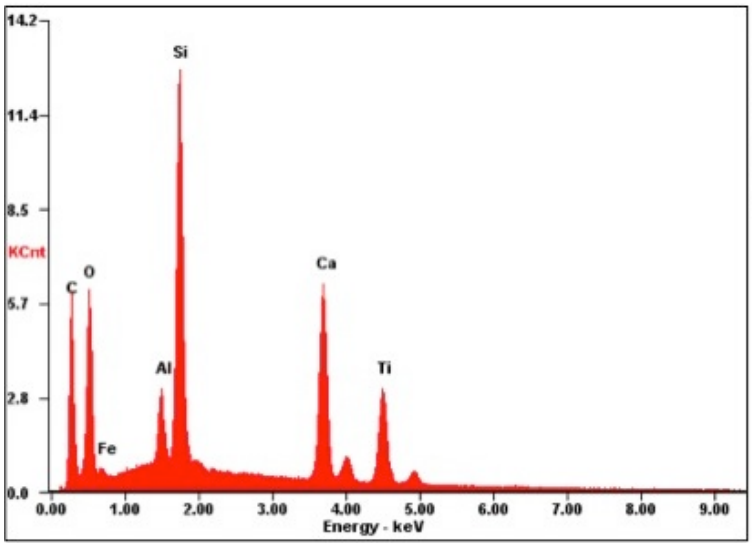

Element	Wt %	At %
FeL	13.39	08.47
AlK	07.48	09.80
SiK	37.56	47.28
P K	00.99	01.13
CaK	23.34	20.59
TiK	17.24	12.73

Figure 127: Chemical composition of titanite, including a table with the amount of elements present.

Intergrown minerals:

Feldspar

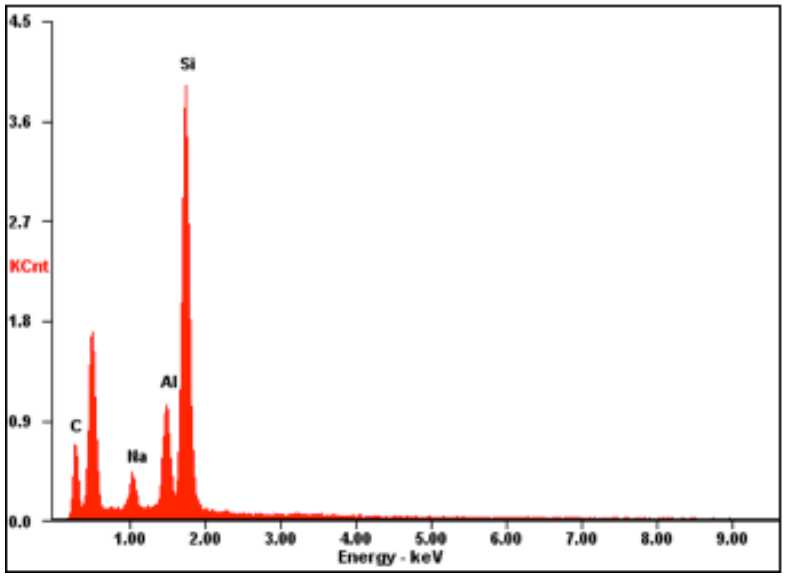

Element	Wt %	At %
NaK	04.40	05.29
AlK	15.93	16.32
SiK	79.67	78.39

Figure 128: Chemical composition of feldspar, including a table with the amount of elements present.

Muscovite

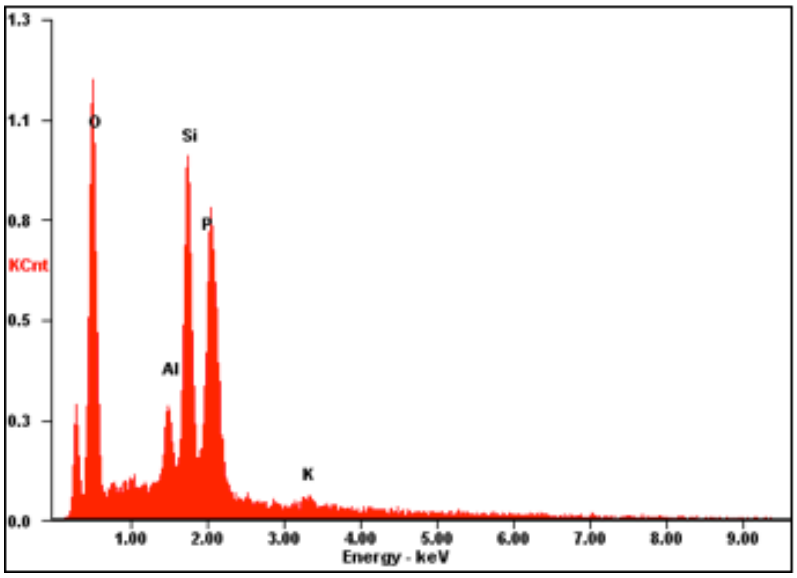

Element	Wt %	At %
AlK	04.92	09.83
SiK	24.32	46.69
ZrL	68.65	40.58
K K	02.10	02.90

Figure 129: Chemical composition of muscovite, including a table with the amount of elements present.

Biotite

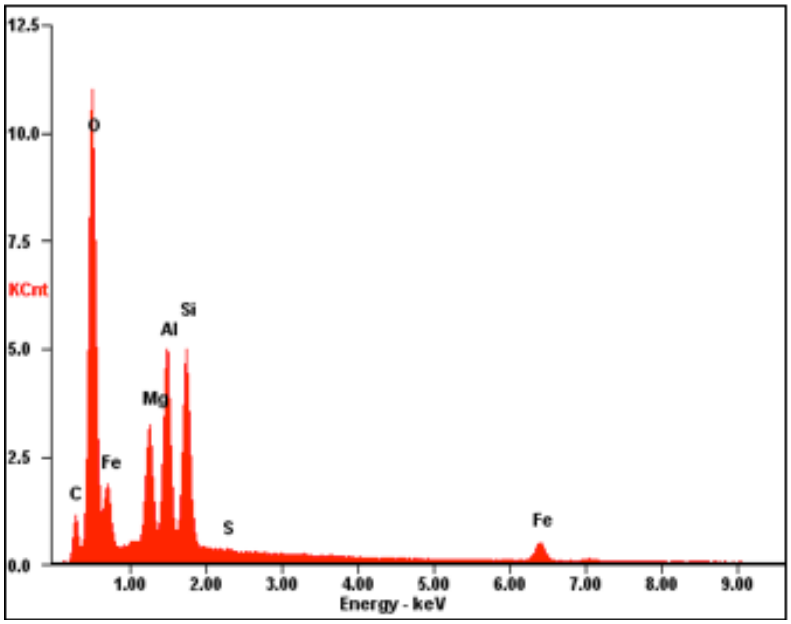

Element	Wt %	At %
FeL	18.57	12.33
MgK	09.46	14.42
AlK	17.75	24.39
SiK	19.49	25.73
S K	00.15	00.17
FeK	34.57	22.95

Figure 130: Chemical composition of biotite, including a table with amount of elements present.

Quartz

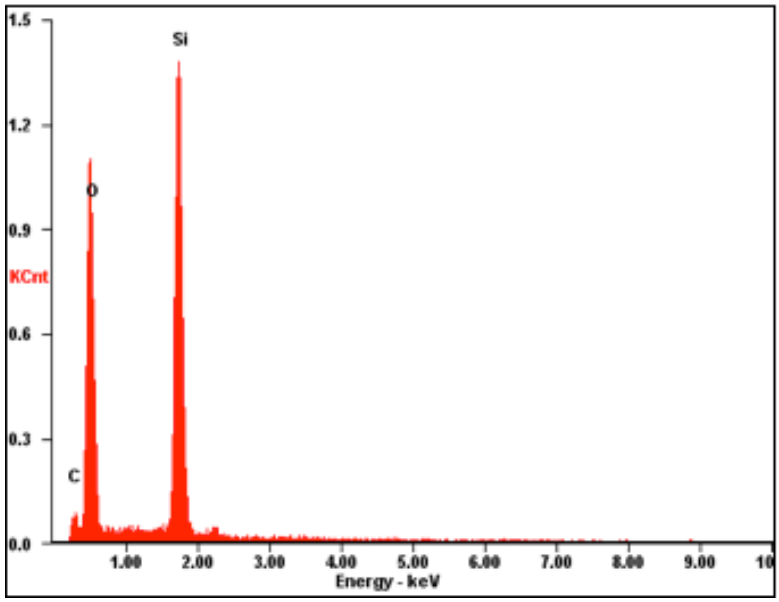

Element	Wt %	At %
SiK	100.00	100.00

Figure 131: Chemical composition of quartz, including a table with amount of element present.

Petrography

Sample CAN 3

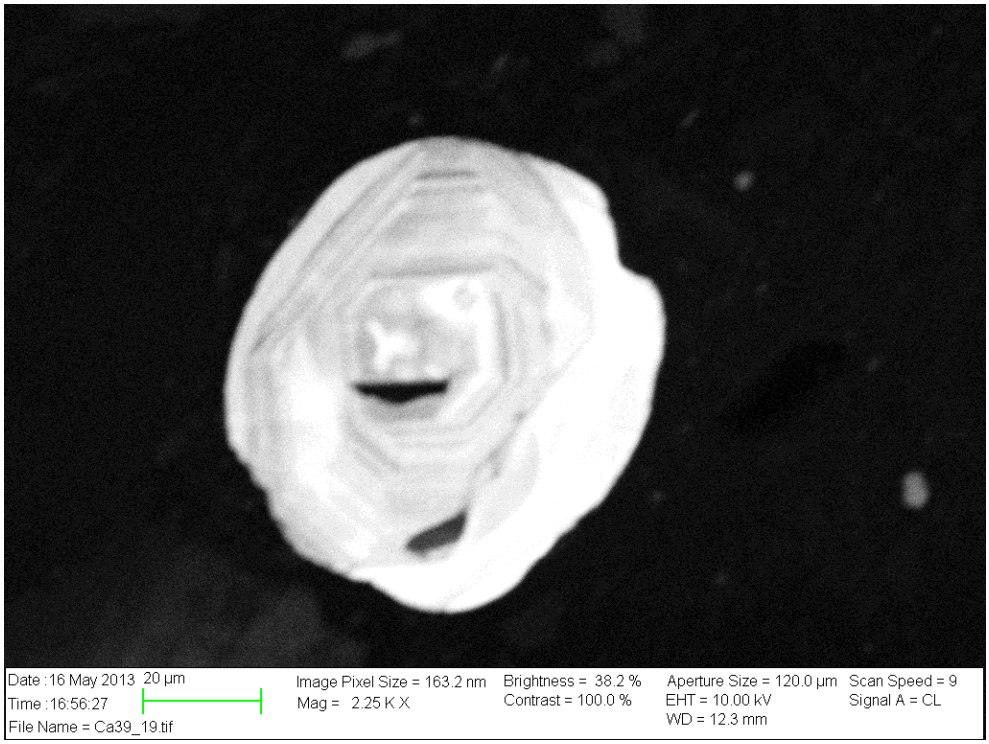

Figure 132: Zonation from a well rounded zircon, taken with a CL detector.

Figures below shows different heavy minerals found in the SEM:

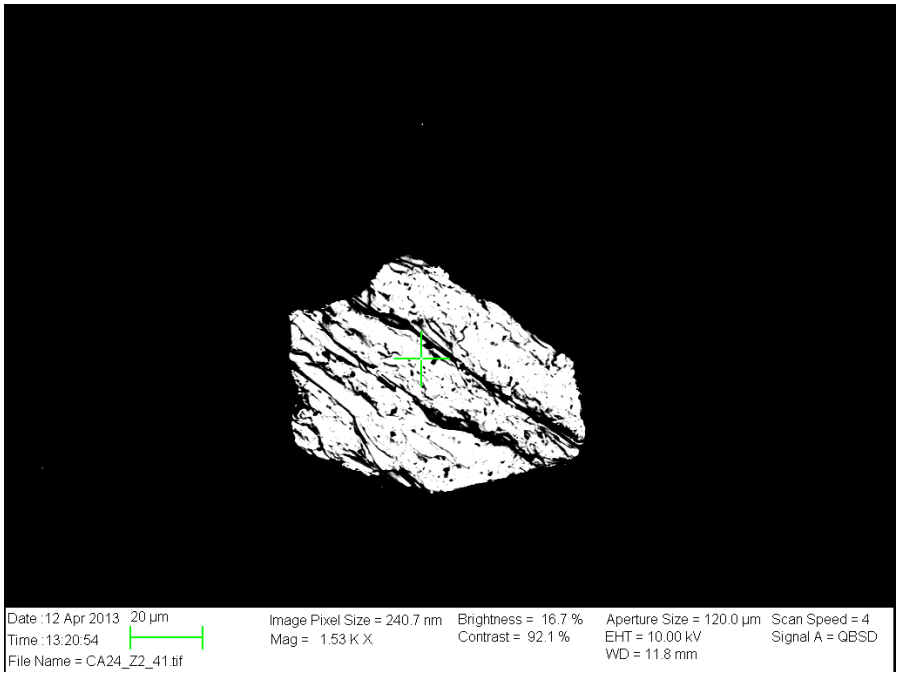

Figure 133: Zircon.

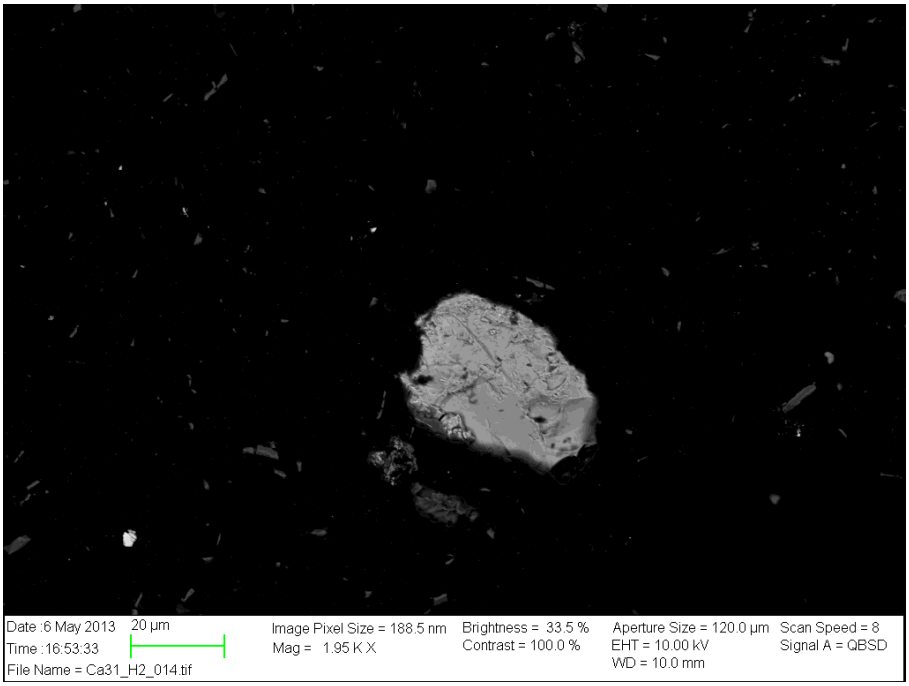

Figure 134: Rounded zircon.

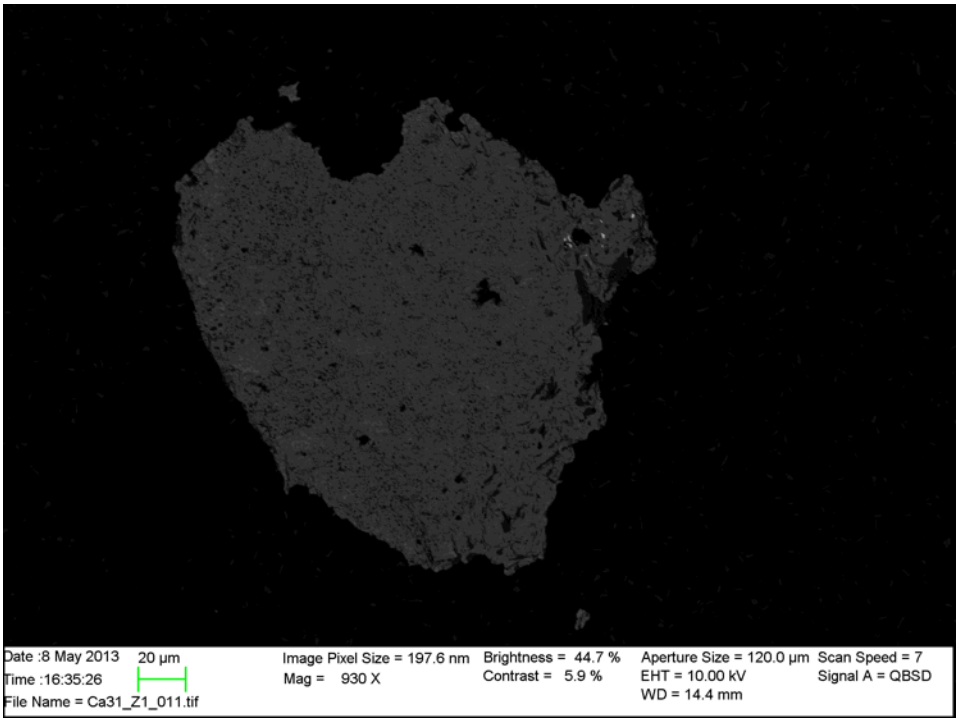

Figure 135: Large pyrite, with some muscovite in the upper right corner (white).

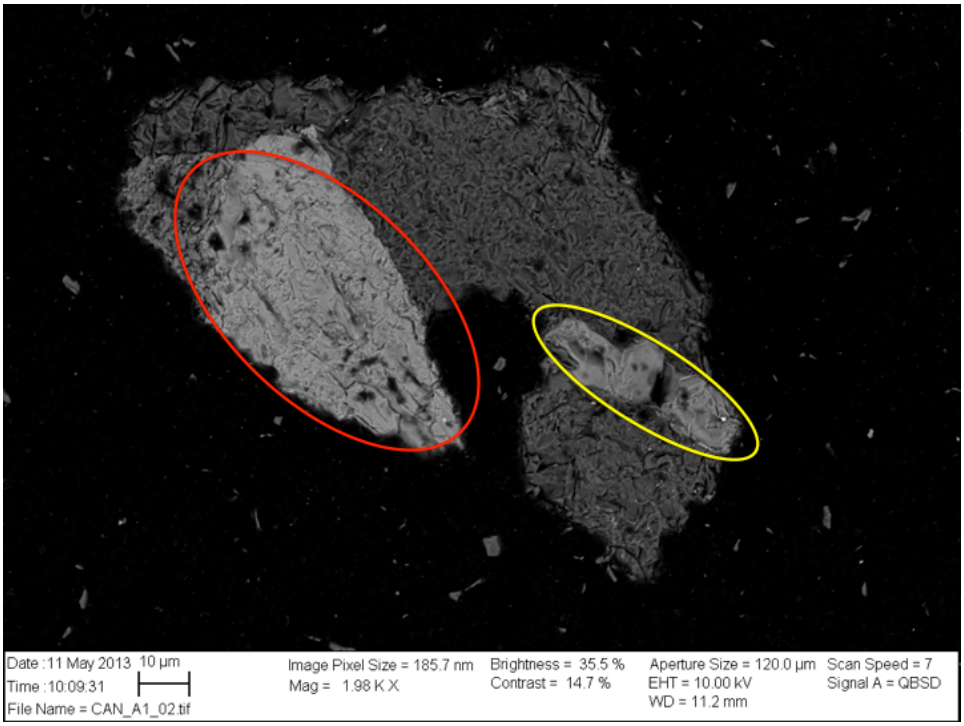

Figure 136: Red circle: rutile, yellow circle: apatite, intergrown mineral dark grey: quartz.

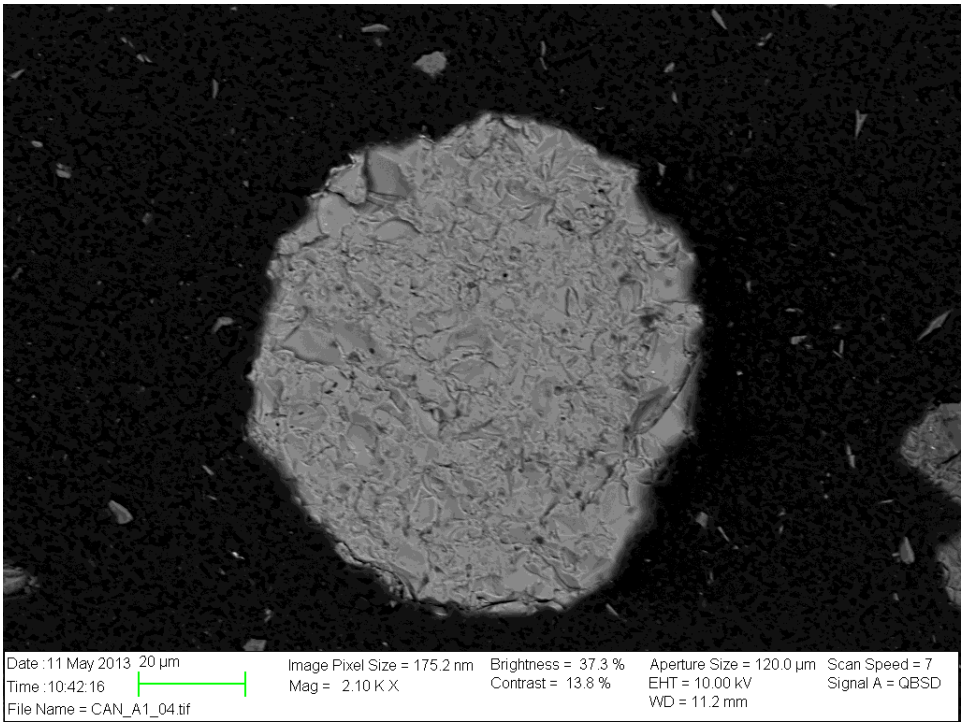

Figure 137: well-rounded apatite.

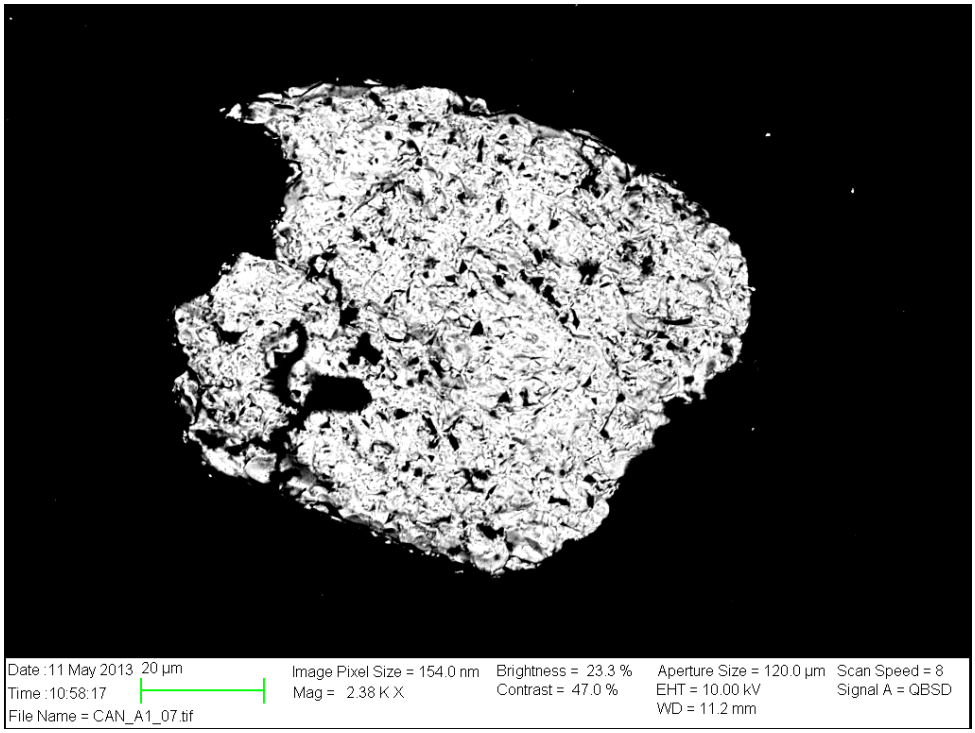

Figure 138: Rounded zircon.

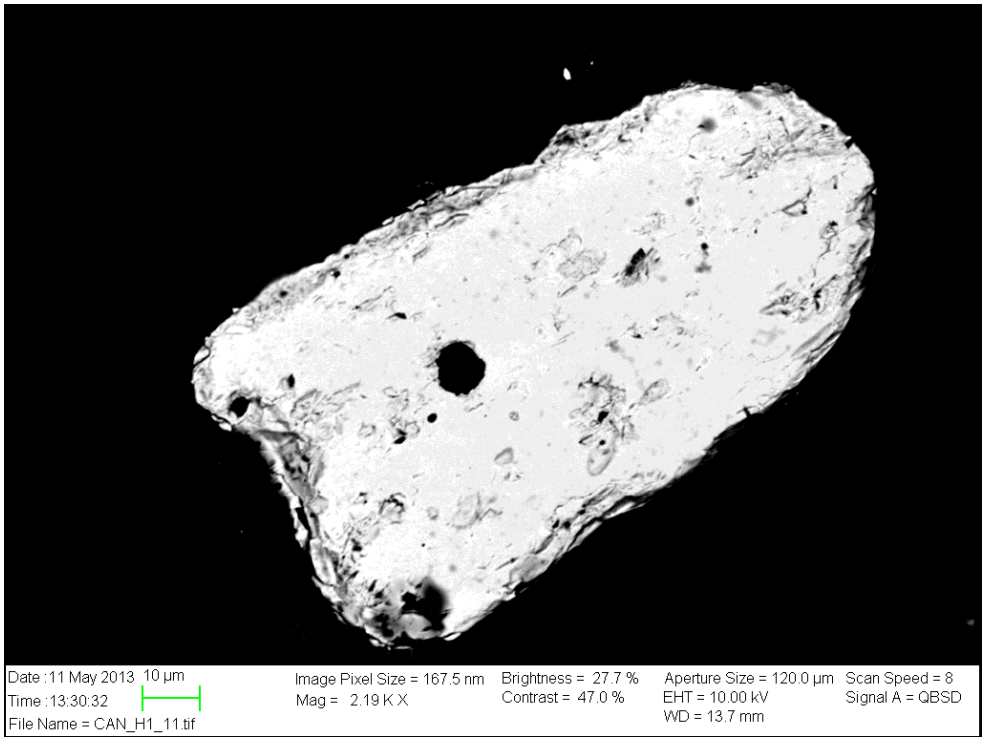

Figure 139: Angular zircon.

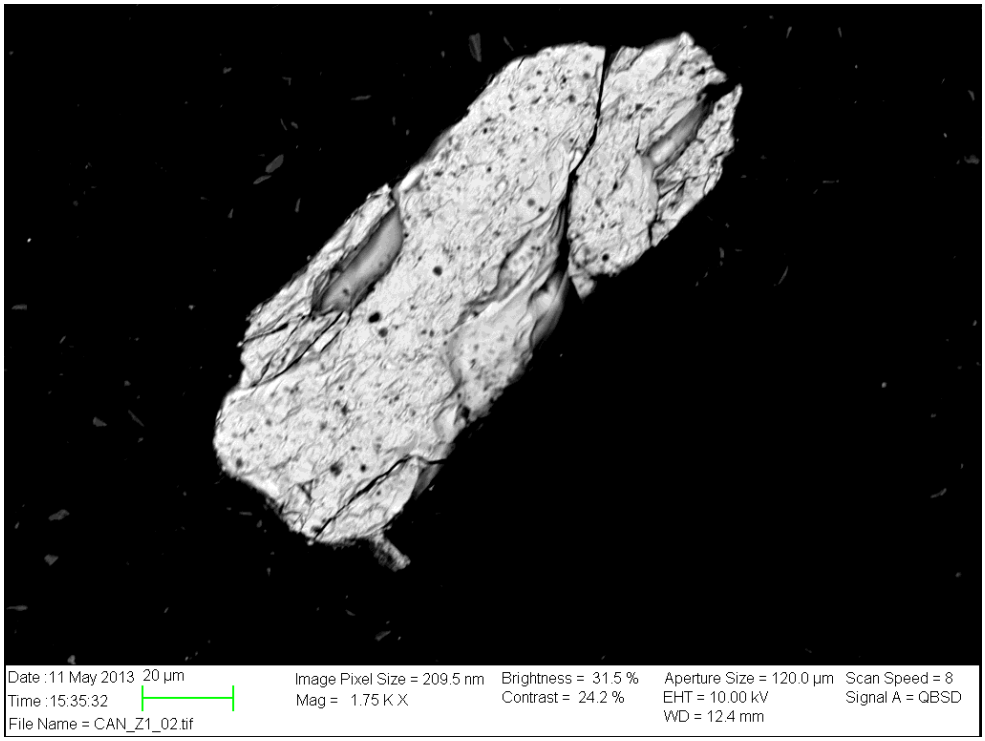

Figure 140: Elongated zircon.

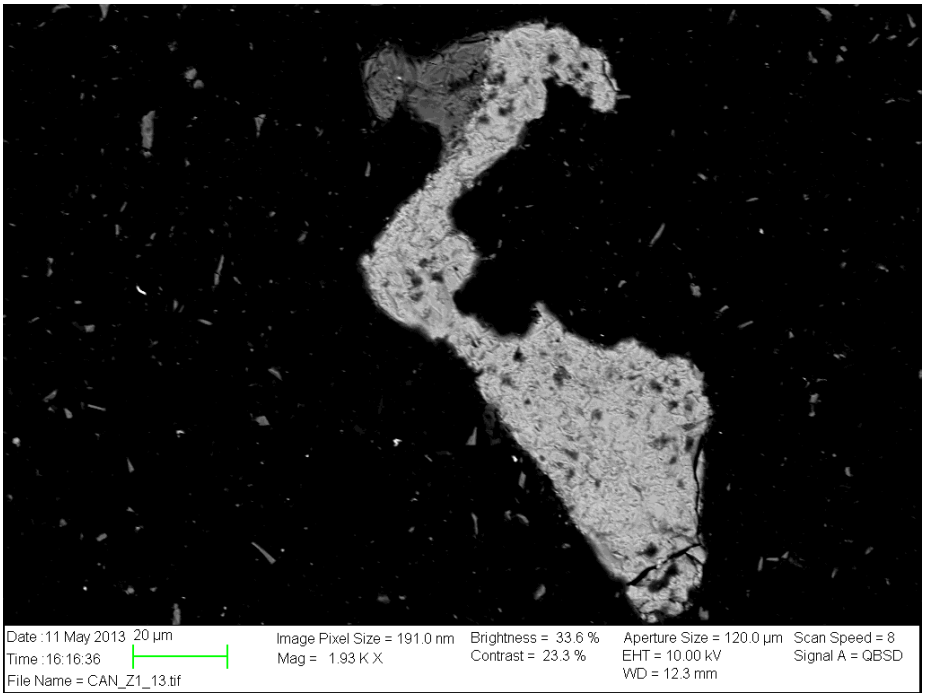

Figure 141: Rutile (light grey), in quartz (dark grey).

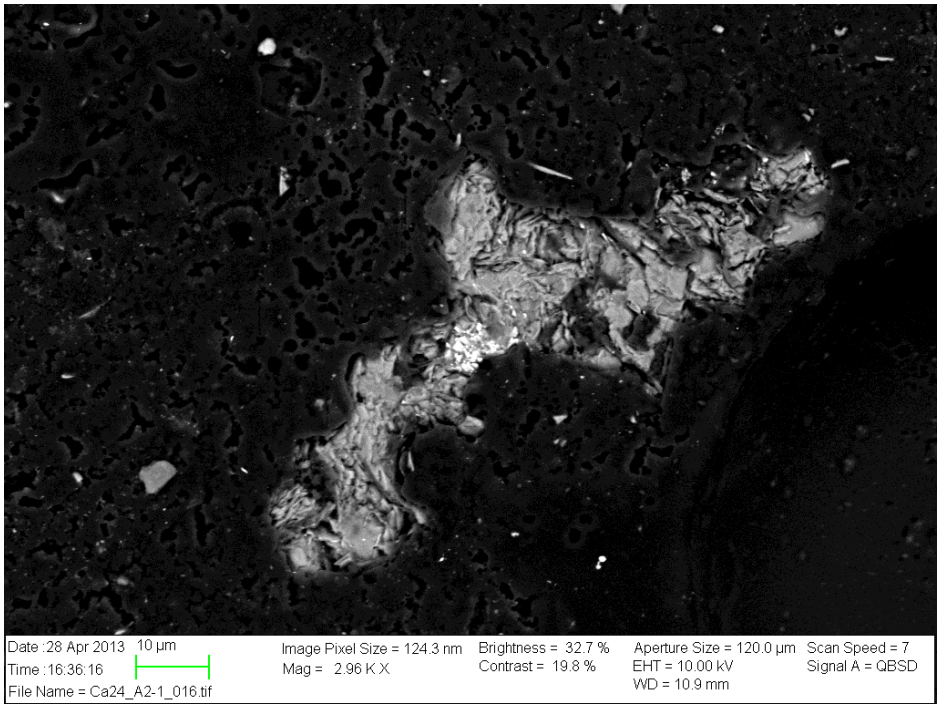

Figure 142: Muscovite dark gray, with a rutile in the middle (white).

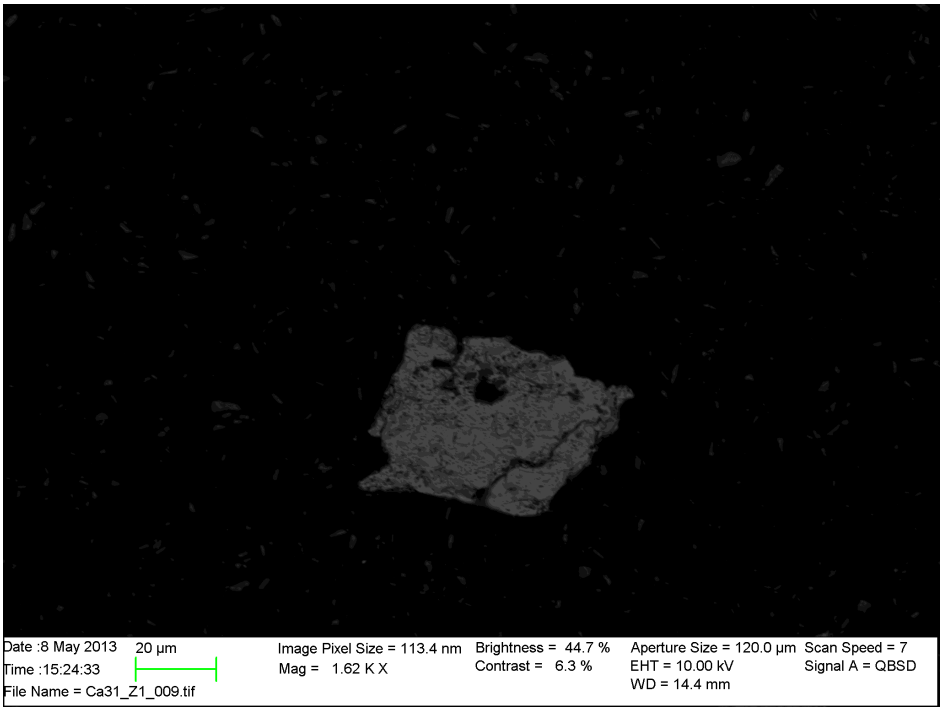

Figure 143: Angular/squared pyrite

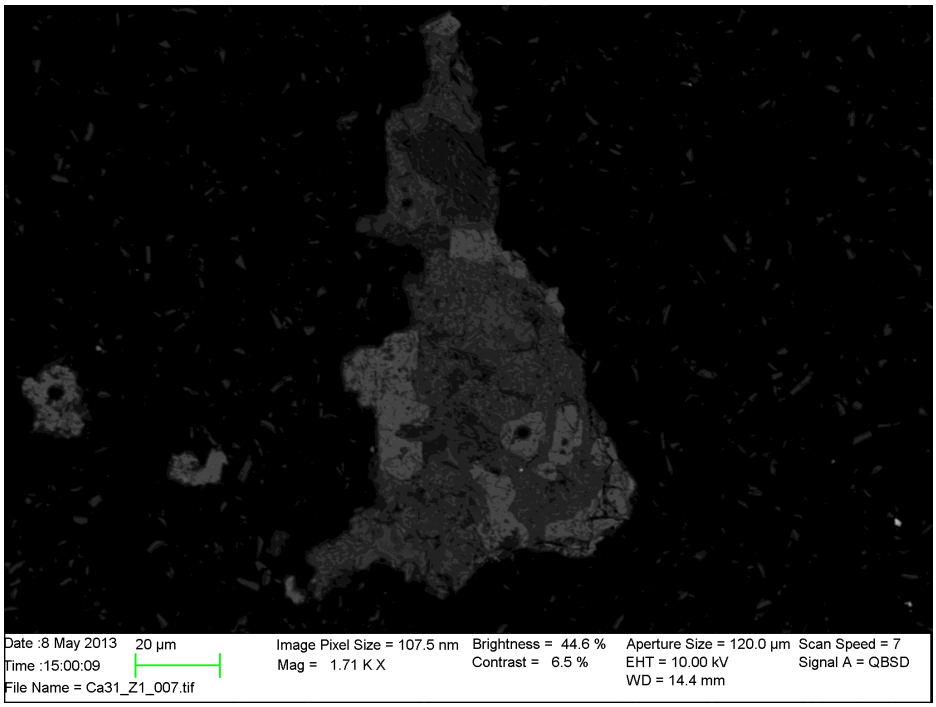

Figure 144: Lithoclast with a variety of heavy minerals: Light grey: pyrite, darker grey: apatite, dark/black in the top: muscovite.

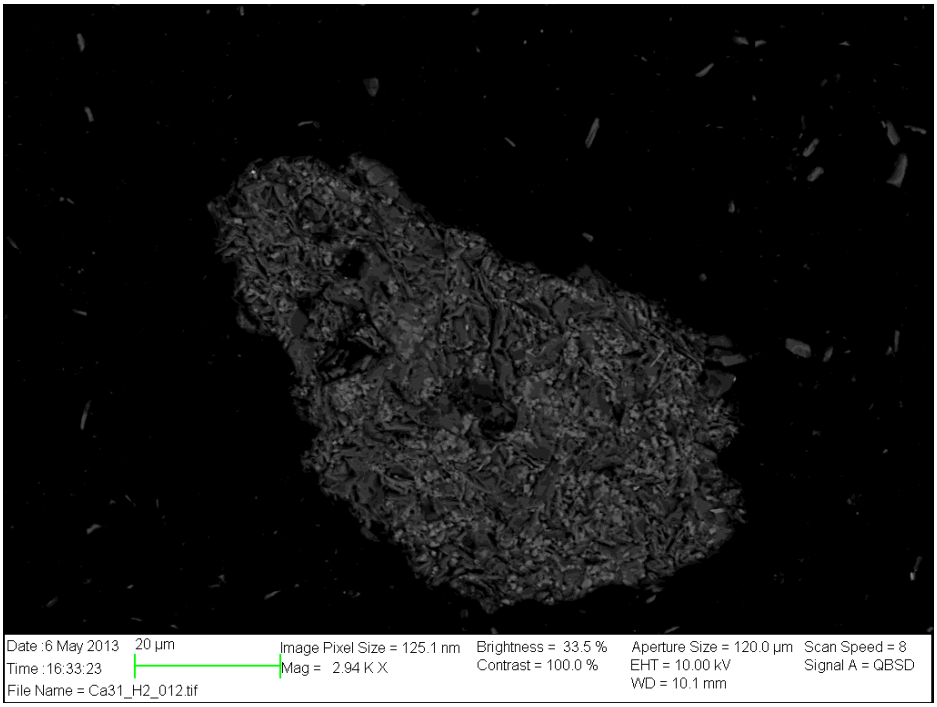

Figure 145: Apatite in light gray, muscovite in dark grey.

APPENDIX D- GEOCHEMISTRY

Basic data table:

Sample	Rock type	SiO2	Al2O3	Fe2O3	MgO	CaO	Na2O	K2O	TiO2	P2O5	MnO	Cr2O3		Ni	Sc	LOI	Sum	Ba	Be	Co	Cs	Ga	Hf	Nb
		%	%	%	%	%	%	%	%	%	%	%	PPM	PPM	PPM	%	%	PPM	PPM	PPM	PPM	PPM	PPM	PPM
		0.01	0.01	0.04	0.01	0.01	0.01	0.01	0.01	0.01	0.01	0.002		20	1	-5.1	0.01	1	1	0.2	0.1	0.5	0.1	0.1
CA1	Sand	64.83	16.64	7.61	1.5	0.19	0.42	3.39	0.79	0.2	0.07	0.011	75.35	<20	14	4.2	99.83	600	2	6.5	5.9	20.9	6.4	14.2
CA2	Shale	61.41	19.49	7.52	1.72	0.26	0.39	4.04	0.88	0.2	0.08	0.013	89.05	28	17	3.8	99.8	742	3	8.1	8.8	23.8	4.7	15.9
CA3	Shale	61.09	19.52	7.56	1.71	0.31	0.37	4.03	0.89	0.22	0.08	0.01	68.5	23	17	4	99.78	768	2	20.4	9.4	23.7	6	15.7
CA4	Sand	69.79	15.16	6.08	1.32	0.13	0.33	3.02	0.8	0.09	0.07	0.008	54.8	<20	13	3	99.83	586	<1	9.9	5.7	17.7	6.9	14
CA5	sand	65.07	17.48	6.89	1.6	0.25	0.39	3.53	0.81	0.17	0.07	0.011	75.35	34	15	3.5	99.8	674	<1	19.9	8.1	21	5.4	14.9
CA6	Shale	61.1	19.83	7.28	1.81	0.26	0.46	3.87	0.89	0.18	0.07	0.013	89.05	30	17	4	99.77	745	<1	17.9	9	24.5	5.3	16.1
CA7	Shale	61.52	19.6	7.08	1.72	0.26	0.51	3.76	0.89	0.19	0.07	0.012	82.2	24	17	4.2	99.8	712	<1	11	7.8	24.6	5	16.4
CA8	Shale	59.12	20.34	7.03	1.82	1.14	0.55	3.93	0.91	0.8	0.08	0.013	89.05	34	18	4	99.76	721	5	14.8	9.8	26.8	4.6	16.4
CA9	Shale	56.29	22.82	7.31	1.86	0.35	0.7	4.49	1.17	0.24	0.09	0.015	102.75	31	21	4.4	99.74	863	3	15.3	7.3	28.4	5.1	21.5
CA10	Shale	55.68	21.68	9.36	2.27	0.26	0.74	3.92	1.16	0.17	0.11	0.013	89.05	34	20	4.4	99.76	749	4	23.4	7.3	27.9	5.3	20.2
CA11	Shale	57.75	21.29	8.05	2.05	0.33	0.71	3.94	1.01	0.23	0.09	0.012	82.2	38	18	4.3	99.75	734	3	19.6	8.4	26.6	4.8	17.1
CA12	Shale	55.23	21.88	9.23	2.32	0.42	0.7	3.94	1.09	0.28	0.1	0.013	89.05	35	20	4.5	99.76	744	<1	20.3	8.5	27	4.5	18.9
CA13	Shale	54.29	22.92	8.85	2.26	0.34	0.73	4.2	1.05	0.25	0.09	0.014	95.9	50	21	4.8	99.76	763	3	16.4	9.7	29	4.4	18.1
CA14	Shale	57.24	21.2	8.67	2.19	0.32	0.82	3.77	1.02	0.23	0.11	0.013	89.05	33	19	4.2	99.77	676	7	16.8	8.2	27.2	5.2	18.8
CA15	Shale	56.72	21.07	9.05	2.27	0.32	0.74	3.73	1.04	0.23	0.1	0.013	89.05	43	18	4.5	99.76	673	<1	20.1	8	26	5.2	18.9
CA16	Shale	57.26	21.74	8.06	2.05	0.33	0.8	3.98	1.05	0.24	0.09	0.014	95.9	37	19	4.1	99.76	711	2	15.8	9.5	26	5.5	19.3
CA17	Shale	56.38	22.49	7.74	1.98	0.31	0.84	4.26	1.08	0.23	0.08	0.012	82.2	24	20	4.4	99.77	750	3	11	9.6	27.4	4.8	18.8
CA18	Shale	54.02	23.18	8.92	2.17	0.4	0.73	4.19	1.04	0.27	0.09	0.014	95.9	38	20	4.7	99.76	744	3	16.6	10.5	27.1	4.6	18.6
CA19	Shale	55.79	22.35	8.15	1.97	0.45	0.7	4.18	1.04	0.3	0.08	0.014	95.9	37	20	4.7	99.76	721	4	16.5	10.9	26.2	4.2	18.1
CA20	Shale	55.58	22.48	8.26	2	0.38	0.79	4.21	1.07	0.27	0.08	0.014	95.9	39	20	4.6	99.76	722	<1	14	10.4	29	5.4	19
CA21	Sand	66.03	19.28	3.36	0.86	0.19	0.92	4.31	1.17	0.14	0.02	0.015	102.75	<20	23	3.5	99.77	671	5	9.3	8.7	29.9	9.6	22
CA22	Sand	88.05	4.66	3.87	0.76	0.1	0.73	0.29	0.35	0.07	0.04	0.002	13.7	<20	3	1	99.93	51	<1	4.3	0.6	10	7.7	8.5
CA23	Shale	54.81	23.52	7.55	1.89	0.35	0.95	4.68	1.13	0.24	0.07	0.013	89.05	50	20	4.6	99.75	783	2	16.4	10.4	32.4	5.5	19.9
CA24	Shale	56.35	21.78	8.55	1.99	0.34	0.68	4.13	1.04	0.25	0.08	0.012	82.2	43	19	4.5	99.75	671	4	10.8	9.3	31	5.5	19
CA25	Shale	56.11	22.48	8.07	1.89	0.32	0.63	4.45	1.11	0.22	0.07	0.013	89.05	45	19	4.4	99.75	717	5	20.3	10.7	31.9	5.9	21.3
CA26	Shale	56.73	22.02	8.06	1.93	0.33	0.78	4.31	1.06	0.23	0.08	0.013	89.05	36	19	4.3	99.8	545	2	6.8	7.4	21.2	4.3	14.9
CA27	Sand	84.84	6.37	4.34	0.94	0.15	1.06	0.47	0.32	0.09	0.06	0.002	13.7	<20	3	1.3	99.93	99	<1	4.8	1	9.6	6	6.4
CA28	Shale	53.81	24.03	7.81	2.02	0.26	0.9	5.07	1.18	0.18	0.07	0.016	109.6	36	22	4.4	99.75	839	4	15	10.4	32.3	5.5	22
CA29	Shale	58.15	21.42	7.19	1.93	0.4	0.88	4.41	1.09	0.26	0.08	0.012	82.2	42	20	3.9	99.76	790	2	15.9	9.7	27.7	5.6	19.9
CA30	Shale	62.92	17.11	7.75	1.94	0.89	0.95	3.1	0.89	0.22	0.11	0.009	61.65	35	15	3.9	99.8	541	5	17.2	6.8	21.5	7	16.2
CA31	Sand	66.52	16.84	5.6	1.46	0.3	0.81	3.63	0.78	0.14	0.06	0.008	54.8	44	14	3.6	99.79	611	2	20.7	9.1	22.8	5.7	13.8
CA32	Shale	64.87	18.33	4.56	1.47	0.49	1.1	4.05	1.09	0.16	0.08	0.011	75.35	35	15	3.5	99.76	735	<1	14.1	7.9	24	7.4	18.8
CA33	Shale	54.6	8.45	8.11	3.75	11.41	0.26	0.93	0.44	0.1	0.88	0.006	41.1	20	8	10.9	99.83	213	2	9.1	1	12.2	3.3	7.8
CA34	Sand	69.61	15.25	3.35	1.05	1.49	1.04	3.4	0.82	1.04	0.07	0.007	47.95	75	14	2.7	99.8	647	3	17.4	5.7	19.9	8	14
CA35	Shale	64.42	17.33	4.38	1.21	0.86	0.54	4.33	0.63	0.12	1.12	0.009	61.65	151	24	4.7	99.71	1069	3	90.3	7.3	23.8	2.6	11.8
CA36	Shale	57.67	16.12	8.18	1.72	1.31	0.51	3.71	0.59	0.09	2.87	0.007	47.95	123	24	7	99.74	971	4	96.5	5.9	23.3	2.4	11.3
CA37	Shale	61.13	17.9	6.38	1.6	1.47	0.57	4.13	0.63	0.15	0.96	0.009	61.65	67	25	4.8	99.73	1053	5	46.2	8	24.9	2.8	12.4
CA38	Shale	60.65	18.22	7.22	1.76	0.94	0.53	4.04	0.65	0.12	0.93	0.009	61.65	122	23	4.6	99.72	1019	6	90.8	9	25.5	2.9	12.6
CA39	Shale	55.95	18.77	9.94	2.12	1.08	0.49	3.71	0.68	0.13	1.3	0.011	75.35	126	24	5.5	99.69	1009	5	138.2	8.2	27	3	13.3
CA40	Shale	41.62	15.45	10.33	1.8	2.65	0.35	3.2	0.56	1.5	10.86	0.008	54.8	109	21	11.4	99.74	826	2	53.7	5.8	36.8	2.3	10.8
CA41	Shale	53.28	20.05	10.96	1.89	0.58	0.63	4.19	0.75	0.15	1.73	0.01	68.5	131	24	5.4	99.66	1168	3	87.9	9.4	27.2	3.7	13.8
CA42	Shale	55.5	19.69	9.15	1.63	0.59	0.68	4.33	0.73	0.11	1.86	0.01	68.5	119	21	5.4	99.72	1192	4	51.7	10	32.2	3.4	13.5
CA43	Shale	60.34	17.84	10.34	1.9	0.25	0.54	3.41	0.67	0.15	0.63	0.01	68.5	104	24	3.6	99.64	896	2	86.9	6.8	22.1	2.8	12.7
CA44-1	Shale	53.36	20.63	13.06	1.94	0.26	0.8	3.86	0.77	0.18	0.75	0.011	75.35	81	21	4.1	99.73	963	7	66.3	11.2	28.3	3.3	14.7
CA44-2	Shale	54.23	20.74	12.15	1.84	0.27	0.83	3.97	0.77	0.18	0.7	0.011	75.35	66	21	4	99.73	1015	5	62.6	10.2	28	3.2	14.4
CA45	Shale	56.2	19.74	7.58	1.54	0.46	0.89	4.59	0.76	0.1	2.55	0.012	82.2	78	20	5.2	99.65	1088	4	50.4	10.4	27.3	3.4	14.3
CA46	Shale	55.52	21.5	9.06	1.73	0.45	0.8	4.48	0.81	0.14	0.83	0.01	68.5	77	20	4.4	99.72	1056	4	53.3	11.3	29	3.8	14.2
CA47	Shale	55.56	21.65	9.38	1.69	0.21	0.83	4.54	0.82	0.19	0.79	0.012	82.2	<20	21	4	99.7	1138	4	48.7	10.7	27.1	3.5	14.9
CA48	Shale	53.96	21.98	10.56	1.81	0.26	0.8	4.4	0.78	0.16	0.7	0.012	82.2	86	22	4.3	99.73	1110	7	55.8	10.7	31.1	3	16
CA49	Shale	55.72	21.19	10.41	1.73	0.24	0.91	4.33	0.8	0.15	0.61	0.013	89.05	59	22	3.6	99.68	1166	3	46.8	10.3	26.6	4.3	13.4
CA50	Shale	54.84	22.34	9.96	1.68	0.21	0.78	4.55	0.83	0.14	0.56	0.011	75.35	75	22	3.8	99.7	1236	5	53.8	13.1	30.4	3.7	15.5
CA51	Shale	54.05	22.22	10.59	1.72	0.21	0.77	4.55	0.83	0.07	0.55	0.012	82.2	50	22	4.1	99.65	1228	6	55.1	13.1	26.9	3.5	15.3
CA52	Shale	54.71	20.02	9.18	1.57	1.72	0.83	4.16	0.73	0.33	1.22	0.012	82.2	42	19	5.2	99.74	1028	5	36.9	10	29.4	3.2	14.5
CA53	Shale	56.71	20.81	9.96	1.61	0.22	0.88	4.33	0.82	0.11	0.64	0.013	89.05	42	20	3.6	99.7	1148	2	54.8	11.1	24.7	3.7	15.2
CA54	Shale	51.92	21.22	11.77	1.71	0.98	0.71	4.2	0.76	0.15	1.15	0.01	68.5	73	21	5.1	99.73	1076	5	52.4	10.9	30.5	2.9	14.2
CA55	Shale	53.79	20.92	12.65	1.84	0.22	0.8	3.79	0.78	0.15	0.73	0.014	95.9	76	20	4	99.71	1133	5	72.5	9.9	30.7	3.4	14.9
CA56	Shale	54.83	21.4	9.16	1.44	0.6	0.93	4.48	0.74	0.13	1.35	0.009	61.65	52	20	4.6	99.72	1228	6	41.7	11.2	28.1	3.3	13.8
CA57	Shale	47.55	18.77	17.07	2.18	1	0.74	2.63	0.64	0.24	2.68	0.013	89.05	117	21	6.2	99.72	775	10	98.2	6.3	27.6	3.8	13.2
CA58	Shale	54.03	20.83	11.7	1.79	0.39	0.98	3.98	0.74	0.24	0.69	0.011	75.35	93	22	4.2	99.58	1010	4	66	10.5	25.5	2.8	12
CA59	Shale	52.14	19.21	15.91	2.15	0.26	0.85	2.74	0.67	0.18	1.14	0.013	89.05	145	24	4.3	99.62	858	<1	121.8	5.7	29.5	3.1	13.3
CAN1	Sand	73.55	12.76	5.58	1.26	0.25	0.62	2.13	0.63	0.18	0.07	0.009	61.65	27	11	2.8	99.83	524	2	8.4	5.8	16.9	7.8	13
CAN2	Sand	72.27	13.59	5.63	1.32	0.27	0.67	2.34	0.66	0.18	0.07	0.008	54.8	22	11	2.8	99.83	514	2	13.3	<0.1	<0.5	<0.1	17.5
CAN3	Shale	65.59	17.36	6.41	1.65	0.25	0.52	3.14	0.83	0.18	0.08	0.011	75.35	32	14	3.8	99.78	686	2	14.4	11.2	20.8	4.5	17.3
CAN4	Shale	64.08	18.34	6.35	1.64	0.23	0.56	3.54	0.83	0.19	0.07	0.012	82.2	27	15	4	99.79	755	3	9.1	11.5	23.6	5.9	15.6
CAN5	Sand	66.05	17.25	6.16	1.51	0.24	0.4	3.55	0.94	0.15	0.05	0.01	68.5	22	14	3.5	99.79	682	3	9.3	8.1	21.5	9.4	16.9
CAN6	Sand	85.26	6.67	3.3	0.83	0.15	0.94	0.82	0.48	0.09	0.05	0.004	27.4	<20	5	1.3	99.92	183	<1	5.4	1.4	7.5	8.3	9.2
CAN7	Sand	88.25	5.87	1.78	0.43	0.11	1.12	0.8	0.38	0.08	0.02	0.005	34.25	<20	4	1	99.9	147	2	3.3	1.2	3.9	11.1	7.5
CAN8	Shale	59.2	20.2	7.77	1.77	0.31	0.4	4.34	1	0.22	0.07	0.013	89.05	48	17	4.5	99.78	716	5	16.7	8.6	25	6.6	18.4
CAN9	Shale	55.9	22.3	7.98	1.93	0.25	0.47	4.83	1.07	0.19	0.08	0.014	95.9	57	18	4.7	99.76	793	2	17.2	9.7	27.8	6.5	20.7
CAN10	Sand	89.55	4.47	2.13	0.5	0.1	0.82	0.49	0.84	0.07	0.04	0.004	27.4	23	4	0.8	99.78	91	2	3.6	0.9	2.2	37.8	14.8
CAN11	Sand	65.79	17.61	5.71	1.51	0.19	0.34	3.95	0.97	0.14	0.04	0.01	68.5	24	14	3.5	99.78	684	<1	7.4	5.9	21.2	10.9	18.1
CAN12	Sand	68.22	16.62	5.01	1.38	0.23	0.67	3.67	0.91	0.16	0.04	0.01	68.5	32	13	2.8	99.77	680	<1	9.3	6.8	19.2	11	19.6
CAN13	Sand	75.79	12.39	3.4	0.99	0.24	0.43	2.57	0.78	0.14	0.04	0.006	41.1	<20	10	3	99.79	434	<1	5.3	5.6	15.1	12	13.9

Rb	Sn	Sr	Ta	Nb/Ta	Th	U	U/Th	V	W	Zr	Zr/Hf	Y	La	Ce	Pr	Nd	Sm	Eu	Gd	Tb	Dy	Ho	Er	Tm
PPM	PPM	PPM	PPM		PPM	PPM		PPM	PPM	PPM		PPM	PPM	PPM	PPM	PPM	PPM	PPM	PPM	PPM	PPM	PPM	PPM	PPM
0.1	1	0.5	0.1		0.2	0.1		8	0.5	0.1		0.1	0.1	0.1	0.02	0.3	0.05	0.02	0.05	0.01	0.05	0.02	0.03	0.01
139.8	3	87.3	1.1	12.91	10.3	2.5	0.24	94	1.8	225.1	35.17	28.3	45.1	89.7	9.65	34.5	6.23	1.22	5.37	0.82	4.89	1.02	3.06	0.45
165.4	3	102.7	1.1	14.45	16.2	2.8	0.17	110	1.8	180.5	38.40	35	54.7	111.2	12.07	45	7.61	1.57	6.75	1.08	6.49	1.33	3.69	0.5
168	3	108.3	1.1	14.27	17.6	3.2	0.18	110	1.7	202.1	33.68	39.2	58.3	117.2	13.31	52.7	9.33	1.96	8.79	1.2	7.22	1.41	4.14	0.59
122.8	2	81.3	1.1	12.73	13.1	3	0.23	90	1.5	245.6	35.59	23.6	47.8	96.6	10.38	34.5	5.63	1.26	4.84	0.68	4.51	0.84	2.46	0.41
151.1	3	115.1	1.1	13.55	15.7	3.2	0.20	91	1.7	192.7	35.69	32.9	53.7	110.3	12.45	48	8.82	1.76	7.78	1.08	6.11	1.23	3.35	0.49
168.9	3	169.8	1.2	13.42	16.2	3.5	0.22	107	1.9	187.1	35.30	34.5	55.6	115.3	12.85	48.3	8.54	1.77	7.85	1.14	6.91	1.35	3.62	0.52
167.1	3	169.9	1.1	14.91	16.1	3.1	0.19	110	1.8	193	38.60	38.2	53.7	108.7	12.4	44.8	8.95	1.76	8.01	1.24	7.46	1.43	4.15	0.6
173.1	3	210.5	1.1	14.91	16.7	3.9	0.23	108	1.9	170	36.96	66.6	66.8	143.3	16.57	69.4	17.58	3.57	18.68	2.41	13.01	2.3	5.9	0.79
196	3	203.7	1.5	14.33	19.5	4	0.21	136	2.3	176.9	34.69	52.4	67.8	142.6	16.11	64.4	12.04	2.4	11.29	1.59	9.77	1.83	4.96	0.76
169.2	4	161.3	1.3	15.54	18.7	3.1	0.17	138	2	174.8	32.98	41.6	69.3	141.5	16.23	63.4	11.77	2.31	9.58	1.37	8.44	1.62	4.47	0.65
172.2	4	179.3	1.3	13.15	16.6	3.1	0.19	120	13.8	161.7	33.69	41.8	63	127.7	14.56	55.5	10.25	2.11	9.36	1.31	8.04	1.52	4.13	0.63
175.5	4	185.2	1.5	12.60	18.4	3.5	0.19	131	2	158.6	35.24	44.8	61.6	126.7	14.2	51.7	10.5	2.17	9.81	1.43	8.06	1.68	4.63	0.65
186.1	4	201	1.4	12.93	17.7	3.6	0.20	137	1.9	144.8	32.91	44.1	66.2	137.5	15.75	61.2	12.1	2.43	10.21	1.45	8.55	1.56	4.53	0.65
165.3	3	174.6	1.3	14.46	17	3.5	0.21	124	10.9	168.2	32.35	39.8	59.2	124.6	13.9	53.9	10.19	2.1	9.13	1.28	8.07	1.4	4.01	0.61
163.9	4	175.8	1.4	13.50	17.2	3.7	0.22	121	2.4	179.3	34.48	39.5	58.9	120.7	13.59	49	9.54	1.91	8.55	1.3	7.48	1.46	3.95	0.61
174.3	4	185.3	1.4	13.79	17.6	3.5	0.20	125	1.9	197.1	35.84	44	65.9	133.4	14.94	60.3	10.71	2.16	9.57	1.35	8.28	1.56	4.48	0.67
183.9	4	194.1	1.4	13.43	18.9	3.7	0.20	136	2.4	179.5	37.40	46.5	71.6	143.9	16.32	64.3	11.95	2.27	10.48	1.52	9.44	1.72	4.86	0.7
182.1	4	198.4	1.4	13.29	18.7	3.7	0.20	133	2.2	155.5	33.80	46.2	72.3	142.6	16.41	63.5	11.76	2.43	10.52	1.49	9.12	1.62	4.47	0.7
184.6	3	205.1	1.5	12.07	17.8	4.1	0.23	126	2	170.3	40.55	44.7	67.3	133.9	15.49	58.4	11.53	2.39	10.29	1.49	8.52	1.56	4.49	0.68
177.8	3	189	1.5	12.67	19.3	4.1	0.21	130	2	180.3	33.39	45	67.5	137.7	15.65	60.2	11.6	2.26	10.44	1.47	8.49	1.68	4.49	0.69
181.1	5	117.2	1.5	14.67	21.1	5.5	0.26	135	2.2	318.8	33.21	31.3	83.2	180.4	19.82	77.8	14.07	2.34	9.25	1.15	6.71	1.24	3.93	0.61
11.6	2	18	0.5	17.00	5.9	1.1	0.19	28	0.6	290.4	37.71	8.6	19.3	42.4	4.39	16.9	2.71	0.59	2.38	0.31	1.77	0.35	1.13	0.18
197.5	5	181.7	1.4	14.21	20.5	4.8	0.23	136	2.4	213.3	38.78	42	68.2	142.7	15.76	57.1	11.37	2.36	9.66	1.46	9.15	1.63	4.61	0.69
173.3	5	163.8	1.4	13.57	18.7	3.9	0.21	126	2.6	199.3	36.24	40	66.3	135.3	14.96	58.9	10.87	2.18	9.7	1.41	7.86	1.64	4.42	0.69
189.8	5	184	1.4	15.21	20	4.4	0.22	127	2.4	198.4	33.63	41.9	66.5	140.4	15.73	60.9	11.33	2.36	10.4	1.48	8.93	1.6	4.81	0.71
139.4	3	117.9	1	14.90	14.9	3	0.20	103	1.5	150	34.88	31	47.8	97.4	10.89	41.7	7.82	1.61	7.2	1.1	6.94	1.22	3.33	0.53
19.9	2	28.6	0.5	12.80	5.4	1.3	0.24	31	0.8	252.6	42.10	17.2	20.2	44.3	4.61	18.9	3.6	0.73	4.01	0.61	3.91	0.72	1.98	0.3
209.2	4	135.1	1.5	14.67	20.9	5	0.24	139	2.3	206.5	37.55	38	69.7	143.2	16.08	60.4	11.22	2.13	8.91	1.24	7.25	1.47	4.43	0.67
181.6	5	133.6	1.4	14.21	18.4	3.5	0.19	123	3	203.5	36.34	40.9	62.6	133.3	14.67	56.8	10.69	2.11	9.66	1.42	8.86	1.69	4.78	0.68
126	4	112.7	1.3	12.46	14.3	3.2	0.22	100	1.8	253.8	36.26	32.7	50	104.5	11.6	45.3	8.66	1.75	7.82	1.13	6.43	1.35	3.73	0.56
151.1	4	117.6	1.1	12.55	14.3	3.4	0.24	98	1.6	221.3	38.82	29.2	53	108.8	12.19	45.6	8.21	1.71	7.27	1.01	6.29	1.2	3.03	0.51
157.8	5	135.8	1.5	12.53	17.6	4.5	0.26	110	2	272	36.76	34.4	59.8	128.7	14.02	55.5	9.74	1.85	8.58	1.28	7.53	1.39	4.02	0.62
36.6	2	239.7	0.7	11.14	8.2	1.7	0.21	48	0.9	137.9	41.79	18	27	55	5.95	22.9	4.57	1	4.79	0.67	4.14	0.73	2.26	0.33
135.7	5	129.3	1.2	11.67	15.3	4	0.26	105	5.9	315.6	39.45	45.8	56.4	127.7	12.31	50.1	10.15	2.13	10.78	1.51	9.15	1.85	4.96	0.7
189.6	4	113.4	0.7	16.86	14.5	1.8	0.12	120	3.9	94.2	36.23	33.5	41.5	197.9	9.99	37.5	7.65	1.61	7.41	1.17	6.63	1.22	3.68	0.57
150.9	4	115.3	0.8	14.13	14.4	1.8	0.13	114	4.2	91.8	38.25	25.7	43.4	189.6	10.21	36.6	7.49	1.53	7.18	0.98	5.9	1.2	3.28	0.52
190.6	4	150.9	0.8	15.50	14.8	2.3	0.16	129	4.6	94.9	33.89	31	39.4	152.9	9.19	34.4	7.26	1.49	6.48	1.06	5.84	1.2	3.62	0.54
169.9	4	115	0.9	14.00	15.4	2.2	0.14	128	5.1	96	33.10	27.4	44.5	164.7	9.89	38.8	7.12	1.58	6.87	1.01	5.91	1.21	3.33	0.55
175	5	107.9	1.2	11.08	14.9	2.3	0.15	136	3.8	109.3	36.43	38	48.2	163.1	11.15	42.5	8.28	1.78	7.95	1.24	6.98	1.42	4.27	0.63
130.2	4	117.3	0.7	15.43	12.6	3.7	0.29	164	3.2	82.8	36.00	46	49.8	185.7	10.78	44.1	11.26	2.37	12.43	1.59	8.12	1.66	5.13	0.71
175.1	3	105.3	1	13.80	15.1	2.4	0.16	154	4.2	108.8	29.41	35.3	50.4	173	11.7	46.8	9.57	1.78	8.13	1.23	6.54	1.29	3.81	0.65
184.8	5	116.9	1.1	12.27	15.6	2.4	0.15	136	3	117.1	34.44	33.6	51.4	174.7	12.14	43.3	9.31	1.81	8.54	1.26	8.12	1.48	3.99	0.62
143.7	3	81.9	0.9	14.11	14.2	2.8	0.20	203	3.6	107	38.21	57.3	78.7	241.1	18.28	72.8	13.44	2.69	12.69	2.08	12.54	2.38	6.59	0.97
166.7	4	74.8	1.2	12.25	15.4	2.4	0.16	149	3	113.6	34.42	36.8	57.2	157.6	13.07	51	9.96	2.1	9.37	1.42	8.64	1.59	4.63	0.66
168.8	5	79.5	0.9	16.00	16.2	2.6	0.16	154	2.6	116.2	36.31	34.8	55.8	152.1	12.88	52.7	9.09	1.95	9	1.35	7.95	1.52	4.26	0.66
193.9	4	87	1.1	13.00	14.8	2.8	0.19	198	4.6	115.4	33.94	27.8	39.2	88	9.18	38.7	6.02	1.22	5.33	0.85	5.23	1.03	3.17	0.44
190.1	5	82.3	1	14.20	15.5	2.4	0.15	205	4.7	122	32.11	33.6	45	111.1	10.57	35.3	7.83	1.66	7.41	1.11	6.32	1.38	3.53	0.54
199.7	4	84.6	1.2	12.42	15.3	2.6	0.17	189	3.6	126.8	36.23	34.8	44.3	108.6	10.71	38.1	8.13	1.54	6.93	1.07	6.48	1.33	3.64	0.57
183.2	5	86.3	1.3	12.31	15.8	2.9	0.18	156	3.6	111.9	37.30	38	48.1	142.7	11.44	45.7	8.58	1.86	7.83	1.25	7.74	1.47	3.94	0.58
182.6	4	88	1.1	12.18	15.3	2.6	0.17	152	3.5	128.5	29.88	39.1	49.2	133.4	11.57	46.8	9.01	1.66	8.04	1.21	7.78	1.48	4.5	0.62
194.4	5	89.9	1.1	14.09	17.3	2.6	0.15	176	3.4	134.9	36.46	38.6	47.6	138.4	12.09	46	8.92	1.77	8.36	1.27	7.56	1.42	4.07	0.61
199.9	4	86.2	1.1	13.91	16.6	2.8	0.17	160	3.9	129	36.86	34.8	46.5	125.8	11.39	41	8.06	1.54	7.81	1.16	7.52	1.36	3.37	0.6
175.5	5	102.6	1	14.50	14.1	2.7	0.19	148	2.7	106.4	33.25	34.9	45.1	117	11.06	46.3	9.41	1.74	8.76	1.33	6.9	1.25	3.74	0.47
193.3	4	83.8	1.4	10.86	15.7	2.5	0.16	172	4.9	129.9	35.11	32.5	45.6	111.8	10.84	41.7	8.57	1.51	7.15	1.06	6.11	1.26	3.07	0.5
178.3	6	93.2	0.9	15.78	15.9	2.3	0.14	163	2.8	105.5	36.38	34.6	50	154.1	12.21	48.6	8.74	1.86	8.19	1.24	6.98	1.38	3.77	0.67
179.5	5	79.5	1	14.90	17	2.6	0.15	179	3.5	124.6	36.65	45	60.7	168.9	14.55	54.8	9.91	2.3	9.93	1.54	9.5	1.72	4.2	0.74
191.6	4	98	0.9	15.33	14	2.2	0.16	137	3	108.5	32.88	31.5	43.1	131.2	10.4	41.6	8	1.68	7.16	1.08	6.54	1.19	3.57	0.52
121	5	84.3	0.9	14.67	16.8	2.4	0.14	170	2.9	120.2	31.63	62.7	79.9	217.2	18.83	69.7	13.67	2.78	14.04	2.11	12.01	2.25	6.43	0.99
165.4	5	94.6	0.9	13.33	15.7	2.7	0.17	207	4.6	102.1	36.46	39.2	46.4	149.6	11.4	45.9	9.59	1.98	9.33	1.27	7.94	1.42	4.28	0.57
132	5	79.5	0.8	16.63	15.9	2.7	0.17	364	6.1	117.9	38.03	64.7	83.6	242.7	18.88	73.3	13.95	3.11	13.2	2.15	13.14	2.62	7.19	1.1
100.4	3	91.9	0.8	16.25	12.7	3.1	0.24	76	0.8	305.4	39.15	30.2	32.1	67.6	7.95	31	6.12	1.25	5.36	0.85	4.79	0.99	3.06	0.49
<0.1	31	94.6	75.4	0.23	<0.2	<0.1		<8	<0.5	274.3		26.7	32	66.5	<0.02	<0.3	<0.05	<0.02	<0.05	<0.01	<0.05	<0.02	<0.03	<0.01
149.4	4	145.6	1.1	15.73	15.5	3.3	0.21	103	1.8	184	40.89	33.8	59.6	123.4	14.45	52.5	9.92	1.97	8.1	1.19	6.79	1.13	3.5	0.51
162.1	4	130.3	1.2	13.00	16.4	3.4	0.21	111	1.7	180.4	30.58	32.4	41	87.7	10.5	40.4	7.37	1.58	6.53	1.05	6.71	1.22	3.42	0.49
143.2	4	78	1.3	13.00	15.6	3.3	0.21	107	1.9	313	33.30	37.2	43.2	88.4	9.08	33.2	6.58	1.47	7.14	1.07	6.86	1.35	4.22	0.61
30.9	<1	30.4	0.7	13.14	7.3	1.8	0.25	34	0.9	309.6	37.30	21.5	18.8	39.4	4.18	17	3.37	0.61	3.37	0.49	3.39	0.71	2.09	0.31
30.9	<1	25.5	0.6	12.50	6.8	1.7	0.25	24	0.9	398.4	35.89	12.7	22.3	43.7	5.08	21.3	3.71	0.67	3.04	0.45	2.51	0.53	1.35	0.2
171.7	4	68.9	1	18.40	17.9	3.5	0.20	126	2.4	221.1	33.50	39.3	44	110.8	10.89	43.1	7.81	1.6	7.81	1.25	6.66	1.37	3.8	0.58
191.4	4	69	1.1	18.82	19.6	3.4	0.17	138	2.1	229.8	35.35	42.3	47	111	12.21	49.4	9.93	1.93	9.15	1.41	8	1.67	4.75	0.71
17.6	2	22.5	1.2	12.33	14.6	4	0.27	24	0.9	1362.5	36.04	32	38	74.5	8.47	30.6	5.56	1.12	5.5	0.87	4.99	1.03	3.48	0.52
148	3	55.7	1.2	15.08	16.9	4.3	0.25	98	1.7	366.9	33.66	39.4	48	96	10.93	42.8	7.48	1.71	7.38	1.18	7.52	1.43	4.43	0.72
139.1	4	60.3	1.3	15.08	16.4	3.7	0.23	109	2	373.4	33.95	42	56.2	119.2	13.98	51.6	10.1	2.11	8.63	1.43	7.53	1.42	4.4	0.68
93.8	3	35.6	0.9	15.44	13.1	3.3	0.25	66	1.7	454.3	37.86	29.9	43.9	89.2	9.9	37.5	6.79	1.36	6.45	0.89	5.44	1.1	3.16	0.51

Yb	Lu	TOT/C	TOT/S	Mo	Cu	Pb	Zn	Ag	Ni	As	Au	Cd	Sb	Bi	Hg	Tl	Se
PPM	PPM	%	%	PPM	PPM	PPM	PPM	PPM	PPM	PPM	PPB	PPM	PPM	PPM	PPM	PPM	PPM
0.05	0.01	0.02	0.02	0.1	0.1	0.1	1	0.1	0.1	0.5	0.5	0.1	0.1	0.1	0.01	0.1	0.5
2.98	0.42	0.15	0.44	1.7	4.8	29.5	51	<0.1	14.4	8.5	<0.5	<0.1	0.9	0.3	<0.01	<0.1	<0.5
3.4	0.54	0.19	0.03	0.3	20.8	10.9	85	<0.1	19.8	13.7	<0.5	<0.1	<0.1	0.3	<0.01	<0.1	<0.5
3.52	0.53	0.18	0.09	0.3	33.4	23.5	110	<0.1	38	13.9	<0.5	<0.1	<0.1	0.5	<0.01	<0.1	<0.5
2.53	0.42	0.17	<0.02	1	7.9	11.3	57	<0.1	27.2	5.2	<0.5	<0.1	<0.1	0.2	<0.01	<0.1	<0.5
3.43	0.49	0.18	0.48	0.3	29.9	16.5	92	<0.1	40.9	10.3	<0.5	<0.1	0.4	0.5	<0.01	<0.1	<0.5
3.75	0.52	0.21	0.23	0.5	33.3	19.2	117	<0.1	39.2	9	<0.5	<0.1	0.2	0.4	<0.01	<0.1	<0.5
3.99	0.58	0.2	0.2	0.5	14.8	15.7	78	<0.1	34.2	11.9	<0.5	<0.1	0.3	0.5	<0.01	<0.1	<0.5
4.88	0.66	0.23	0.09	0.6	29.6	19.3	112	<0.1	47.5	11	<0.5	<0.1	0.1	0.3	<0.01	<0.1	<0.5
4.98	0.72	0.19	<0.02	0.3	39.7	16.1	94	<0.1	40	7.9	<0.5	<0.1	<0.1	0.3	<0.01	<0.1	<0.5
4.31	0.59	0.21	<0.02	0.3	34.2	18.1	94	<0.1	46.9	15.3	<0.5	<0.1	0.1	0.4	<0.01	<0.1	<0.5
3.95	0.55	0.22	0.02	0.5	38.6	18.2	139	<0.1	45	9.5	<0.5	<0.1	0.2	0.5	<0.01	<0.1	<0.5
4.23	0.61	0.23	<0.02	0.3	34.7	19.9	119	<0.1	45.8	8.3	<0.5	<0.1	0.1	0.4	<0.01	<0.1	<0.5
3.93	0.63	0.21	<0.02	0.2	33.4	17.2	124	<0.1	50	6.5	<0.5	<0.1	<0.1	0.3	<0.01	<0.1	<0.5
3.99	0.58	0.16	0.02	0.5	30.7	14.3	89	<0.1	43.5	11.4	<0.5	<0.1	0.1	0.3	<0.01	<0.1	<0.5
4.21	0.62	0.18	0.17	0.2	30.6	20.6	131	<0.1	51.6	12.1	<0.5	<0.1	0.2	0.7	<0.01	<0.1	<0.5
4.26	0.64	0.23	<0.02	0.4	32.5	13.2	109	<0.1	42.9	11.6	<0.5	<0.1	<0.1	0.2	<0.01	<0.1	<0.5
4.75	0.63	0.22	<0.02	0.3	25.5	11.8	84	<0.1	42.5	13.1	<0.5	<0.1	0.1	0.3	<0.01	<0.1	<0.5
4.4	0.63	0.22	<0.02	0.6	32.6	13.7	111	<0.1	48.2	16.6	<0.5	<0.1	<0.1	0.3	<0.01	<0.1	<0.5
4.22	0.59	0.24	<0.02	0.2	32.3	13.6	92	<0.1	41.3	16.1	<0.5	<0.1	0.1	0.2	<0.01	<0.1	<0.5
4.22	0.63	0.25	<0.02	0.3	26.5	19.9	76	<0.1	44	21.2	<0.5	<0.1	0.1	0.4	<0.01	<0.1	<0.5
4.16	0.62	0.21	<0.02	0.2	15.4	18.3	21	<0.1	14.6	11.6	0.8	<0.1	<0.1	0.2	<0.01	<0.1	<0.5
1.21	0.2	0.04	0.08	0.2	8.4	8.4	36	<0.1	10.9	2.2	<0.5	<0.1	<0.1	0.2	<0.01	<0.1	<0.5
4.52	0.67	0.25	<0.02	0.2	33.8	3.7	89	<0.1	51.4	19.8	<0.5	<0.1	<0.1	0.4	<0.01	<0.1	<0.5
3.98	0.61	0.22	0.04	0.5	21.7	9.7	107	<0.1	44	19.4	<0.5	<0.1	0.3	0.5	<0.01	<0.1	<0.5
4.73	0.61	0.24	0.06	0.3	37.8	13.6	138	<0.1	46.2	29.4	<0.5	<0.1	0.2	0.6	<0.01	<0.1	<0.5
3.35	0.48	0.31	0.1	0.2	34.9	14.4	101	<0.1	41.3	32.1	<0.5	<0.1	0.3	0.6	<0.01	<0.1	<0.5
2.32	0.28	0.06	<0.02	<0.1	3.7	13.6	97	<0.1	15.9	4.3	<0.5	<0.1	<0.1	0.1	<0.01	<0.1	<0.5
4.4	0.7	0.18	0.06	1	13.1	6.7	60	<0.1	36.7	33.7	<0.5	<0.1	<0.1	0.3	<0.01	<0.1	<0.5
4.46	0.67	0.14	0.04	0.4	26.3	9.1	66	<0.1	39.1	37.3	<0.5	<0.1	0.1	0.3	<0.01	<0.1	<0.5
3.66	0.53	0.2	0.62	0.3	31.5	20.4	86	<0.1	37.3	39.6	<0.5	<0.1	0.6	0.6	<0.01	<0.1	<0.5
3.15	0.46	0.14	1.04	4	33.8	28.5	100	<0.1	47.7	20.4	<0.5	<0.1	0.6	0.4	<0.01	<0.1	<0.5
4.12	0.56	0.19	1.01	0.3	22.2	13.6	179	<0.1	35.7	7.4	<0.5	0.1	0.4	0.2	0.01	<0.1	<0.5
2.16	0.36	2.7	2.48	0.8	18.9	21.4	48	<0.1	15.6	30.8	<0.5	<0.1	1.2	0.3	<0.01	<0.1	<0.5
5.2	0.72	0.08	0.74	6.4	19.6	15.4	43	<0.1	82.2	13.6	0.8	<0.1	0.6	0.2	<0.01	<0.1	<0.5
3.84	0.57	0.63	0.07	5.7	148.5	31.4	67	<0.1	137.5	252.3	1.9	<0.1	<0.1	0.2	<0.01	<0.1	<0.5
3.52	0.49	1.37	0.13	2.4	93.2	38.2	114	<0.1	132.9	238.5	1.8	<0.1	<0.1	0.5	0.01	<0.1	<0.5
3.43	0.52	0.53	0.06	0.4	50.5	11.2	104	<0.1	81.3	71.4	<0.5	<0.1	0.5	0.2	<0.01	<0.1	<0.5
3.44	0.54	0.38	0.04	1.8	80.9	126.2	143	<0.1	125.2	150.8	1.3	<0.1	1.1	2	<0.01	<0.1	<0.5
4.02	0.64	0.51	0.1	1.2	24.8	83.4	129	<0.1	140.8	181.8	2.7	<0.1	0.7	1	<0.01	<0.1	<0.5
4.6	0.7	2.67	0.06	2.2	47.2	126.3	156	<0.1	108.9	30.2	7.4	<0.1	0.3	2.9	<0.01	<0.1	<0.5
3.6	0.63	0.52	0.08	<0.1	13.4	6.8	124	<0.1	134.4	111.1	1.9	<0.1	0.2	0.3	<0.01	<0.1	<0.5
4.13	0.63	0.55	0.04	0.5	7	4.6	140	<0.1	116	67	1.2	<0.1	0.1	0.7	<0.01	<0.1	<0.5
6.35	0.96	0.05	0.05	<0.1	23.1	12.2	144	<0.1	136.2	108.5	1.8	<0.1	0.3	0.4	<0.01	<0.1	<0.5
4.49	0.7	0.04	<0.02	<0.1	12.1	16	151	<0.1	86.4	26	0.8	<0.1	<0.1	0.4	<0.01	<0.1	<0.5
4.01	0.62	0.04	<0.02	<0.1	11.1	20.1	132	<0.1	77.7	23.1	1.1	<0.1	0.4	0.5	<0.01	<0.1	<0.5
3.56	0.52	0.51	<0.02	0.2	27.9	26.1	95	<0.1	55.7	37.3	1.5	<0.1	0.6	0.4	<0.01	<0.1	<0.5
3.86	0.55	0.15	<0.02	0.4	17	9.9	131	<0.1	75.2	23.9	<0.5	<0.1	0.3	0.5	<0.01	<0.1	<0.5
3.65	0.53	0.04	<0.02	0.4	9.7	10	103	<0.1	66.3	23.2	1.9	<0.1	0.7	0.3	<0.01	<0.1	<0.5
3.79	0.59	0.1	<0.02	0.2	10	11.5	144	<0.1	91.7	26.5	<0.5	<0.1	1	0.7	<0.01	<0.1	<0.5
3.67	0.59	0.03	0.03	<0.1	6.2	16.1	108	<0.1	69.7	23.6	<0.5	<0.1	0.7	0.3	<0.01	<0.1	<0.5
3.83	0.65	0.07	0.02	0.2	4.2	8.7	123	<0.1	79.9	23.9	<0.5	<0.1	0.3	0.6	<0.01	<0.1	<0.5
3.69	0.64	0.04	0.02	0.1	6	11.3	109	<0.1	69.8	24.7	2.7	<0.1	0.4	0.7	<0.01	<0.1	<0.5
3.88	0.54	0.54	<0.02	0.3	7.8	12.8	104	<0.1	55.8	18.6	<0.5	<0.1	0.5	0.2	<0.01	<0.1	<0.5
3.42	0.57	0.09	0.04	0.2	13	40.8	110	<0.1	57.6	40.4	2.4	<0.1	0.7	0.7	<0.01	<0.1	<0.5
3.46	0.57	0.34	<0.02	0.3	5.8	7.6	118	<0.1	65.8	24.3	<0.5	<0.1	0.5	0.5	<0.01	<0.1	<0.5
4.88	0.64	0.04	<0.02	0.2	15.8	20.6	121	<0.1	71.8	48.1	4.2	<0.1	0.3	0.8	<0.01	<0.1	<0.5
3.4	0.53	0.27	<0.02	0.3	6.5	6.8	98	<0.1	71.8	22	<0.5	<0.1	0.9	0.5	<0.01	<0.1	<0.5
6.28	0.85	0.63	0.03	0.7	14.8	36.7	154	<0.1	111.6	57.4	2	<0.1	0.6	1	<0.01	<0.1	<0.5
4.06	0.58	0.06	0.13	0.5	1174	66	177	<0.1	115.4	56.6	22.4	<0.1	1	0.9	0.01	<0.1	<0.5
6.9	1.02	0.05	0.02	0.5	107	13.6	516	<0.1	128	79.2	2.5	1.4	0.2	0.3	0.15	<0.1	<0.5
3.21	0.46	0.17	0.21	0.2	11.1	19.9	45	<0.1	16.5	5.4	0.8	<0.1	0.2	0.2	<0.01	<0.1	<0.5
<0.05	<0.01	0.2	0.11	0.2	11.7	16.6	57	<0.1	18.3	5.7	0.9	<0.1	0.2	0.2	<0.01	<0.1	<0.5
3.24	0.49	0.29	0.07	0.4	27.2	27.4	119	<0.1	32.3	9.8	0.6	0.2	0.2	0.3	<0.01	<0.1	<0.5
3.23	0.45	0.27	0.07	0.4	20.5	36.8	61	<0.1	14.4	6.8	1.9	0.2	0.2	0.3	<0.01	0.1	<0.5
3.67	0.56	0.21	<0.02	0.1	11.5	49.4	93	<0.1	29.5	13.1	<0.5	0.3	0.2	0.3	<0.01	<0.1	<0.5
2.22	0.33	0.08	<0.02	0.1	5.4	37.3	81	<0.1	11.8	3.2	<0.5	0.3	0.1	0.2	<0.01	<0.1	<0.5
1.47	0.24	0.03	0.04	<0.1	2.4	41.2	31	<0.1	5.1	1	3.3	0.1	<0.1	<0.1	<0.01	<0.1	<0.5
3.65	0.58	0.27	0.04	0.2	19.8	74.9	138	0.1	33.3	13.2	1.7	0.5	0.3	0.6	<0.01	<0.1	<0.5
4.24	0.64	0.32	0.05	<0.1	13.1	33.6	100	<0.1	38.4	6.3	1.4	0.3	0.2	0.2	<0.01	<0.1	<0.5
3.88	0.62	0.03	0.03	0.2	4	6.4	31	<0.1	9.5	<0.5	0.8	<0.1	<0.1	<0.1	<0.01	<0.1	<0.5
4.27	0.62	0.17	<0.02	0.3	7.2	20.9	85	<0.1	25.9	5.8	<0.5	0.5	0.1	0.3	<0.01	<0.1	<0.5
4.13	0.58	0.19	0.04	0.1	11.9	44.9	78	<0.1	23.2	6	<0.5	0.3	0.2	0.2	<0.01	<0.1	<0.5
3.04	0.49	0.1	<0.02	<0.1	12.6	99.9	345	0.1	18.1	5.8	<0.5	1	0.4	<0.1	<0.01	<0.1	<0.5

Table 5: All geochemistry data (basic data), before calculations.

Calculated values:

Sample	Rock type	Zr/Sc	La/Sc	Ti/Zr	Nb/Y	Zr/Ti	La/Th	Hf	Sc/Th	Zr/10	Th/U	K/Sc	Th/Sc	Sc	K	Eu/Eu*	LaN/YbN
CA1	Sand	16.08	3.22	21.04	0.50	0.05	4.38	6.40	1.36	22.51	4.12	2,013.47	0.74	14.00	28,188.52	0.63	10.23
CA2	Shale	10.62	3.22	29.23	0.45	0.03	3.38	4.70	1.05	18.05	5.79	1,976.68	0.95	17.00	33,603.50	0.65	10.87
CA3	Shale	11.89	3.43	26.40	0.40	0.04	3.31	6.00	0.97	20.21	5.50	1,972.18	1.04	17.00	33,527.04	0.64	11.19
CA4	Sand	18.89	3.68	19.53	0.59	0.05	3.65	6.90	0.99	24.56	4.37	1,931.68	1.01	13.00	25,111.90	0.72	12.77
CA5	sand	12.85	3.58	25.20	0.45	0.04	3.42	5.40	0.96	19.27	4.91	1,957.43	1.05	15.00	29,361.47	0.63	10.58
CA6	Shale	11.01	3.27	28.52	0.47	0.04	3.43	5.30	1.05	18.71	4.63	1,894.07	0.95	17.00	32,199.17	0.64	10.02
CA7	Shale	11.35	3.16	27.65	0.43	0.04	3.34	5.00	1.06	19.30	5.19	1,839.68	0.95	17.00	31,274.54	0.62	9.09
CA8	Shale	9.44	3.71	32.09	0.25	0.03	4.00	4.60	1.08	17.00	4.28	1,816.76	0.93	18.00	32,701.66	0.58	9.25
CA9	Shale	8.42	3.23	39.65	0.41	0.03	3.48	5.10	1.08	17.69	4.88	1,779.47	0.93	21.00	37,368.93	0.61	9.20
CA10	Shale	8.74	3.47	39.78	0.49	0.03	3.71	5.30	1.07	17.48	6.03	1,630.92	0.94	20.00	32,618.45	0.65	10.87
CA11	Shale	8.98	3.50	37.45	0.41	0.03	3.80	4.80	1.08	16.17	5.35	1,821.56	0.92	18.00	32,788.15	0.64	10.78
CA12	Shale	7.93	3.08	41.20	0.42	0.02	3.35	4.50	1.09	15.86	5.26	1,639.24	0.92	20.00	32,784.87	0.63	9.84
CA13	Shale	6.90	3.15	43.47	0.41	0.02	3.74	4.40	1.19	14.48	4.92	1,664.21	0.84	21.00	34,948.33	0.65	11.38
CA14	Shale	8.85	3.12	36.35	0.47	0.03	3.48	5.20	1.12	16.82	4.86	1,650.90	0.89	19.00	31,367.15	0.65	10.03
CA15	Shale	9.96	3.27	34.77	0.48	0.03	3.42	5.20	1.05	17.93	4.65	1,724.30	0.96	18.00	31,037.45	0.63	9.45
CA16	Shale	10.37	3.47	31.94	0.44	0.03	3.74	5.50	1.08	19.71	5.03	1,743.04	0.93	19.00	33,117.71	0.63	10.45
CA17	Shale	8.98	3.58	36.07	0.40	0.03	3.79	4.80	1.06	17.95	5.11	1,772.20	0.95	20.00	35,444.04	0.60	10.19
CA18	Shale	7.78	3.62	40.10	0.40	0.02	3.87	4.60	1.07	15.55	5.05	1,743.26	0.94	20.00	34,865.12	0.65	11.10
CA19	Shale	8.52	3.37	36.61	0.40	0.03	3.78	4.20	1.12	17.03	4.34	1,739.10	0.89	20.00	34,781.91	0.65	10.78
CA20	Shale	9.02	3.38	35.58	0.42	0.03	3.50	5.40	1.04	18.03	4.71	1,751.58	0.97	20.00	35,031.54	0.61	10.81
CA21	Sand	13.86	3.62	22.00	0.70	0.05	3.94	9.60	1.09	31.88	3.84	1,559.13	0.92	23.00	35,860.05	0.61	13.51
CA22	Sand	96.80	6.43	7.23	0.99	0.14	3.27	7.70	0.51	29.04	5.36	803.00	1.97	3.00	2,408.99	0.69	10.78
CA23	Shale	10.67	3.41	31.76	0.47	0.03	3.33	5.50	0.98	21.33	4.27	1,947.32	1.03	20.00	38,946.33	0.67	10.20
CA24	Shale	10.49	3.49	31.28	0.48	0.03	3.55	5.50	1.02	19.93	4.79	1,808.91	0.98	19.00	34,369.31	0.63	11.26
CA25	Shale	10.44	3.50	33.54	0.51	0.03	3.33	5.90	0.95	19.84	4.55	1,949.07	1.05	19.00	37,032.30	0.65	9.50
CA26	Shale	7.89	2.52	42.36	0.48	0.02	3.21	4.30	1.28	15.00	4.97	1,886.80	0.78	19.00	35,849.27	0.64	9.64
CA27	Sand	84.20	6.73	7.59	0.37	0.13	3.74	6.00	0.56	25.26	4.15	1,301.41	1.80	3.00	3,904.23	0.57	5.88
CA28	Shale	9.39	3.17	34.26	0.58	0.03	3.33	5.50	1.05	20.65	4.18	1,917.81	0.95	22.00	42,191.86	0.63	10.70
CA29	Shale	10.18	3.13	32.11	0.49	0.03	3.40	5.60	1.09	20.35	5.26	1,834.79	0.92	20.00	36,695.75	0.62	9.48
CA30	Shale	16.92	3.33	21.02	0.50	0.05	3.50	7.00	1.05	25.38	4.47	1,718.99	0.95	15.00	25,784.86	0.63	9.23
CA31	Sand	15.81	3.79	21.13	0.47	0.05	3.71	5.70	0.98	22.13	4.21	2,156.88	1.02	14.00	30,196.27	0.66	11.37
CA32	Shale	18.13	3.99	24.02	0.55	0.04	3.40	7.40	0.85	27.20	3.91	2,246.68	1.17	15.00	33,700.18	0.60	9.81
CA33	Shale	17.24	3.38	19.13	0.43	0.05	3.29	3.30	0.98	13.79	4.82	966.64	1.03	8.00	7,733.13	0.63	8.45
CA34	Sand	22.54	4.03	15.58	0.31	0.06	3.69	8.00	0.92	31.56	3.83	2,020.01	1.09	14.00	28,280.17	0.60	7.33
CA35	Shale	3.93	1.73	40.09	0.35	0.02	2.86	2.60	1.66	9.42	8.06	1,502.01	0.60	24.00	36,048.14	0.63	7.30
CA36	Shale	3.83	1.81	38.53	0.44	0.03	3.01	2.40	1.67	9.18	8.00	1,286.55	0.60	24.00	30,877.22	0.62	8.33
CA37	Shale	3.80	1.58	39.80	0.40	0.03	2.66	2.80	1.69	9.49	6.43	1,375.05	0.59	25.00	34,376.20	0.64	7.76
CA38	Shale	4.17	1.93	40.59	0.46	0.02	2.89	2.90	1.49	9.60	7.00	1,462.19	0.67	23.00	33,630.45	0.67	8.74
CA39	Shale	4.55	2.01	37.30	0.35	0.03	3.23	3.00	1.61	10.93	6.48	1,287.20	0.62	24.00	30,892.71	0.65	8.10
CA40	Shale	3.94	2.37	40.55	0.23	0.02	3.95	2.30	1.67	8.28	3.41	1,268.22	0.60	21.00	26,632.64	0.59	7.32
CA41	Shale	4.53	2.10	41.33	0.39	0.02	3.34	3.70	1.59	10.88	6.29	1,454.17	0.63	24.00	34,900.11	0.60	9.46
CA42	Shale	5.58	2.45	37.37	0.40	0.03	3.29	3.40	1.35	11.71	6.50	1,716.41	0.74	21.00	36,044.52	0.60	8.41
CA43	Shale	4.46	3.28	37.54	0.22	0.03	5.54	2.80	1.69	10.70	5.07	1,183.70	0.59	24.00	28,408.89	0.61	8.38
CA44-1	Shale	5.41	2.72	40.64	0.40	0.02	3.71	3.30	1.36	11.36	6.42	1,529.95	0.73	21.00	32,128.85	0.64	8.61
CA44-2	Shale	5.53	2.66	39.73	0.41	0.03	3.44	3.20	1.30	11.62	6.23	1,573.54	0.77	21.00	33,044.43	0.64	9.40
CA45	Shale	5.77	1.96	39.48	0.51	0.03	2.65	3.40	1.35	11.54	5.29	1,911.78	0.74	20.00	38,235.70	0.64	7.44
CA46	Shale	6.10	2.25	39.80	0.42	0.03	2.90	3.80	1.29	12.20	6.46	1,864.66	0.78	20.00	37,293.18	0.65	7.88
CA47	Shale	6.04	2.11	38.77	0.43	0.03	2.90	3.50	1.37	12.68	5.88	1,800.01	0.73	21.00	37,800.22	0.61	8.20
CA48	Shale	5.09	2.19	41.79	0.42	0.02	3.04	3.00	1.39	11.19	5.45	1,664.71	0.72	22.00	36,623.55	0.67	8.58
CA49	Shale	5.84	2.24	37.32	0.34	0.03	3.22	4.30	1.44	12.85	5.88	1,639.04	0.70	22.00	36,058.99	0.58	9.06
CA50	Shale	6.13	2.16	36.89	0.40	0.03	2.75	3.70	1.27	13.49	6.65	1,721.98	0.79	22.00	37,883.48	0.61	8.40
CA51	Shale	5.86	2.11	38.57	0.44	0.03	2.80	3.50	1.33	12.90	5.93	1,722.84	0.75	22.00	37,902.49	0.58	8.52
CA52	Shale	5.60	2.37	41.13	0.42	0.02	3.20	3.20	1.35	10.64	5.22	1,822.23	0.74	19.00	34,622.43	0.57	7.85
CA53	Shale	6.50	2.28	37.84	0.47	0.03	2.90	3.70	1.27	12.99	6.28	1,802.59	0.79	20.00	36,051.75	0.57	9.01
CA54	Shale	5.02	2.38	43.19	0.41	0.02	3.14	2.90	1.32	10.55	6.91	1,664.71	0.76	21.00	34,958.85	0.65	9.77
CA55	Shale	6.23	3.04	37.53	0.33	0.03	3.57	3.40	1.18	12.46	6.54	1,577.63	0.85	20.00	31,552.53	0.69	8.41
CA56	Shale	5.43	2.16	40.89	0.44	0.02	3.08	3.30	1.43	10.85	6.36	1,864.66	0.70	20.00	37,293.18	0.66	8.57
CA57	Shale	5.72	3.80	31.92	0.21	0.03	4.76	3.80	1.25	12.02	7.00	1,042.53	0.80	21.00	21,893.09	0.60	8.60
CA58	Shale	4.64	2.11	43.45	0.31	0.02	2.96	2.80	1.40	10.21	5.81	1,508.07	0.71	22.00	33,177.57	0.62	7.72
CA59	Shale	4.91	3.48	34.07	0.21	0.03	5.26	3.10	1.51	11.79	5.89	951.32	0.66	24.00	22,831.67	0.68	8.19
CAN1	Sand	27.76	2.92	12.37	0.43	0.08	2.53	7.80	0.87	30.54	4.10	1,610.12	1.15	11.00	17,711.37	0.65	6.76
CAN2	Sand	24.94	2.91	14.42	0.66	0.07		<0.1		27.43		1,768.87		11.00	19,457.56		
CAN3	Shale	13.14	4.26	27.04	0.51	0.04	3.85	4.50	0.90	18.40	4.70	1,865.91	1.11	14.00	26,122.80	0.65	12.43
CAN4	Shale	12.03	2.73	27.58	0.48	0.04	2.50	5.90	0.91	18.04	4.82	1,963.17	1.09	15.00	29,447.60	0.68	8.58
CAN5	Sand	22.36	3.09	18.00	0.45	0.06	2.77	9.40	0.90	31.30	4.73	2,109.34	1.11	14.00	29,530.78	0.64	7.95
CAN6	Sand	61.92	3.76	9.29	0.43	0.11	2.58	8.30	0.68	30.96	4.06	1,362.46	1.46	5.00	6,812.32	0.54	5.72
CAN7	Sand	99.60	5.58	5.72	0.59	0.17	3.28	11.10	0.59	39.84	4.00	1,661.87	1.70	4.00	6,647.50	0.59	10.25
CAN8	Shale	13.01	2.59	27.11	0.47	0.04	2.46	6.60	0.95	22.11	5.11	2,123.88	1.05	17.00	36,106.04	0.61	8.15
CAN9	Shale	12.77	2.61	27.91	0.49	0.04	2.40	6.50	0.92	22.98	5.76	2,232.81	1.09	18.00	40,190.58	0.60	7.49
CAN10	Sand	340.63	9.50	3.70	0.46	0.27	2.60	37.80	0.27	136.25	3.65	1,019.12	3.65	4.00	4,076.49	0.60	6.62
CAN11	Sand	26.21	3.43	15.85	0.46	0.06	2.84	10.90	0.83	36.69	3.93	2,347.25	1.21	14.00	32,861.49	0.68	7.60
CAN12	Sand	28.72	4.32	14.61	0.47	0.07	3.43	11.00	0.79	37.34	4.43	2,348.86	1.26	13.00	30,535.13	0.67	9.20
CAN13	Sand	45.43	4.39	10.29	0.46	0.10	3.35	12.00	0.76	45.43	3.97	2,137.86	1.31	10.00	21,378.62	0.61	9.76

Table 6: Calculated values, used in the diagrams.

Major trace elements:

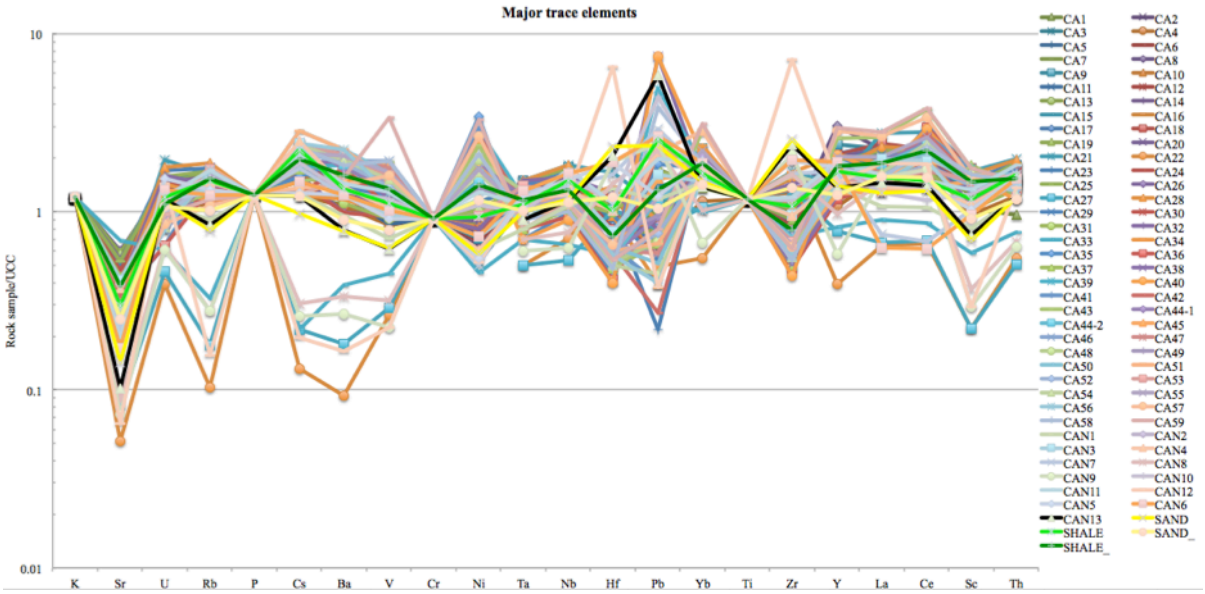

Figure 146: Major trace elements for both formations, all samples (CA Fm and CAN Fm).

REE- normalized to UCC:

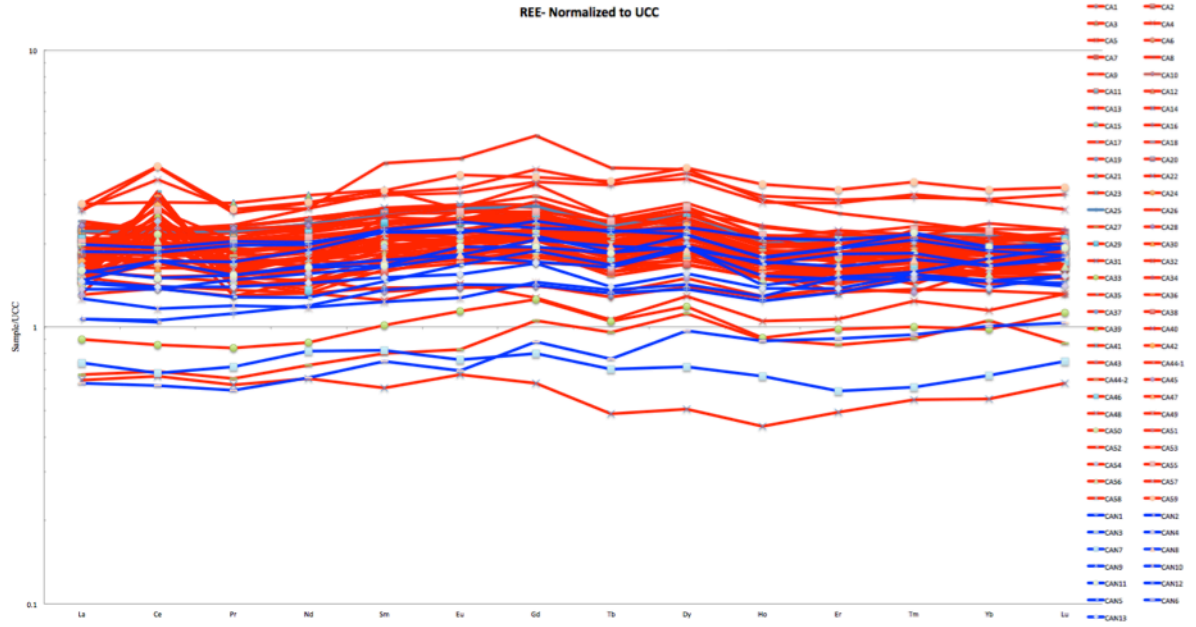

Figure 147: All trace elements for REE- normalized to UCC, red values are CA Fm, while blue values are CAN Fm

REE- normalized to chondrite:

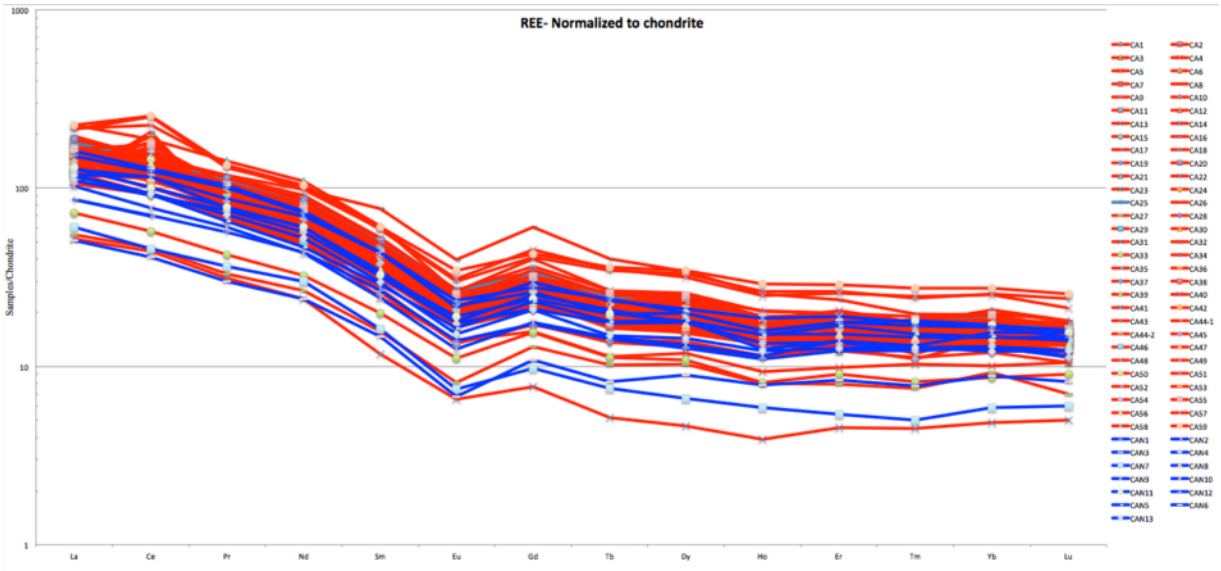

Figure 148: Trace elements for REE- normalized to chondrite, red values are CA Fm, while blue values are CAN Fm.